

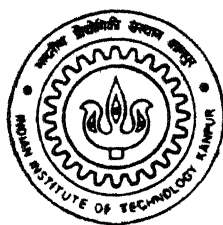
9810608

# EFFECT OF $\beta$ PROCESSING DURING THERMOMECHANICAL TREATMENT OF Ti-6Al-4V ALLOY ON ITS GRAIN REFinement AND SUPERPLASTIC BEHAVOUR

by

INDRANIL LAHIRI

TH  
MME/1999/M  
L139c



DEPARTMENT OF MATERIALS AND METALLURGICAL ENGINEERING  
**INDIAN INSTITUTE OF TECHNOLOGY KANPUR**

December, 1999

**EFFECT OF  $\beta$  PROCESSING DURING THERMOMECHANICAL  
TREATMENT OF Ti-6Al-4V ALLOY ON ITS GRAIN REFINEMENT AND  
SUPERPLASTIC BEHAVOUR**

A Thesis Submitted in Partial Fulfilment of the Requirements  
For the Degree of  
**MASTER OF TECHNOLOGY**

By  
**INDRANIL LAHIRI**

to the  
**DEPARTMENT OF MATERIALS AND METALLURGICAL ENGINEERING**  
**INDIAN INSTITUTE OF TECHNOLOGY KANPUR**  
**DECEMBER, 1999**

15 MAY 2000 / MME

**CENTRAL LIBRARY**  
I.I.T., KANPUR

130842

TH

MME/1999/M  
L139c



A130842

**Dedicated**

**To**

*My Parents*

## **ACKNOWLEDGEMENT**

I wish to express my deep sense of gratitude and indebtedness to Dr. S. Bhargava for his valuable guidance, encouragement and inspirational discussions throughout the course of this investigation. It has truly been a learning experience to associate with him and work towards the completion of this work.

I am thankful to Mr. Manasij Kumar Yadava and Dr. Satyam Suwas for their endless help and moral support extended to me at different times.

I am also thankful to Dr. Mungole, Mr. K.P.Mukherjee, Mr. Jain, Mr. Umashankar Singh, late Mr. Pal, Mr. Lal, Mr. Agnihotri, the metallurgical workshop staffs and especially to Mr. Kumar for their assistance in the experimental works.

And, last but not the least, I want to mention the name of Debrupa Mondal, who is also my co-worker.

December'1999

I.I.T.,Kanpur

Indranil Lahiri

# CONTENTS

<b>ABSTRACT</b>	1 - 2
<b>Chapter 1. Introduction</b>	3 - 5
<b>Chapter 2. Literature Review</b>	6 - 57
2.1 Titanium and its Alloy	
2.1.1 Properties of Ti-Alloys	
2.1.2 Important Uses of Ti and its Alloys	
2.1.3 Classification of Ti-Alloys	
2.1.4 Microstructural Features Ti-Alloys	
2.1.5 Importance of ( $\alpha+\beta$ ) Alloys	
2.1.6 Microstructure and Property Control	
2.1.6.1 Effect of Heat Treatment	
2.1.6.2 Effect of Working	
2.1.6.3 Effect of Thermo-Mechanical Treatment	
2.2 Texture in ( $\alpha+\beta$ ) Ti-Alloys	
2.3 Deformation Characteristics of Ti and its Alloys	
2.4 Forming Characteristics of Ti-Alloys	
2.5 Superplasticity	
2.5.1 What Is Superplasticity	
2.5.2 Mechanical Equations of Superplasticity	
2.5.3 Metallurgical Variables Affecting Superplasticity	
2.5.4 Importance of Superplasticity	
2.5.5 Superplasticity and Ti-Alloys	
<b>Chapter 3. Experimental Procedure</b>	58 - 67
3.1 Starting Material	
3.2 $\beta$ -Transus Determination	
3.3 Thermo-Mechanical Treatment	
3.3.1 Equipments for Thermo-Mechanical Processing	
3.3.2 Working Schedule	
3.4 Characterization	

3.4.1	Microstructural Characterization
3.4.2	Phase Characterization
3.4.3	Mechanical Property (Superplasticity) Determination
<b>Chapter 4. Results and Discussions</b>	<b>68 – 150</b>
4.1	Characterization of the As Received Ti-6Al-4V Alloy
4.1.1	Structure of the As Received Alloy
4.1.2	$\beta$ -Transus of the Alloy
4.1.3	Effect of $\beta$ Annealing Temperature on $\beta$ Grain Size
4.1.4	Type of Martensite Formed by Water Quenching
4.2	Thermomechanical Processing Variables in The $\beta$ Phase Field and Their Effect on Conditioning of $\beta$ Grains
4.2.1	Effect of Thickness Reduction on $\beta$ Grain Characteristics
4.2.2	Effect of Recrystallization Annealing on Microstructure
4.2.3	Morphology of Martensite Formed by Different $\beta$ Processing Routes
4.3	Effect of Thermomechanical Processing in ( $\alpha+\beta$ ) Phase Field on Microstructural Refinement of The Alloy
4.3.1	Effect of Cooling Rate on the Structure
4.3.2	Type of Martensite Formed as a Function of Processing
4.3.3	Effect of Conditioning of $\beta$ Grains on Microstructural Refinements After Rolling in Two-Phase Field

4.4	Effect of Recrystallization Annealing Treatment on Evolution of Equiaxed $\alpha$ Structure on Thermomechanically Processed Ti-6-4 Alloy	
4.4.1	Effect of Recrystallization Temperature on the Evolution of Low Aspect Ratio $\alpha$ Morphology in Ti-6-4 Alloy	
4.4.2	Effect of Recrystallization Temperature on the $\alpha$ Grain Size	
4.5	Superplastic Behaviour of Thermomechanically Processed Ti-6-4 Alloy	
4.5.1	Flow Curves and the Strain Rate Sensitivity of Thermomechanically Processed Ti-6-4 Alloy Before Recrystallization Annealing	
4.5.2	Flow Curves and the Strain Rate Sensitivity of Thermomechanically Processed Ti-6-4 Alloy After Recrystallization Annealing	
<b>Chapter 5. Conclusions</b>		151 - 153
<b>References</b>		154 - 162

## ABSTRACT

Though two-phase ( $\alpha+\beta$ ) titanium alloys have poor workability, they may be thermo-mechanically processed to display excellent superplastic behaviour in fine equiaxed  $\alpha$  condition. Ti-6Al-4V alloy, hereafter referred to as Ti-6-4 alloy, is one of the most important ( $\alpha+\beta$ ) titanium alloy having wide applications in space, aeronautical and chemical industries. Further, in the extra-low interstitial (ELI) condition, Ti-6-4 alloy shows excellent fracture toughness in cryogenic environment and hence is considered to be an extremely useful material for making gas bottles for space vehicles. The conventional thermo-mechanical processing route for this alloy consists of heavy hot deformation in the ( $\alpha+\beta$ ) phase field followed by mill annealing at a lower temperature to obtain a fine equiaxed  $\alpha$  phase structure surrounded by the  $\beta$  phase. Evolution of the equiaxed  $\alpha$  structure, however, is expected to be influenced by the conditioning of prior  $\beta$  grains. The present study deals with the superplastic behaviour of an ELI grade Ti-6-4 alloy as influenced by its thermo-mechanical processing involving different routes affecting the conditioning of prior  $\beta$  grains as well as the aspect ratio of the lamellar  $\alpha$  prior to rolling in ( $\alpha+\beta$ ) field.

Plates of the given Ti-6-4 alloy, before their rolling in the ( $\alpha+\beta$ ) field, were subjected to five thermo-mechanical treatments involving heating in the  $\beta$  phase field followed by (a) furnace cooling, (b) water quenching with no deformation in the  $\beta$  phase field, (c) water quenching with 30% deformation in the  $\beta$  phase field, (d) water quenching with 60% deformation in the  $\beta$  phase field and (e) recrystallization of the 60% deformed sample for 30 seconds at 10°C above the  $\beta$ -transus temperature followed by water quenching. Samples obtained from these routes were further hot rolled to give a thickness reduction of 75% in the ( $\alpha+\beta$ ) field at a temperature of 90°C below the  $\beta$ -transus temperature and were subsequently mill-annealed at the temperatures of 250°C, 150°C and 100°C below the  $\beta$ -transus temperature.

Results of the present study show that the unconventional routes investigated in this study produce considerably finer structures than those obtained by the conventional route. Microstructures obtained by each of the new routes were found to have an average  $\alpha$  phase size  $< 2\mu\text{m}$ . It was also found that though the alloy water-quenched from the  $(\alpha+\beta)$  field contains only the hexagonal martensite, that water-quenched from the  $\beta$  field, even subjected to these unconventional thermo-mechanical routes, possessed hexagonal as well as orthorhombic martensites. Characterization of the superplastic behaviour of different thermo-mechanically processed alloy was done by (a) 'step strain-rate test' and (b) 'elongation to failure test'. The samples obtained from different processing routes were found to have strain rate sensitivity ranging from 0.25 to 0.87. Samples of ELI grade of Ti-6-4 alloy, treated by route (d), were found to have the maximum elongation of 695% at the strain rate of  $1.5 \times 10^{-3} \text{ s}^{-1}$  at the testing temperature of  $850^\circ\text{C}$ .

# CHAPTER 1

## INTRODUCTION

Interest in the properties of Ti and its alloys began to accelerate during the late 1940s and early 1950s as their potential as high temperature, high strength/weight materials with aeronautical applications became more and more widely recognized. By now, these alloys have found widespread use in the chemical and related industries also, where advantage can be taken of its excellent corrosion resistance[4,95].

Titanium alloys are usually divided into three major classes depending on the phases present in their microstructure at room temperature and are referred to as  $\alpha$  alloys,  $\alpha+\beta$  alloys and  $\beta$  alloys. The group  $\alpha+\beta$  alloys consists of largest number of superplastic alloys. These are alloys whose compositions are such that they support a mixture of  $\alpha$  and  $\beta$  phases in the microstructure. They also have high room temperature strength and moderate elevated temperature strength. The properties of  $\alpha+\beta$  alloys can be controlled by heat treatment and thermomechanical treatment, which are used to adjust the microstructural and precipitational states of the  $\beta$  component.

Morphology of the primary  $\alpha$  phase in the  $\alpha+\beta$  titanium alloys is of considerable importance from the point of view of controlling their static and dynamic mechanical properties. Equiaxed microstructures often show a higher tensile ductility and superior fatigue strength values, especially when the  $\alpha$  grain size is reduced, whereas they are inferior to lamella structures concerning fatigue crack propagation and fracture toughness values[96]. Slow cooling into the  $\alpha+\beta$  phase field leads to a very coarse lamellar arrangement while water quenching from the  $\beta$  phase field followed by an annealing treatment in the two phase field leads to a finer lamellar structure. Equiaxed microstructures require an additional deformation treatment within the  $\alpha+\beta$  phase field followed by mill annealing at about 700°C.

Though  $\alpha+\beta$  titanium alloys possess good mechanical properties, they have poor workability. Hence, superplastic forming has emerged as one of the commercially viable production route. The microstructure of the alloy has important bearing on the superplastic properties and one of the essential requirements of superplasticity in these alloys is that the structure should consist of  $\alpha+\beta$  structure in which the primary  $\alpha$  exists in a very fine equiaxed morphology. Therefore obtaining fine equiaxed structure in the material, so that they can be further processed by superplastic forming, has become one of the major objectives in processing of  $\alpha+\beta$  titanium alloys.

The deformation behaviour of the  $\alpha+\beta$  alloys in the two phase field is strongly influenced by the deformation characteristics of the difficult-to-form hcp  $\alpha$  phase. It occurs both by slip and twining. Further as observed by the nature of the stress-strain curves and TEM analysis of the structure, these alloys soften by dynamic recovery and/or by dynamic recrystallization during their hot deformation[97]. Hot deformation degree, if exceeding a critical value, may also lead to the fracturing of deforming  $\alpha$  lamellae and give rise to primary  $\alpha$  lamellae of smaller aspect ratio[98]. Subsequent break-up of  $\alpha$  lamellae to equiaxed morphology occurs during subsequent recrystallization annealing when the  $\beta$  phase penetrates across the lamellar width along the sub-boundaries or shear bands. The mode of deformation also affects the transformation of lamellar  $\alpha$  to equiaxed  $\alpha$  by primarily influencing texture.

To reduce structural weight and fabrication cost of titanium alloys, increasing attention is being given to near-net shape processing techniques like superplastic forming and to improve SPF by optimizing the material and process parameters. Recently widespread results have shown that SPF with or without concurrent diffusion bonding can result in substantial cost savings, creating great interest in SPF method.

To date most SPF works were concentrated on Ti-6Al-4V in the temperature range 900-925°C. The required microstructure for SPF were produced by conventional thermomechanical processing schedules in most of

these works. The scope of refining the structure by proper  $\beta$  treatment prior to the conventional thermomechanical processing is not investigated thoroughly for this alloy. The results and understanding of the refinement process for development of suitable microstructures for superplastic forming can lead to more precision shapes to be formed by superplastic forming in this alloy.

The present study was undertaken to investigate

- (i) the microstructural refinement in Ti-6Al-4V alloy by involving the conditioning of  $\beta$  grains and acicular  $\alpha$  prior to hot rolling in the  $\alpha+\beta$  field,
- (ii) the superplastic behaviour of the material before and after recrystallization annealing in the  $\alpha+\beta$  phase field.

## CHAPTER 2

### LITERATURE REVIEW

#### **2.1 Titanium and Its Alloys**

##### **2.1.1 Properties of Ti and Its Alloys**

Titanium possesses an outstanding combination of physical, chemical and mechanical properties. Titanium metal exists in two allotropic forms. The low temperature form, stable below 882.5°C, has a hexagonal close-packed structure and is known as  $\alpha$ -titanium. The high temperature form, stable above 882.5°C, has a body centred cubic structure and is known as  $\beta$ -titanium. Titanium is a low density element. Density of  $\alpha$ -titanium at  $25\pm2^\circ\text{C}$ , as calculated by Clark[1], is  $4.505 \text{ gm/cm}^3$ , whereas that of  $\beta$ -titanium at  $900^\circ\text{C}$ , as calculated by Burgers and Jacob[2], is  $4.32 \text{ gm/cm}^3$ . Young's modulus of titanium generally lies in the range  $(11.0\pm0.4)\times10^{11} \text{ dyne/cm}^2$ [3]. It is paramagnetic in nature and shows a relatively lower coefficient of linear thermal expansion and high electrical resistivity. Some important physical properties of titanium are shown in Table 2.1[3,5].

With strength capability most equal to that of low carbon steels and density nearly half (56 %) of them, titanium alloys can be strengthened to achieve a specific strength (strength per unit weight) equal to that of ultra high strength steels. Table 2.2[4] shows typical room temperature tensile strength of some commercial titanium alloys. Titanium approaches the high hardness value possessed by some of the heat-treated alloy steels[29].

Titanium and its alloys have exceptionally high fatigue strength, if the surface is carefully prepared. It is 0.82 and 0.31 of tensile strength for unnotched and notched samples, respectively and thus lies in the same range as the steels[3,6]. Fatigue crack growth rates of annealed Ti-6Al-4V alloy in distilled water are enhanced as compared with that in air; the growth rates are found to decrease with increasing temperature and frequency[7]. These alloys

**Table 2.1 : Physical Properties of Elemental Titanium**

Atomic Number	22
Atomic Weight	47.90
Atomic Volume	10.6 W/D
Covalent Radius	1.32 A
First Ionisation Energy	158 K-cal/gm-mole
Thermal Neutron Absorption Cross Section	5.6 barns/atom
Colour	Dark Gray
Density	$\alpha$ - 4.505 gms/cm <sup>3</sup> at 25±2°C $\beta$ - 4.32 gms/cm <sup>3</sup> at 900°C
Melting Point	1941±10 K
Solidus/Liquidus	1998±10 K
Boiling Point	3533 K
Specific Heat(at 25°C)	0.518 J/kg K
Thermal Conductivity	9.0 BTU/hr ft <sup>2</sup> °F
Heat of Fusion	440 kJ/kg
Heat of Evaporation	9.83 MJ/kg
Heat of Transformation	678 cal/mole
Yong's Modulus	$10.7 \times 10^{11}$ dyne/cm <sup>2</sup>
Temp. Coeffn. Of Young's Modulus	$6.28 \times 10^8$ dyne/cm <sup>2</sup> °C
Modulus of Rigidity	$(3.87 \pm 0.1) \times 10^{11}$ dyne/cm <sup>2</sup>
Poisson's Ratio	0.36
Coefficient of Friction	0.8 at 40 m/min
Coefficient of Linear Expansion	$(8.35 \pm 0.15) \times 10^{-6}$ /°C at 15°C
Electrical Resistivity	$(42.05 \pm 0.5) \times 10^{-6}$ ohm-cm
Magnetic Susceptibility	3.2±0.4 emu/gm
Work Function	4.05±0.1 eV
Electronic Specific Heat	$8.0 \pm 10^{-4}$ cal/°C mol

**Table 2.2 : Typical Room Temperature Tensile Strengths Of Some Commercial Titanium-base Alloys**

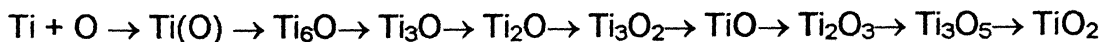
Alloy Name	Nominal Composition	Condition	UTS $10^8 \text{ Nm}^{-2}$	YS $10^8 \text{ Nm}^{-2}$	Elong %
5-2.5	Ti-5Al-2.5Sn	A,.25-4h,1300-1600°F	8.3-9.0	7.9-8.3	13-18
3-2.5	Ti-3Al-2.5Sn	A,1-3h,1200-1400°F	6.5	6.2	22
6-2-1-1	Ti-6Al-2Nb-1Ta-1Mo	A,.25-2h,1300-1700°F	8.6	7.6	14
8-1-1	Ti-8Al-1Mo-1V	A,8h,1450°F	10.0	9.3	12
Corona 5	Ti-4.5Al-5Mo-1.5Cr	$\alpha$ - $\beta$ A, after $\beta$ processing	9.7-11.0	9.3-103	12-15
Ti-17	Ti-5Al-2Sn-2Zr-4Mo-4Cr	$\alpha$ - $\beta$ or $\beta$ processed + Ag.	1.4	10.7	8
6-4	Ti-6Al-4V	A,2h,1300-1600°F Ag.	9.6 11.7	9.0 11.0	17 12
6-6-2	Ti-6Al-6V-2Sn	A,3H,1300-1550°F Ag.	10.7 12.8	10.0 12.1	14 10
6-2-4-2	Ti-6Al-2Sn-4Zr-2Mo	A,4H,1300-1550°F	10.0	9.3	15
6-2-4-6	Ti-6Al-2Sn-4Zr-6Mo	A,2h,1500-1600°F Ag.	10.3 12.1	9.7 11.4	11 8
6-22-22	Ti-6Al-2Sn-2Zr-2Mo-2Cr-.25Si	$\alpha$ - $\beta$ processed+Ag.	10.0	10.1	14
10-2-3	Ti-10V-2Fe-3Al	A,1h,1400°F Ag.	9.7 12.4-13.4	9.0 11.4-12.4	9 7
15-3-3-3	Ti-15V-3Cr-3Sn-3Al	A,.25h,1450°F Ag.	7.9 11.4	7.7 10.7	20-25 8
13-11-3	Ti-13V-11Cr-3Al	A,.5h,1400-1500°F Ag.	9.3-9.7 12.1	8.6 11.4	18 7
38-6-44	Ti-3Al-8V-6Cr-4Mo-4Zr	A,.5h,1500-17--°F Ag.	8.3-9.0 12.4	7.8-8.3 11.7	10-15 7
$\beta$ -III	Ti-4.5Sn-6Zr-11.5Mo	A,.5h,1300-1600°F Ag.	6.9-7.6 12.4	6.5 11.7	23 7

A → Annealed Ag. → Aged

showed creep at room temperature; creep strength of titanium normally decreases at first, but at 120°C begins to increase again, reaching a maximum at 200°C, thereafter falls gradually with increase in temperature. Cold working of titanium increases its creep resistance at room temperature[3,6]. The Charpy impact strength dropped from an average of 15 ft-lb at room temperature to about 6 ft-lb at liquid nitrogen temperature[6]. The specific fracture toughness (fracture toughness,  $K_{IC}$ , per unit weight) of titanium alloys is superior to most of the structural materials. Table 2.3 and 2.4 compares some mechanical properties of Ti and its alloys with some other metals and alloys.

Titanium and its alloys are resistant to corrosion by most reactive substances, their resistance is better than that of stainless steel. It is attacked by hydrofluoric acid and acids containing fluorides, at room temperature[8], but resistant to almost all other corroding media. They also show excellent stress corrosion behaviour except in red fuming nitric acid[3]. They show excellent atmospheric and marine corrosion resistance. Cavitation resistance of Ti-6Al-4V in water is superior to stainless steel[9].

Titanium reacts with oxygen, nitrogen, hydrogen and most gaseous compounds like CO, CO<sub>2</sub>, H<sub>2</sub>O, NH<sub>3</sub> etc. at elevated temperature. Nitrogen is a strong  $\alpha$  stabilizer and not only forms nitride scale, also goes into the lattice. The reaction is irreversible, though kinetics of this reaction is very slow[16]. Oxygen is also a strong  $\alpha$  stabilizer, which forms oxide scales and goes into the solid solution, increasing the  $\alpha/\beta$  transition temperature and increasing the hardness of the oxygen enriched zone near the surface. This reaction is also irreversible. In the oxidation of titanium, the following reaction may be expected to occur at metal/oxygen interface[17].



Hydrogen is one of the most dangerous contaminants in Ti, though its reaction with Ti being reversible, vacuum annealing can cause dehydrogenation. The effects of hydrogen are :

**Table 2.3 : Comparative Properties of Some Metals**

Metal	UTS ( $10^3$ psi)	Yield ( $10^3$ psi)	Elong. (%)	R.A. (%)	Modulus Elastic. ( $10^6$ psi)	Modulus Rigid. ( $10^6$ psi)	BHN <sup>*</sup>	Charpy Impact (ft lb)
Al	9	3	60	70	10	3.87	15	19
Cu	37	14	15	52	16	6	47	16
Fe (pure)	40	20	40	80	29.7	10	90	—
Mg	27	10	15	50	6.25	2.4	37	—
Fe (ingot)	44.3	22.7	47	75	29.1	11.6	120	19
Ti (pure)	35	20	55	80	15	5	85	100
Ti (ingot)	75	55	25	50	16	5	180	30

\* Ferrous and titanium metals measured with 3000-kg load and a 10-mm ball, other metal measured with a 500-kg load and a 10-mm ball.

**Table 2.4 : Comparative Properties of Some Alloys**

Metal	UTS ( $10^3$ psi)	Yield ( $10^3$ psi)	Elong. (%)	R.A. (%)	Modulus Elastic. ( $10^6$ psi)	Modulus Rigid. ( $10^6$ psi)	BHN *	Charpy Impact (ft lb)
Ti (3Al-5Cr)	150	135	18	45	17	6	290	24
Steel (4340)	145	135	20	58	28.7	12	285	52
Stainless Steel (18-8)	89.4	28	61	75	29	—	140	—
Al (4S-O)	26	10	25	50	10	3.9	45	—
Al (75S-T6)	82	72	11	40	10.4	3.9	150	—
Mg (AZ 31)	37	22	21	25	6.5	2.4	56	3.2

\* Ferrous and titanium metals measured with 3000-kg load and a 10-mm ball, other metal measured with a 500-kg load and a 10-mm ball.

- a) Causing strain aging
- b) increasing notch sensitivity, specially below 0°C
- c) causing strain rate sensitivity, tensile strength and elongation to be lower at lower strain rates
- d) stabilizing  $\beta$  phase
- e) forming hydrides and causing embrittlement.

Ti alloys containing hydrogen above 150 ppm become brittle under stress at high temperature[8].

In air titanium is most readily attacked by water vapour, which is dissociated by titanium at high temperature into hydrogen and oxygen. Hence, care should be taken starting from melting to heat treatment of titanium and its alloys.

All the customary techniques used in joining metals have been successfully applied to titanium and its alloys, except for soft soldering. But care should be taken during joining to prevent  $\alpha \rightarrow \beta$  transformation to get a metallurgically sound structure.

Most of the dual phase titanium alloys of the family represented by Ti-6Al-4V can show a high value of strain rate sensitivity of stress approaching to unity which puts them among the most desirable candidate materials for isothermal forging and superplastic forming-diffusion bonding.

### **2.1.2 Important Uses of Ti and Its Alloys**

Interest in the properties of Ti and its alloys began to accelerate during the late 1940s and early 1950s as their potential as high temperature, high strength/weight material with aeronautical applications becoming more and more widely recognized. Ti and its alloys have, by now, found widespread use in the aerospace industry and in the chemical and related industries.

As a consequence of their high strength/weight ratio, resistance to corrosion and low thermal conductivity, Ti alloys are likely candidate for low temperature; structural applications. Due to the heat resistant property, alloys like Ti-6242 are being used at temperature up to 480-510°C. Ti-11, having heat resistance, surface stability and improved creep strength, is intended for use in aircraft gas turbine engines[4]. Ti-alloy forgings for landing gear components, compressor blades and discs; sheets for turbine liners, baffles, skin assembly, tail cones etc. are prescribed by the Bureau of Aeronautics, USA[6]. Ti-6Al-4V and other Ti-alloys are used in different parts in Boeing 777 due to advantages in weight savings, volume constraints, operating temperature, electrical compatibility with carbon-free-reinforced polymer (CFRP) composites and corrosion resistance[10]. It is also used in racing car springs. Good hot strength and low thermal conductivity enhances the use of Ti-alloys in firewalls, nacelles and compressor blades in supersonic aircrafts[6,8]. High static and fatigue strength, reasonable ductility, resistance to corrosion and pitting and better fatigue property of Ti-6Al-4V replaces stainless steel in producing steam turbine blading[11]. It also replaces monel in producing ball valves. It is also used in manufacturing equipments for subsurface geological exploration. Ti-6Al-4V is reported to be used in producing different parts like wheel hubs, centrifuges etc in Airbus A320 and Airbus A300/A310[12]. High-strength Ti-6Al-4V alloy is used in producing six different parts in new turbo-fan engines like V2500, by superplastic forming[13]. Figure 2.1[12] shows aircraft applications of titanium.

Titanium is currently used widely in under water structures due to its unique combination of high strength to weight ratio, excellent corrosion resistance, good fabricability, weldability and shock resistance characteristics[14]. Titanium is used in flash suppressors for artillery, field gun, anti-aircraft gun and airborne missiles in military applications[6] and also in some parts in Navy submarine ships. It is used in mortar base plates, guided missiles, rockets etc. Titanium armour plates replacing steel gives up to 44 % weight saving with equal resistance to ballistic attack[29].

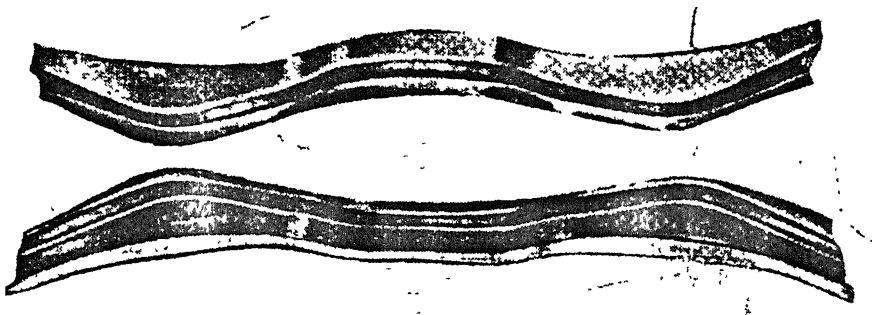


**Figure 2.1(a) Titanium Aircraft Channel Sections**

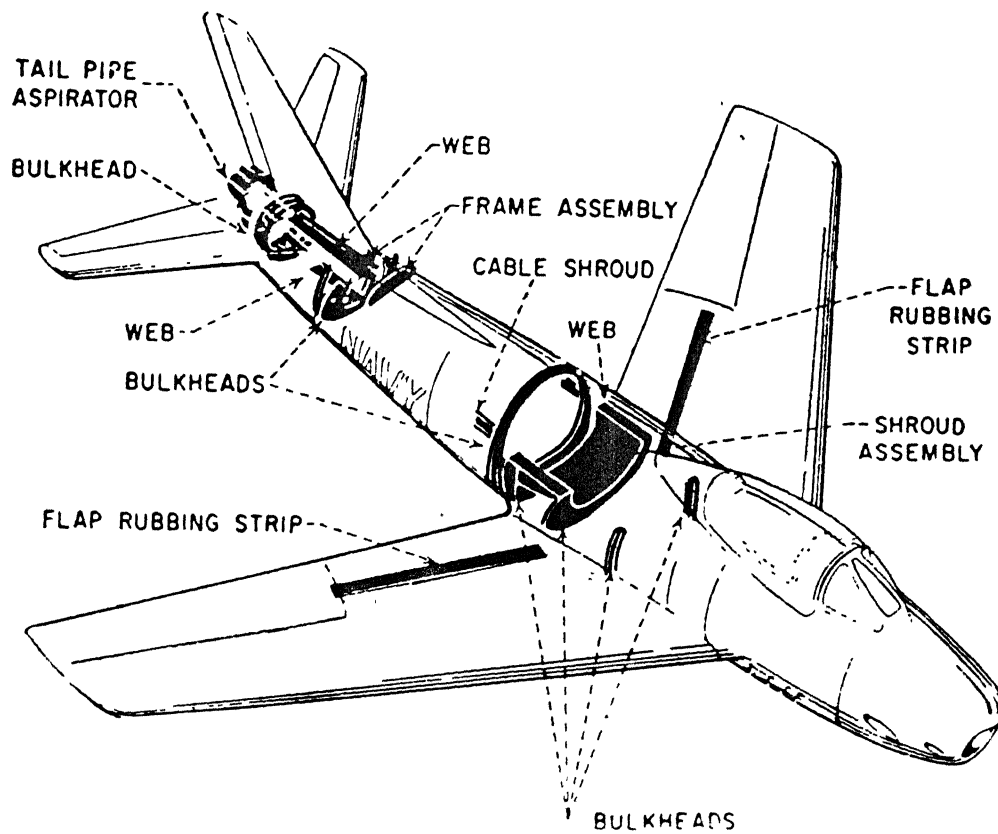


**Figure 2.1(b) Major Fabricated Titanium Parts of The North American FJ-2 Jet Fighter**

Decreased fuel consumption, better fatigue strength is obtained in piston rods of titanium in automobile industries, specially in Formula I racing cars[29,30]. Titanium's high electrical resistance and nonmagnetic property is utilized as cable armour material in electrical industries[29].

Seamless titanium tubings are developed for possible use in aircraft, hydraulic systems of aircraft, tennis racket, bicycle frame and wheel chairs[31].

Good strength, resistance to pitting and crevice corrosion even in acidified hot sea water, resistance to stress corrosion cracking and capability of resisting any local destruction of passive oxide films makes Ti-6Al-4V a potential candidate for offshore petroleum hostile environment exploitations[32].

Due to excellent corrosion resistance displayed by titanium and its alloys, they find extensive applications in heat exchangers, reactor vessels in desalination plants, condenser tubings and several other components in chemical, marine, petrochemical, offshore and power generation industries. Chemical process related industries use about 25 % of the current titanium production and this usage has been growing now at about 12 % per year. Its non-toxicity, excellent corrosion resistance under body condition and biocompatibility is made use of in prosthetic devices such as cages and balls of heart-valves, housings of pacemakers and leg bone replacements or splints[15,33].

Though strength efficiency is the prime consideration for structural applications and in aerospace industries, which have majority of demand for titanium alloys, other requirements like fatigue life, fracture toughness, creep, microstructural stability at high temperature may also have to be met depending on the nature of application. To meet these multifarious requirements, different alloys have been developed.

### 2.1.3 Classification of Ti-Alloys

Pure titanium has two allotropic modifications,  $\alpha$ -titanium and  $\beta$ -titanium, as mentioned earlier. The allotropic transformation temperature is 882.5°C (1155.5 K)[19,20]. Table 2.5 lists lattice parameters of the two phases[1,2,21]

**Table 2.5 : Lattice Parameter(mean) Values of  $\alpha$ - and  $\beta$ -Titanium**

	A	c	c/a
$\alpha$	$2.9503 \pm 0.0004 \text{ \AA}$	$4.6831 \pm 0.0004 \text{ \AA}$	$1.5873 \pm 0.0004$
$\beta$	$3.283 \pm 0.003 \text{ \AA}$		

Alloy additions to titanium except tin and zirconium tend to stabilize either the  $\alpha$  or the  $\beta$  phase. Sn and Zr are interesting alloying elements in that they have extensive solid solubility in both the  $\alpha$  and  $\beta$  phases. They only slow down reaction kinetics and are useful strengthening agents.

Elements which when dissolved in Ti produce little change in the transformation temperature or cause it to increase are known as “ $\alpha$  stabilizers”. They are simple metals or interstitial elements, eg., Al, C, N, O etc. Rosenburg[22] has suggested an expression for the aluminium equivalent Al\* of the alloy :

$$\text{Al}^* = [\text{Al}] + [\text{Zr}]/6 + [\text{Sn}]/3 + 10[\text{O} + \text{C} + \text{N}] \quad \text{wt \%}$$

Alloying additions which decrease the phase-transformation temperature are referred to as “ $\beta$  stabilizers”. They are generally transition metals or noble metals, eg., Mo, V, Ni, Mn, Cu, Cr, Fe, H, Si etc.

Molchanova[19] has suggested an expression for Mo equivalent Mo\* of the alloy :

$$\text{Mo}^* = [\text{Mo}] + [\text{Ta}]/5 + [\text{Nb}]/3.6 + [\text{W}]/2.5 + [\text{V}]/1.5 + 1.25[\text{Cr}] + 1.25[\text{Ni}] + 1.7[\text{Mn}] + 1.7[\text{Co}] + 2.5[\text{Fe}]$$

$\beta$ -stabilized systems can be of two types :  $\beta$  isomorphous and  $\beta$  eutectoid, depending upon whether decomposition of  $\beta$  to  $\alpha$  plus eutectoid products occur under equilibrium condition. Figure 2.2 to 2.4 shows some typical phase diagrams of  $\alpha$  and  $\beta$  stabilized systems[23]. Figure 2.5 shows a simple classification scheme for binary Ti-alloy phase diagrams[4]. The type and concentration of alloying elements determine the equilibrium condition, which forms the basis for classification of titanium alloys. Depending on the type of alloying additions made, technical alloys of Ti are classified as “ $\alpha$ ”, “ $\alpha+\beta$ ” and “ $\beta$ ”. Table 2.6 lists some examples of commercial Ti-alloys with their classes[4].

#### 2.1.3.1 $\alpha$ -alloys

These alloys contain no or only  $\alpha$  stabilizers as alloying additions and at ordinary temperature these have hcp  $\alpha$  phase only. Due to single phase nature of these alloys, no microstructural strengthening can be achieved in them. Solid solution strengthening [22] of them is also limited because an aluminium equivalent of more than 9.0 promotes the formation of the brittle phase  $\alpha_2$ . These alloys, according to Wood[24], are characterized by satisfactory strength, toughness, creep resistance and weldability. Furthermore, the absence of a ductile-brittle transformation, a property of the bcc structure, renders  $\alpha$  alloys suitable for cryogenic applications[25]. These alloys have poor workability. Examples are unalloyed Ti and Ti-5Al-2.5Sn.

#### 2.1.3.2 ( $\alpha + \beta$ ) alloys

These alloys have a mixture of  $\alpha$  and  $\beta$  phase at room temperature and in practice, they usually contain mixtures of both  $\alpha$  and  $\beta$  stabilizers. The simplest of such alloys and undoubtedly the most important is

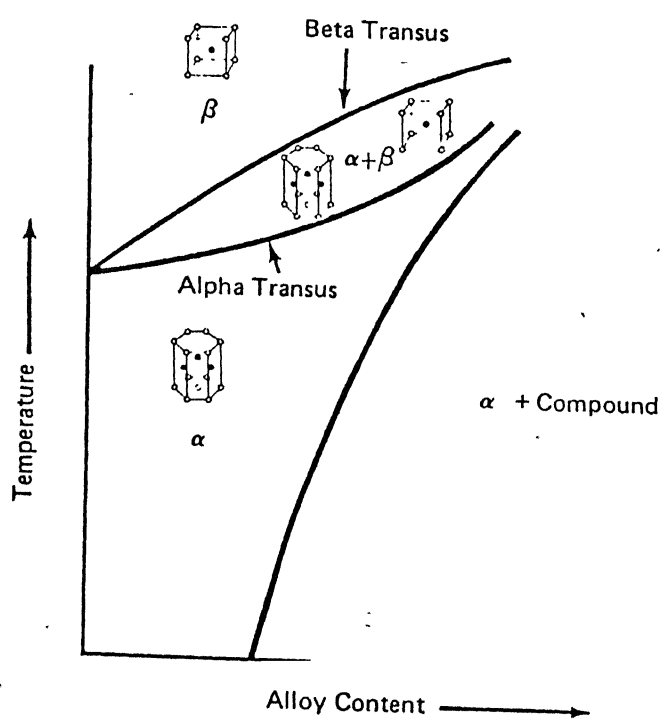
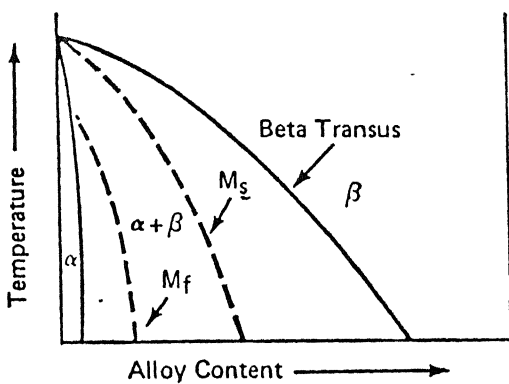
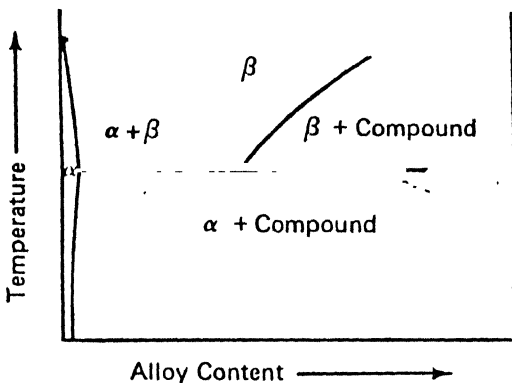


Figure 2.2  $\alpha$ -Stabilized S<sub>v</sub> stem



**Figure 2.3  $\beta$ -Isomorphous System**



**Figure 2.4  $\beta$ -Eutectoid System**

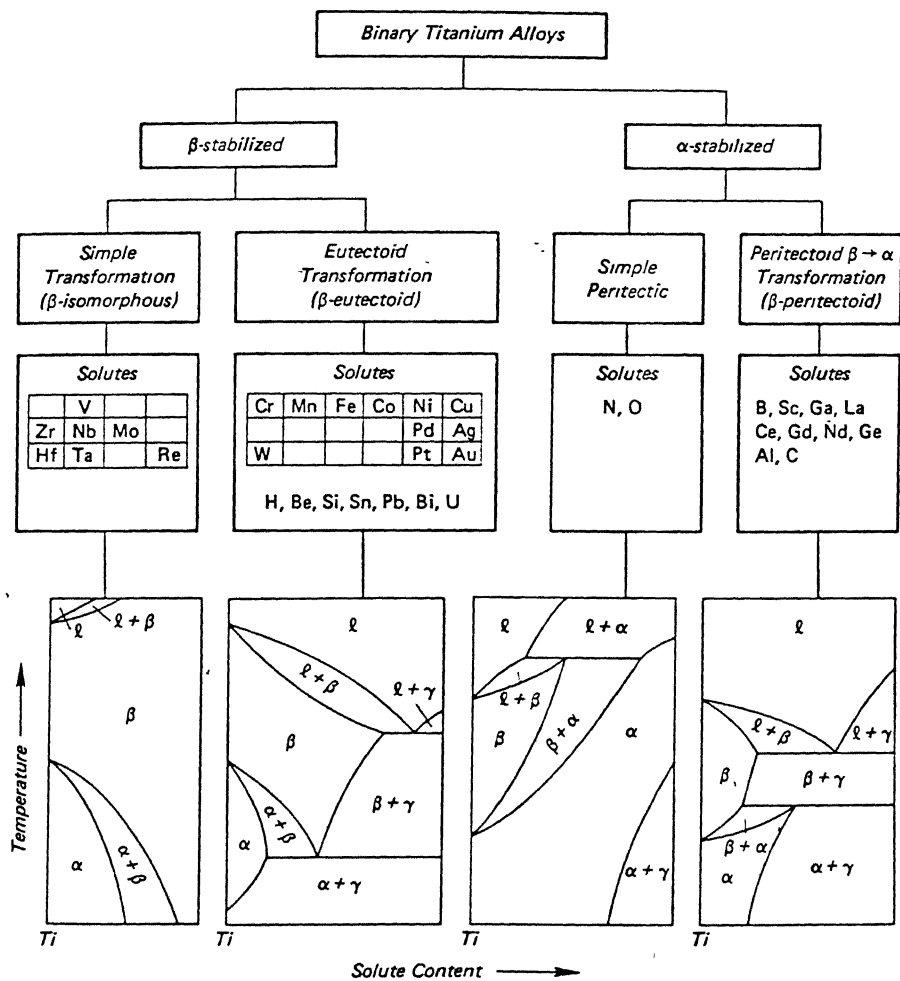


**Figure 2.5 Classification Scheme for Binary Ti-Alloy Phase Diagrams**

$\alpha$  and  $\beta$  are solid solution alloys,  $\gamma$  represents an intermetallic compound.

**Table 2.6 : Structural Classes Of Commercial Titanium-base Alloys**

<b>Alloy</b>	<b>Classification</b>
Ti-5Al-2.5Sn	$\alpha$
Ti-8Al-1Mo-1V Ti-6Al-2Sn-4Zr-2Mo Ti-6Al-4V Ti-6Al-2Sn-6V Ti-3Al-2.5V	$\alpha+\beta$
Ti-6Al-2Sn-4Zr-4Mo Ti-5Al-2Sn-2Zr-4Cr-4Mo Ti-3Al-10V-2Fe	
Ti-13V-11Cr-3Al Ti-15V-3Cr-3Al-3Sn Ti-4Mo-8V-6Cr-4Zr-3Al Ti-8Mo-8V-2Fe-3Al Tu-11.5Mo-6Zr-4.5Sn	$\beta$

Ti-6Al-4V, which is difficult to form even in the annealed condition[25]. But  $(\alpha+\beta)$  alloys generally exhibit good fabricability, high room temperature strength and moderate elevated temperature strength. Alloys containing more than 20 %  $\beta$  phase at room temperature are not weldable. The properties of  $(\alpha+\beta)$  alloys can be controlled by heat treatment, which is used to adjust the microstructural and precipitational states of the  $\beta$  component. Figure 2.6 and 2.7 show vertical and horizontal sections of Ti-Al-V system, respectively[4].

### 2.1.3.3 $\beta$ alloys

Generally transition metal solutes are stabilizers of the bcc,  $\beta$  phase and hence, the  $\beta$  alloys contain one or more of them. Typical examples of  $\beta$  alloys, which have  $\beta$  phase at room temperature, are Ti-15Mo-5Zr and Ti-15Mo-5Zr-3Al. The  $\beta$  alloys have high density, poor ductility, poor oxidation resistance and hence, of less commercial importance. They are extremely formable[24], prone to ductile-brittle transformation[26] and unsuitable for low temperature applications[25].

Since the present investigation is concerned with the titanium alloy, Ti-6Al-4V, an  $(\alpha+\beta)$  alloy, the discussion henceforth will only be confined to the family of  $(\alpha+\beta)$  alloys.

### 2.1.4 Importance of $(\alpha+\beta)$ Alloys

As a class,  $(\alpha+\beta)$  alloys account for more than 75 % of all titanium used[27] and Ti-6Al-4V accounted for 56 % of the total output in 1972[24].  $(\alpha+\beta)$  alloys have been designed to combine the better part of properties of both  $\alpha$  and  $\beta$  alloys. Because of its dual phase nature, a wide range of microstructural features, varying in size and morphology of both the constituent phases, can be obtained in them. Since the rule of mixture is not followed by them[28], a considerable amount of microstructural strengthening can be imparted to them. Thus, for the same alloy, it is possible to have a wide range of property levels by altering the morphology and size of its

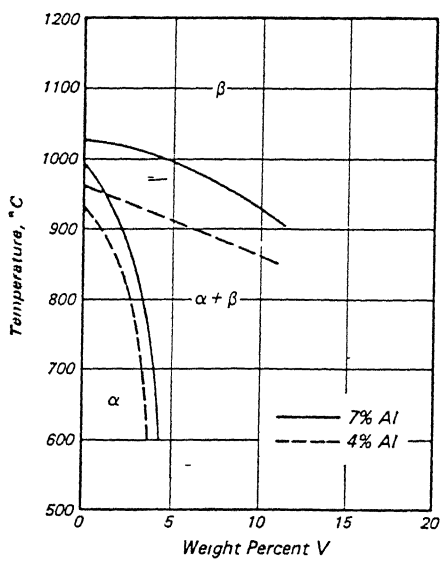


**Figure 2.6(a) Vertical section of The Ti-Al-V Vs T Equilibrium Phase Prism at 4 and 7 Wt% Al**

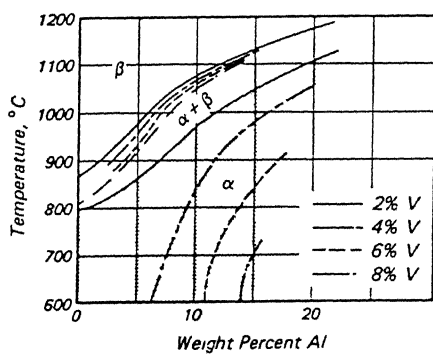


**Figure 2.6(b) Vertical section of The Ti-Al-V Vs T Equilibrium Phase Prism at 2,4,6 and 8 Wt% V**

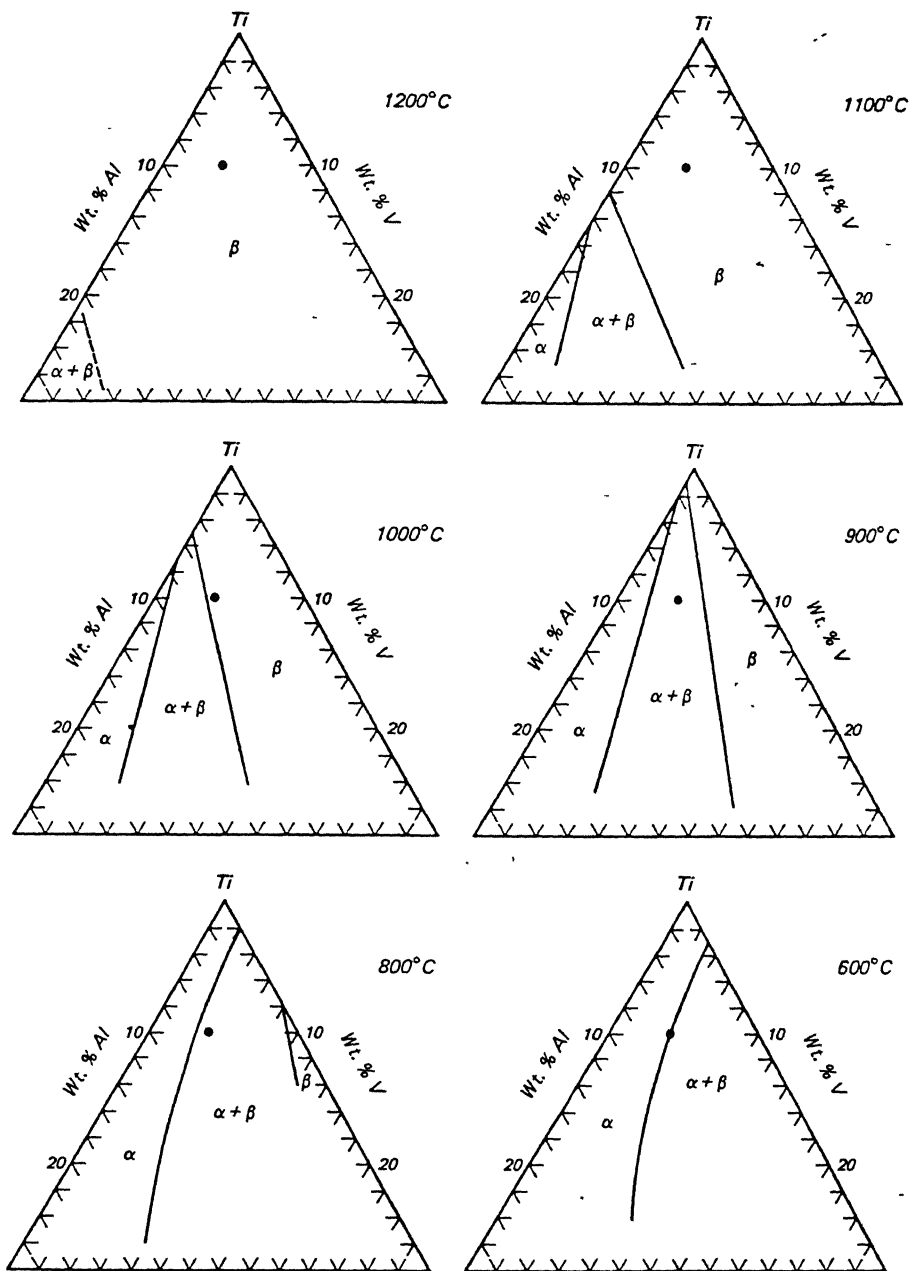


**Figure 2.7 Isothermal (Horizontal) Sections of The Ti-Al-V Vs T Equilibrium Phase Prism at The Temperatures Indicated**

The solid circle represents the alloy Ti-6Al-4V.

microstructural constituents. Yield strength, tensile strength and ductility are not influenced much by a change in microstructure, whereas fracture toughness, fatigue strength, fatigue crack propagation rate, creep resistance, creep rupture strength and above all, the superplastic behaviour, with which the present investigation is concerned, vary drastically with the microstructural states of the material.

### **2.1.5 Microstructural Features of Ti-Alloys [42,43,44]**

Microstructures are characterized by nature of phases present, their shape, size, morphology which, in turn, are functions of heat treatment and working schedule. Before going to the details of microstructure and property control, hence, it is necessary to have a look at common microstructural features in Ti-alloys.

a) Primary  $\alpha$  ( $\alpha_p$ ) :

It refers to the  $\alpha$  phase in crystallographic structure which is retained from the last high temperature ( $\alpha+\beta$ ) working or heat treatment. The morphology of  $\alpha_p$  is influenced by the prior thermo-mechanical treatment and can be lamellar, equiaxed or mixed.

b) Secondary  $\alpha$  or transformed  $\beta$  :

A local or continuous structure, comprised of decomposition products arising by nucleation and growth during cooling through the subtransus region. Primary and regrowth  $\alpha$  may be present, it typically consists of  $\alpha$  platelets which may or may not be separated by  $\beta$  phase.

c) Blocky  $\alpha$  :

$\alpha$  phase, which is considerably larger and more polygonal than the  $\alpha_p$ . It may arise from long exposure high in the ( $\alpha+\beta$ ) field or by slow cooling through the  $\beta$  transus.

d) Elongated  $\alpha$ :

A fibrous type of  $\alpha$  structure brought about by unidirectional metal working. It may be enhanced by the prior presence of blocky and/or grain boundary  $\alpha$ .

e) Widmanstatten structure:

A structure of  $\alpha$  platelets or  $\alpha$  and  $\beta$  platelets resulting from cooling from a temperature above the  $\beta$  transus. The platelets often produce a basket-weave appearance.

f) Grain boundary  $\alpha$ :

Primary  $\alpha$  outlining prior  $\beta$  grain boundaries. It occurs by slow cooling from the  $\beta$  field into ( $\alpha+\beta$ ) field and may be continuous, unless broken up by subsequent work.

g) Acicular  $\alpha$ :

This is a product of nucleation and growth from  $\beta$  to the lower temperature allotrope  $\alpha$ . It may have a needle-like appearance.

h) Alpha case:

The oxygen, nitrogen or carbon enriched alpha stabilized surface, which results from elevated temperature exposure.

i) Hexagonal martensite ( $\alpha'$ ):

A supersaturated, non-equilibrium hexagonal phase formed by a diffusionless transformation of the  $\beta$  phase.

j) Orthorhombic martensite ( $\alpha''$ ):

A supersaturated, non-equilibrium orthorhombic phase formed either by transformation of metastable  $\beta$  during quenching ( $M_o$ , the maximum temperature at which  $\alpha''$  begins to form on cooling) or by stress-induced transformation of retained metastable  $\beta$ .

k) FCC and FCO martensites :

Face-centered cubic and face-centered orthogonal martensites found during TEM analysis of some binary Ti alloys, produced probably as a result of hydrogen contamination.

l)  $\alpha_2$  stucture :

A structure consisting of the ordered  $\alpha$  phase,  $Ti_3Al$ .

m) Equilibrium  $\beta$  :

Some equilibrium  $\beta$  phase present at room temperature due to partitioning of  $\beta$  stabilizers, in  $(\alpha+\beta)$  and  $\beta$  alloys.

n) Beta flecks :

Regions enriched in a  $\beta$ -stabilized element due to segregation during ingot solidification, present in, generally,  $\beta$  alloys having high amount of  $\beta$ -stabilizer.

o) Metastable  $\beta$  :

$\beta$  phase composition that can be partially or fully transformed to martensites,  $\alpha$  or eutectoid decomposition products with thermal or strain energy activation during subsequent processing or service exposure.

p) Intergranular  $\beta$  :

$\beta$  phase situated between  $\alpha$  grains.

q) Omega phase ( $\omega$ ) :

A non-equilibrium, submicroscopic phase formed either isothermally during aging at about  $475^\circ C$  or athermally during quenching, often thought to be a transition phase during the formation of  $\alpha$  from  $\beta$ .

r) Gamma phase ( $\gamma$ ) :

An ordered structure of Ti-Al compound.

s) Hydride phase :

The phase  $TiH_x$  formed in titanium when the hydrogen content exceeds the solubility limit.

t) Silicides :

In high silicon bearing alloys, Si combines with Ti and other alloying elements to form complex compounds as precipitates known as silicates, eg.,  $Ti_5Si_3$ , Ti-Mo-Si etc.

u) Interface phase :

It is a reaction product that forms at the interface between  $\alpha$  and  $\beta$  phases of alloys like Ti-6Al-4V, probably due to hydrogen absorption. It has both fcc and hcp forms.

Different microstructural standards for  $(\alpha+\beta)$  titanium alloys are given in [42].

## 2.1.6. MICROSTRUCTURE AND PROPERTY CONTROL:

The microstructure of  $(\alpha+\beta)$  titanium alloys strongly depends on both processing and heat-treatments, varying which, a wide range of microstructural varieties are produced and these result in the widest range of properties. It has been observed that the percentage, size and distribution of the  $\alpha$  phase as well as prior and/or recrystallized  $\beta$  grain size play a key role in determining fatigue, fracture toughness and tensile properties. Especially morphology of primary  $\alpha$  phase in  $\alpha+\beta$  titanium alloys is of considerable importance from the point of view of controlling their static and dynamic mechanical properties. The presence of equiaxed primary  $\alpha$  phase in microstructure promotes ductility at low temperatures, fatigue crack initiation resistance and elevated temperature flow characteristics. Similarly, improved fracture toughness, fatigue crack propagation resistance, creep and stress rupture strengths are obtained in microstructure possessing lamellar primary

$\alpha$  phase. A bimodal microstructure with the smallest amount of primary equiaxed  $\alpha$  phase - embeded into a fine lamellar  $\alpha$ - $\beta$  structure - called 'quasilamellar', combines the creep rupture properties and fatigue behaviour almost same as lamellar structure and also high temperature tensile strength and ductility comparable to equiaxed structure. It has been found out by Margolin et.al.[99] that in the microstructure containing equiaxed  $\alpha$  in an aged  $\beta$ -matrix, the mean free path,  $\lambda$ , between  $\alpha$  particles appears to play an important role in determining tensile RA. They observed that voids form at the equiaxed  $\alpha$ -aged  $\beta$ -interfaces at low tensile strains. As the strain is increased, these voids readily grow along the interfaces before they by necessity must grow through the matrix. They proposed that their ease of growth depends upon the spacing of the  $\alpha$ -particles, which act as obstacle to growth. As  $\lambda$  decreases, a growing void encounters more obstacles and growth is impeded. This results in greater strain to fracture and higher attainable ductility. It has also been shown that refinement of the prior  $\beta$  grain-size creates a more tortuous path for fracture, the net result being more difficult void growth and hence higher achievable tensile ductility.

Greenfield and Margolin [99] have shown the effect of prior  $\beta$ -grain size and grain-boundary  $\alpha$  thickness on fracture toughness of accicular  $\alpha$  morphologies. Fracture toughness increases in both equiaxed and accicular  $\alpha$ -structure as the prior  $\beta$  grain size decreases, presumably due to more tortuous crack propagation path encountered. High fracture toughness is also a result of shape characteristics of the accicular  $\alpha$  phase.

Work by Ho and Margolin [99] shows that fatigue crack initiation at low stress occurs more readily in structures with coarser  $\alpha$ , both in accicular and equiaxed. Again in strain controlled low cycle fatigue tests it has been found that number of cycles to pin-point crack initially was significantly lower with an accicular structure as compared to an equiaxed microstructure [99-101].

### **2.1.6.1. EFFECT OF HEAT-TREATMENT:**

The microstructural changes that can be brought about through thermal treatments are numerous. Generally lamellar microstructures are obtained by only heat treatments without any mechanical working.

When quenched from above  $\beta$ -transus temperature it is difficult to form a fully martensitic structure in Ti-6Al-4V alloy which is leaner in  $\beta$ -stabilizers, since the kinetics of  $\alpha$ -phase nucleation and growth reaction are more rapid. Thus in thick sections of Ti-6Al-4V, it is unlikely that fully martensitic structure will be produced during quenching. As a result of nucleation and growth of  $\alpha$ -phase, it is frequently present at preferred nucleation sites such as prior  $\beta$ -phase grain boundaries.

Lamellar microstructures require only thermal treatments. The martensitic structure ( $\alpha'$ ) established by water quenching from above the  $\beta$ -transus is very unstable. Short annealing in the  $\alpha+\beta$  phase field are sufficient to precipitate the  $\beta$  phase at boundaries of martensitic needles which results in a fine lamellar  $\alpha+\beta$  microstructure. Remarkable coarsening of the lamella takes place only at high annealing temperatures in the two phase field near the phase boundary. This coarsening process demands a relatively long time due to long diffusion paths. Coarse lamellar structures are achieved by slow cooling from above the  $\beta$ -transus into the two phase field. In this case,  $\alpha$  phase precipitates from the  $\beta$  phase. Length of the lamella is restricted by the former  $\beta$  grain size, whereas the width is diffusion controlled and can be coarsened by decreasing the cooling rate. Duplex heat treatment mode has also been developed to synthesize a microstructure with the high toughness characteristics of accicular structure and high ductility of equiaxed morphologies. A volume fraction of 10 - 25 % globular or nearly equiaxed  $\alpha$  is developed by processing or heat-treating high in the two phase region. Subsequent thermal treatment at a lower solution temperature results in the formation of accicular  $\alpha$  phase termed secondary  $\alpha$ . The final step involves aging the remaining  $\beta$  to the desired strength level [23,96,98,99].

### **2.1.6.2 EFFECT OF WORKING:**

Microstructural changes brought about through processing are numerous and varied and are dependant on alloy content and working history. If working is initiated and completed at temperatures in the  $\beta$ -field, the resulting microstructure will be entirely transformed. The transformation product will consist of acicular or plate-like  $\alpha$ , depending on section size and cooling rate. The structure will also show evidence of coarse equiaxed prior  $\beta$  grains. Structures developed in this manner are not changed significantly through the use of subsequent thermal treatments. Fine acicular structure can be coarsened somewhat by heating in the  $(\alpha+\beta)$  field, but the coarse prior  $\beta$  structure can be altered only by further working at a temperature below the  $\beta$  transus.

If the work is initiated in the  $\beta$  field and finished in the  $(\alpha+\beta)$  field, the resulting microstructure will be predominantly transformed  $\beta$ . The prior  $\beta$  grain boundaries will be distorted and partially broken up due to lower finishing temperature. Work carried out entirely in the  $(\alpha+\beta)$  field generally yields a fine grain structure with little or no evidence of transformation product.

When total strain is kept same and strain ratios in  $(\alpha+\beta)$  and  $\beta$  phase field are varied, material deformed more in  $\beta$  phase field have been observed to have microstructure with coarser  $\alpha$  lamella in comparison to those observed in samples given a higher deformation in the  $(\alpha+\beta)$  phase field [23,100].

### **2.1.6.3. EFFECT OF THERMO-MECHANICAL TREATMENT:**

Thermo-mechanical processing, both in single phase  $\beta$  as well as two phase  $(\alpha+\beta)$  field, is the most effective method of modifying and controlling the morphology of the primary  $\alpha$ -phase. While the lamellar  $\alpha$ -morphology arises during slow cooling of the alloy through the  $(\alpha+\beta)$  two phase field, equiaxed morphology generally results from the recrystallization/ mill annealing of the structure which is obtained by imparting sufficient deformation in the alloy

below its  $\beta$ -transus temperature. Thermo-mechanical processing is strongly influenced by the factors,

- 1) the degree of prior deformation in the  $\beta$ -phase field.
- 2) working temperature and,
- 3) the mode of deformation.

The first two influence the morphology of primary  $\alpha$  as well as the texture, and the third one primarily influence the texture which, in turn, affects the  $\alpha$ -phase morphology during recrystallization annealing.

When the material is warm-worked below the recrystallization temperature, equiaxed  $\alpha$ -grains are nucleated at the  $\alpha/\beta$  interface upon subsequent annealing. The rate at which lamellar  $\alpha$  transform to equiaxed  $\alpha$  is a function of annealing temperature, time and the amount of work  $\alpha$ -phase has received.

It has been observed that keeping the deformation temperature and annealing procedure constant, the percentage of equiaxed morphology in resulting microstructure depends on the degree of deformation, i.e, with increasing degree of deformation, percentage of equiaxed morphology increases in the microstructure.

Degree of hot deformation, if exceeds a critical value, may also lead to fracturing of deforming  $\alpha$ -lamella and may give rise to primary  $\alpha$ -lamella of smaller aspect ratio. Subsequent break-up of  $\alpha$ -lamella to equiaxed morphology occurs during subsequent recrystallization annealing when  $\beta$ -phase penetrates across the lamellar widths along the sub-boundaries [100].

In alloys which are  $(\alpha+\beta)$  finish worked, air cooled and then solution treated at a temperature lower than the finishing temperature, a low density of smaller elongated  $\alpha$ -phase particles develop in addition to primary  $\alpha$ . This phase often occurs at  $\beta$ -phase grain boundaries. This  $\alpha$ -phase develops as a result

of coarsening unsolutionized Widmanstatten  $\alpha$  during the solution treatment. The resulting microstructure is actually triplex, since it consists of tempered  $\alpha'$ , small elongated  $\alpha$  and much coarser equiaxed or elongated primary  $\alpha$ .

The increasing fineness of equiaxed microstructure with the aging effect resulting from the thermo-mechanical treatment yields an improvement in tensile properties also. This helps in improvement in superplastic behaviour of the material.

In order to combine good creep rupture behaviour with high tensile ductility at room temperature, it is favourable to produce the quasilamellar microstructure by thermo-mechanical treatment. Because it exhibits the same creep rupture strength as the lamellar one without suffering from extreme drop in tensile ductility related to the complete transformation into the  $\beta$ -phase when exceeding the transus during solution treatment. Also the quasi-lamellar structure possesses good fatigue strength at room temperature which is significantly superior to that of the as-received condition. Even its drop at very high number of cycles is smaller than that of the lamellar or bimodal structure. Anyway the thermo-mechanical treatment has a strong potential to achieve a significant improvement in static and dynamic mechanical properties at room temperature combined with good elevated temperature strength[96,100,101,102].

### **2.1.7 IMPORTANCE OF $\beta$ -PROCESSING:**

Very fine equiaxed structure for Ti-6Al-4V alloys are required to have good superplastic properties. Now, it has been observed that for a given amount of deformation, thin  $\alpha$ -lamella material is more easily converted into fine equiaxed morphology than thick lamella material. The morphology

changes from  $\alpha$ -lamella to lower aspect ratio grains was identified to be a breaking of the  $\alpha$ -lamella essentially by two step process: fraction of low and high angle  $\alpha$ - $\alpha$  boundaries or shear bands across the  $\alpha$ -plates followed by penetration of  $\beta$ -phase to complete the separation. This break-up takes place during hot deformation and subsequent annealing. The separation by  $\beta$ -phase penetration is easier in thin  $\alpha$ -lamella. In thick lamella structure  $\beta$ -phase penetration is incomplete leading to aggregates of needle-like structure. When the plates are thinner and finer they break-up to form fine grains of equiaxed  $\alpha$ -phase. Now, these plates are formed from martensitic needles, when they are heated in the two phase  $\alpha$ - $\beta$  region. So, to get finer equiaxed grains, the needles also are required to be finer. When the material is solutionized above  $\beta$ -transus and water quenched, the martensitic needles are obtained in the quenched microstructure. So, if some deformation is given in the  $\beta$ -phase field before quenching, the fineness of the martensitic needles in the quenched structure increases. Thus,  $\beta$ -processing helps in getting the finer equiaxed structure with very good superplastic behaviour. There is another advantage of  $\beta$ -processing also. When the material is only solutionized above  $\beta$ -trasus and water quenched from there, coarser martensitic needles are obtained. When these are taken in  $\alpha$ - $\beta$  phase field for giving thermo-mechanical treatment, those martensitic needles transform into  $\alpha$ -plates and with increase in temperature the  $\alpha$ -plates become coarser. So, to get fine structure the hot deformation is required to be given in the lower temperature range in the  $\alpha$ - $\beta$  phase field. But in this lower temperature range it is difficult to give heavy deformation as the resistance to plastic flow is higher. And so it is difficult to get fine equiaxed microstructure. But, when the material is  $\beta$ -worked, finer matensitic needles are obtained through water-quenching, which, on heating in the  $\alpha$ - $\beta$  phase field yields finer  $\alpha$ -plates. So, this structure can be given thermo-mechanical treatment at the higher range of temperature in the  $\alpha$ - $\beta$  phase field without hampering the fineness of the equiaxed structure. And also heavy amount of deformation can be given as

resistance to plastic-flow is less at higher range of temperature. So, to establish a fine equiaxed microstructure, working in  $\beta$ -phase field is quite useful[96,102].

## 2.2 Texture in ( $\alpha+\beta$ ) Ti-Alloys

Ti and its alloys show texture which produce pronounced anisotropy in mechanical properties due to lower crystallographic symmetry of hcp  $\alpha$  Ti. By proper control of the variables, texture, as a measure of strengthening can be utilized to fabricate components having higher strength along a particular direction.

The main feature of cold-rolled texture of pure Ti is that the [1010] direction is parallel to the rolling direction and (0002) or basal poles are concentrated in regions  $\pm 30^\circ$  to  $\pm 40^\circ$  in the transverse direction away from the sheet normal[3,45]. Such a texture is supposed to be produced from a competition between {0001}<1120> slip and {1122} twinning[4]. Inagaki[46] proposed a three dimensional mechanism of development of cold rolling texture. Below 30 % reduction, initial textures are weakened by twinning and slip rotations, between 30 and 50 % reductions{0001}<0110> texture is developed mainly through slip rotations and above 50 % reductions {2115}<0110> orientation is developed which is stable end orientation of cold-rolling texture of Ti. It is observed that annealing at low temperatures( $\sim 540^\circ\text{C}$ ) results in the sharpening of the cold-rolled texture, though true recrystallization does not take place at that temperature[3].

Textures observed in titanium, hot rolled at temperatures below  $800^\circ\text{C}$  are essentially same as the cold rolling texture, {2115}<010>. Hot rolling between 800 and  $850^\circ\text{C}$  enhances the development of {2110}<0110> and {2118}<8443>, formed by the recrystallization which occurs during and after hot rolling. Hot rolling above  $880^\circ\text{C}$  results in the formation of a strong transformation texture {2110}<0110>, derived from the {100}<011> of the bcc  $\beta$  phase rolling texture via Burgers' orientation relationship[47].

In the Ti-alloy specimens, hot rolled at temperature above the  $\beta$  transus, transformation textures inherited from the rolling textures of  $\beta$  phase are observed, main orientations being  $(\bar{1}010)[0001]$  and  $(\bar{2}110)[0\bar{1}10]$ . These are much stronger in  $(\alpha+\beta)$  alloys. On hot rolling, at temperatures below the  $\beta$  transus, but above the recrystallization temperature of the  $\alpha$  phase, weak recrystallization textures alongwith transformation textures inherited from rolling textures of  $\beta$  are observed, main orientation being  $(\bar{2}110)[0\bar{1}10]$ . If rolling is done below the recrystallization temperature of  $\alpha$  phase, rolling textures of  $\alpha$  phase,  $(\bar{2}111)[0\bar{1}10]$  as a main component, are observed, which are much stronger in  $(\alpha+\beta)$  alloys[48,49].

The strong prismatic texture,{1120}<1100>, present in hot rolled Ti-6Al-4V systems, is associated with high anisotropy of the strength of the sheets. To obtain isotropic properties, a deformation texture of basal or near basal type must be created. Such a basal plane texture would show texture strengthening and very high bi-axial strengths. One way of achieving this is round rolling(with 45° rotation after every pass) and cross rolling(with 90° rotation after every pass). Temperature range of such rollings is 811 to 1089 K for Ti-6Al-4V[50,51,52]. For a prismatic texture to be preserved in the metals, recrystallization annealing should be done at temperatures below the polymorphic transformation point[52]. Figure 2.8 shows the main textural components observed in Ti and its alloys.

There has been considerable interest recently in the use of textured titanium alloy sheet for pressure vessel applications due to the large amount of bi-axial strengthening achieved when the through-thickness strain is minimized by the sheet texture. Ideal texture of this application is found to be (0002) parallel to sheet normal[53]. Different factors that affect texture development are :

- 1) starting microstructure[49],
- 2) temperature of deformation[48],
- 3) heat treatment[48],

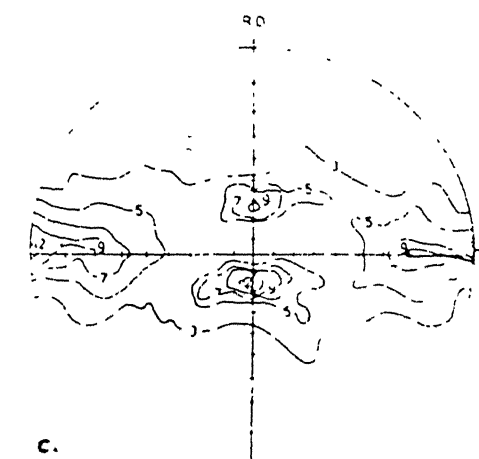
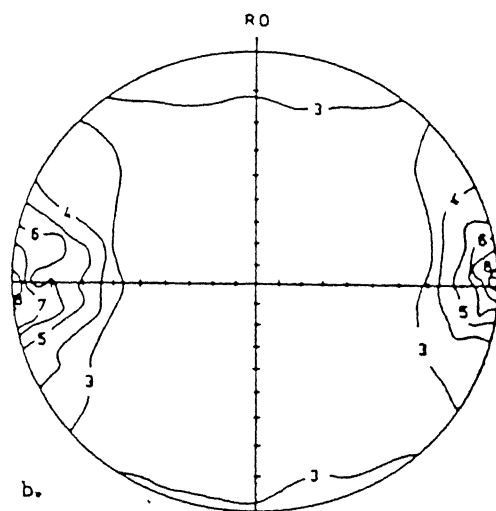
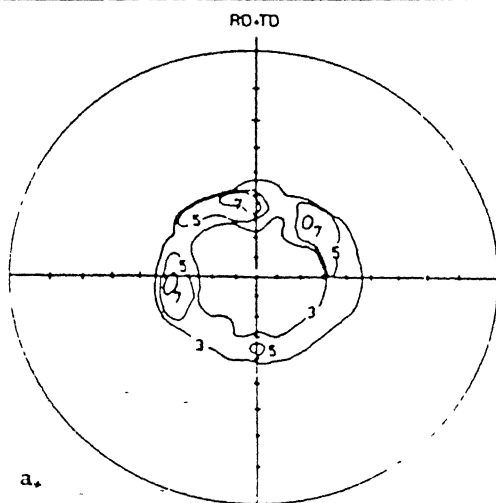


**Figure 2.8 Textures in ( $\alpha+\beta$ ) Titanium Alloys**

(a) Basal Texture

(b) Transverse Texture

(c) Mixed (Basal+Transverse) Texture

- 4) cooling rate[48],
- 5) initial texture[46],
- 6) rolling direction[50],
- 7) degree of deformation[54],
- 8) thickness of the specimen[51],
- 9) annealing texture[52],
- 10) alloy composition[48].

### **2.3 Deformation Characteristics of Ti and Its Alloys**

Pure titanium deforms at room temperature both by slip and by twinning. The greater part of the slip observed occurs on the system  $\{10\bar{1}0\}[11\bar{2}0]$ . Slip in the  $\{10\bar{1}1\}[11\bar{2}0]$  system also occurs, but it is less important and occurred in coarse grained specimens of commercial titanium, only when all three  $\{10\bar{1}0\}$  systems are operative[35]. Slip on the basal plane in the  $[11\bar{2}0]$  direction has been reported for the single crystals of commercially pure titanium by Churchman[36], but most of the workers failed to find basal plane slip. Churchman[36] found the CRSS for slip on the basal plane to be greater than that for  $\{10\bar{1}1\}$  slip which, in turn, is greater than that for  $\{10\bar{1}0\}$  slip. The critical shear stresses for slipping and twinning processes occurring in titanium ( $C_s$  and  $C_t$ , respectively) are related by the equation[3] :

$$C_{s(0001)} = 1.1 C_{s\{10\bar{1}1\}} = 1.02 C_{s\{10\bar{1}0\}} = C_{t\{10\bar{1}2\}} = C_{t\{11\bar{2}2\}}$$

Twinning occurring in titanium as a result of room temperature deformation takes place on the  $\{10\bar{1}2\}$ ,  $\{11\bar{2}1\}$ ,  $\{11\bar{2}2\}$ ,  $\{11\bar{2}3\}$  and  $\{11\bar{2}4\}$  planes, last two being observed only in single crystal titanium flakes. At liquid nitrogen temperature (-196°C), slip is confined to  $\{10\bar{1}0\}[11\bar{2}0]$  system and greater part of deformation is due to twinning in the same plane as in room

temperature. At higher temperature, eg., at 500°C and 815°C, slip in {1010} planes is the predominant mechanism of slip, though secondary slip of the {1011} type is also present[37,38].

Titanium is reported to have a SFE value of 300 MJm<sup>-2</sup> in the basal planes of the hcp phase, suggesting that it should be characterized as a high SFE metal and hence, dynamic recovery should occur in the  $\alpha$  phase. SFE values of the bcc  $\beta$  phase has not been established. In the alloy Ti-6Al-4V, the influence of Al and V on the SFE values has not been investigated, but the two phase structure, below the transus, appears to modify the hot deformation behaviour, suggesting that differing dynamic restoration mechanisms may be operative. It was observed that the slip in the near- $\alpha$  Ti alloy having a fully martensitic structure is homogeneous in nature. The Widmanstatten  $\alpha$ - $\beta$  structure deforms by planar slip. Slip bands in Widmanstatten  $\alpha$  are not impeded by  $\beta$  films, but the  $\beta$  layers are severely distorted due to deformation[58].At a glance, the deformation characteristics can be summerized as follows[34] :

- ◆ the hot ductility of the ( $\alpha$ + $\beta$ ) alloys is much greater in the  $\beta$  region and decreases fairly rapidly with temperature,
- ◆ the flow stress in the ( $\alpha$ + $\beta$ ) regime is very sensitive to strain rate and temperature,
- ◆ in the  $\beta$  region, the activation energy of 169.962 kJmol<sup>-1</sup> is similar to that for self diffusion; in the ( $\alpha$ + $\beta$ ) region the activation energy is almost three times that in the  $\beta$  region at 521.697 kJmol<sup>-1</sup>, indicating that deformation is more difficult below the transus,
- ◆ the mode of deformation is dynamic recovery in the  $\beta$  region and dynamic recrystallization in the ( $\alpha$ + $\beta$ ) region.

## **2.4 Forming Characteristics of Ti-Alloys**

Titanium and its alloys can be formed in standard machines to tolerances similar to those obtained in the forming of stainless steel.

Commercially pure titanium and the most ductile titanium alloys (like Ti-8Al-1Mo-1V) can be formed cold to a limited extent, but it generally strain hardens the materials resulting into increase in yield and tensile strengths and a straight drop in ductility. Cold forming of other alloys generally results in excessive springback, requires stress relieving between operations and requires more power. In general, springback in forming Ti and its alloys varies directly with the ratio of bend radius to work-metal thickness and inversely with forming temperature. Springback is generally reduced by increasing the forming pressure. Higher ratios of yield strength to tensile strength generally result in greater springback. However, in order to lessen the effect of springback variation on accuracy and to gain the advantages of increased ductility the great majority of formed titanium parts are made by hot forming or by cold preforming followed by hot sizing[39].

Hot forming does not greatly affect the final properties. Forming at temperatures from 595 to 815°C allows the material to slip more readily and simultaneously stress relieves the deformed material. The commercial conventional hot forging operations should be done at rapid deformation rates (using mechanical press) in order to avoid shear bands and cracks in temperature sensitive alloys, like titanium[40]. Titanium metals also tend to creep at elevated temperature and holding under load at high temperature (creep forming) is another alternative to achieve the desired shape without extensive springback.

In all forming operations, titanium and its alloys are susceptible to the Bauschinger Effect, which is most pronounced at room temperature. Increase in the temperature reduces the Bauschinger Effect, subsequent full thermal stress relieving completely removes it[41].

Various methods of forming of  $(\alpha+\beta)$  titanium alloys include[4,39,41] :

1. Isothermal forging,
2. Hot sizing,
3. Press-brake forming,
4. Deep drawing,
5. Power spinning,
6. Rubber-pad forming,
7. Stretch forming,
8. Roll forming,
9. Creep forming,
10. Vacuum forming,
11. Drop hammer forming,
12. Explosive forming,
13. Superplastic forming.

However, of the above mentioned methods, superplastic forming is replacing all other conventional methods, for it offers some unique advantages over other processes, which are discussed in the next section.

## **2.4 Superplasticity**

Prior to 1945 the deformation behaviour of the class of alloys that possessed "viscous properties between those of glass and pitch" was known under different names. The term 'superplasticity' became common after 1945 when a Russian word (pronounced as sverkhplastichnost), introduced by Bochvar and Sviderskya, got so translated.

Superplastic forming has now emerged as a viable manufacturing process over the past decade or so, and is now used to fabricate number of sheet metal components for a range of aerospace systems. More than 200 parts are in production for a number of aircraft and spacecraft vehicles. This process offers unique advantages over the conventional forming operations :

1. Reduced machining,
2. No springback,
3. Uniform metal flow,
4. No resultant residual stresses,
5. No cavitation, in general,
6. Formability of shapes, not possible by any other method.

While the alloy Ti-6Al-4V is quite superplastic as conventionally produced, there are desirable properties of other alloys which form a basis for interest in the superplasticity of those materials as well. A number of titanium alloys have been evaluated for superplastic behaviour and a summary of some of those alloys and their superplastic properties are shown in Table 2.7[62].

#### **2.4.1 What Is Superplasticity**

Superplasticity is the deformation process that produces essentially large neck-free elongation (of many hundreds of percent) in metallic materials deformed in tension[59]. Superplastic materials also show high ductility during torsion, compression and indentation hardness testing. The highest elongation, on uniaxial tension, reported, are 4850 % in a Pb-Sn eutectic alloy[60] and greater than 5500 % for an aluminium bronze[61].

Superplasticity can be induced both in materials possessing a stable, ultra-fine grain size ( $< 10\mu\text{m}$ , generally) at the narrow temperature range of deformation ( $\geq 0.5 T_m$ , where  $T_m$  is the absolute melting point) and in

**Table 2.7 : Superplastic Characteristics of Titanium Alloys**

Alloy	Test Temp.(°C)	Strain Rate( $\text{sec}^{-1}$ )	m	Elongation %
Ti-6Al-4V	840-870	$1.3 \times 10^{-4}$ To $10^{-3}$	0.75	750-1170
Ti-6Al-5V	850	$8 \times 10^{-4}$	0.70	700-1100
Ti-6Al-2Sn-4Zr-2Mo	900	$2 \times 10^{-4}$	0.67	538
Ti-4.5Al-5Mo-1.5Cr	871	$2 \times 10^{-4}$	0.63-0.81	>510
Ti-6Al-4V-2Ni	815	$2 \times 10^{-4}$	0.85	720
Ti-6Al-4V-2Co	815	$2 \times 10^{-4}$	0.53	670
Ti-6Al-4V-2Fe	815	$2 \times 10^{-4}$	0.54	650
Ti-5Al-2.5Sn	1000	$2 \times 10^{-4}$	0.49	420
Ti-15V-3Cr-3Sn-3Al	815	$2 \times 10^{-4}$	0.5	229
Ti-13Cr-11V-3Al	800	—	—	<150
Ti-8Mn	750	—	0.43	150
Ti-15Mo	800	—	0.60	100
C.P. Ti	850	$1.7 \times 10^{-4}$	—	115

those, subjected to special environmental conditions, eg., thermal cycling through a phase change. These two, categories are best described as "structural" and "environmental" superplasticity, respectively. There are two main types of structurally superplastic alloys : pseudo single phase and microduplex. In the former class of materials fine scale distribution of dispersoids are developed to have a small grain size upon recrystallization and to prevent grain growth during superplastic deformation, eg., precipitation strengthened Al alloys, dispersion strengthened Cu alloys etc. The microduplex materials have a fine grain microstructure consisting roughly equal proportions of two or more chemically and structurally different phases to prevent grain growth, eg.,  $\alpha$ - $\beta$  titanium alloys,  $\alpha/\tau$  stainless steels,  $\alpha$ - $\beta$  Cu alloys etc.[63,64].

#### **2.4.2 Mechanical Equations of Superplasticity**

In the original form of the mechanical equation of state the plastic flow stress was considered an instantaneous function of strain, strain rate and temperature, though later it was proved to be non-existing. Rather, for isothermal straining a relation of the form

$$\sigma_t = f(\varepsilon_t, \dot{\varepsilon}_t)$$

is feasible. The two general explicit forms of this equation are

$$\sigma_t = K' \varepsilon_t^N \dot{\varepsilon}_t^m$$

where  $K'$  and  $N$ , the strain hardening exponents are constants and

$$\sigma_t - \sigma_Y = K_1 \varepsilon_t^N \dot{\varepsilon}_t^m$$

where  $\sigma_Y$  is a yield stress and  $K_1$  is another constant.

For superplastic deformation  $N$  is very small or zero, frequently  $\sigma_Y$  can be neglected and  $m$  is non-integral and lies in the range 0.3 to 0.9. then the empirical equation[65]

$$\sigma_t = K \dot{\varepsilon}_t^m$$

describes the nature of the stress-strain rate relation adequately.

Frequently terms are included which account the temperature and the grain size dependence. A commonly used general form[63] is

$$\dot{\epsilon}_t = \text{constant } \sigma_t^{1/m} / L^a \exp(-Q/kT)$$

where  $L$  is the average grain size,  $a$  is a constant usually in the range 2 to 3,  $Q$  is an activation energy,  $k$  is Boltzmann's constant and  $T$  is absolute temperature of deformation.

In a constant velocity ( $V$ ) tensile test, the true strain rate at any time  $t$  is given by

$$\dot{\epsilon}_t = d\epsilon/dt = d[\ln(L/L_0)]/dt = (dL/dt) / L = V/L$$

Therefore, there is a gradual fall in strain rate with deformation. This may lead to a measurable decrease in stress in superplastic materials, which are significantly strain rate sensitive material. So, this leads to carry out constant true strain rate tests. A typical true stress-true strain behaviour of a superplastic material tested in tension at constant true strain rate is shown in Figure 2.9. It is suggested that strain hardening, wherever observed is due to grain growth or phase coarsening and strain softening is due to grain refinement and/or morphological changes. Strain independent behaviour is seen when the structure is fully stable.

The variation of  $\ln \sigma_t$  with  $\ln \dot{\epsilon}_t$  is sigmoidal and for convenience, the curve is divided into three regions (Figure 2.10). The region of maximum strain-rate-sensitivity (region II) delineates the strain rate range over which superplasticity occurs. At both low and high strain rates (regions I & III) the strain rate sensitivity is small and this corresponds to more conventional form of plastic deformation.

#### **2.4.3 MEASUREMENT OF SUPERPLASTICITY**

The total elongation to failure will contain contribution from uniform deformation and strain in necked region. For superplastic materials

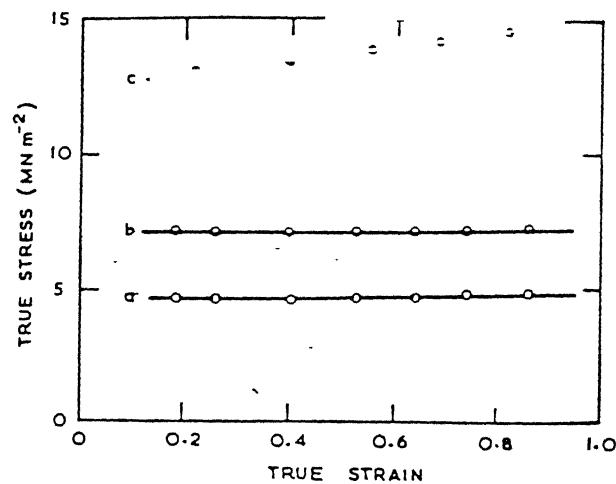


**Figure 2.9 Typical True Stress – True Strain Curve at Constant True Strain Rate (Tested in Tension)**

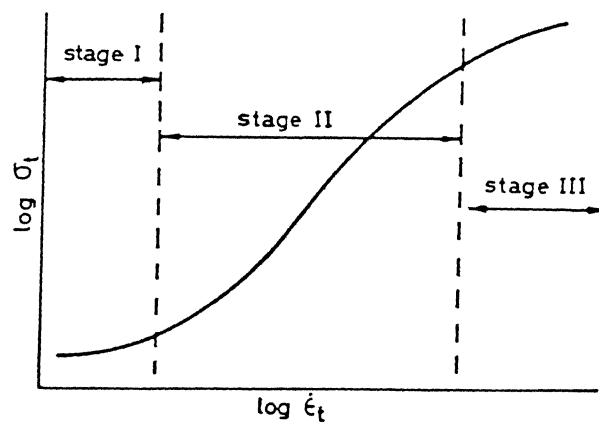


**Figure 2.10 Typical True Stress – True Strain Rate Behaviour for Structurally Superplastic Materials (Schematic)**

where multiple, diffused necks form, the latter contribution could be substantial.

Total elongations of superplastic materials can not be considered as a dependent variable of the deformation process because of its poor reproducibility even in standard specimens, of its dependence on specimen geometry, composition, initial grain size, strain rate, temperature, grain growth etc. Hence it will only be of limited use in understanding superplastic deformation. Rather, strain rate sensitivity index,  $m$ , is a very important parameter in characterizing superplastic deformation. The value of  $m$  also varies with temperature and structure (grain size). It can be determined from the slope of experimental  $\ln \sigma_t - \ln \epsilon_t$  plots or by stress relaxation tests or step strain rate test. The latter is favoured most due to its simple test procedure and consistency in obtaining values for  $m$ . As shown in Figure 2.11 if the crosshead velocity suddenly increased from  $V_1$  to  $V_2$ , there is a corresponding increase in load. If straining is continued for a few percent to eliminate transient effects, a load comparison can be made. The lower velocity curve extrapolated to establish a common strain for measurement. If  $m$  is assumed to be nearly independent of strain rate in the range covered by the velocity increase, then , according to the Figure ,

$$m = \ln(P_A/P_B)/\ln(V_2/V_1)$$

In general , a direct relation between the value of  $m$  and elongation exists [59], but there is considerable scatter. For the mutual comparisons of relative superplasticity of different materials, the  $m$  value alone can not do so as different materials of the same  $m$  value may have entirely different strain or total elongation. It is proposed [66] that the best way is to use  $\delta/m$  ratio, which is either the strain or total elongation caused by unit value of  $m$  at any instance and can be called the "strength of superplasticity" of the  $m$  value of the material. In the fundamental equation of superplasticity,  $\sigma = k\epsilon^m$  , both  $m$  and  $k$  vary with increase in strain ( $\delta$ ). The interdependence of them is expressed by the C.L.m- $\delta$  equation [67]:

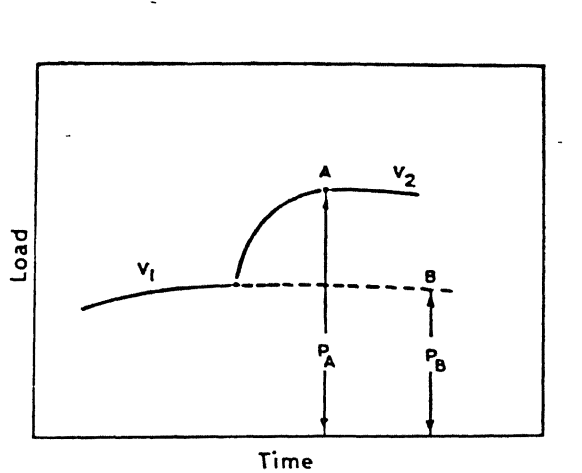


**Figure 2.11 Schematic Diagram for Step Strain Rate Test**

$V_1$  and  $V_2$  are cross head velocities before and after change.

$$\delta(\%) = [C\varepsilon^{(m-m_0)} - 1] \times 100$$

where  $m_0$  ( $\neq 0$ ) is value of  $m$  corresponding to  $\delta_0$  ( $= 0.00\%$ ),

$$C_0 = k_0 + dk_0/k_0$$

Where  $k_0$  ( $\neq 0$ ) is value of  $k$  corresponding to  $\delta_0$  ( $= 0.00\%$ ),

By this equation, not only the total elongation at fracture, but also the strains at any instant during stretching can be predicted, if the corresponding  $m$  values are known.

#### **2.4.4 Metallurgical Variables Affecting Superplasticity**

Several metallurgical variables, which have been found to affect the superplasticity in titanium, are as follows.

**(1) Grain size :** Grain size is known to strongly influence the superplasticity of titanium alloys(Figure 2.12). As is typically found for most superplastic materials , increasing grain size increases the flow stress and reduces the maximum  $m$  value as well as the strain rate at which the maximum  $m$  is observed. It is reported [68] that for Ti-6Al-4V alloy average  $\alpha$  grain diameter of 3.3  $\mu\text{m}$  gives large elongation over 800% at 850-900°C and lower flow stress. This behaviour is attributed to the limitation of void formation and resistance against localized necking. It is also observed that grain size has a strong influence on region transition in the  $\ln\sigma$  -  $\ln\varepsilon$  curves. With a decrease in grain size the transition between regions II & III is displaced to higher strain rates [69-70].

**(2) Grain Size Distribution:** Grain size has the strongest influence on superplasticity of metals. But as polycrystalline materials generally possess a distribution of grain size, it is expected that grain size distribution will also affect the superplastic behaviour (Figure 2.13). The flow stresses for the material having the smallest distribution of grain sizes

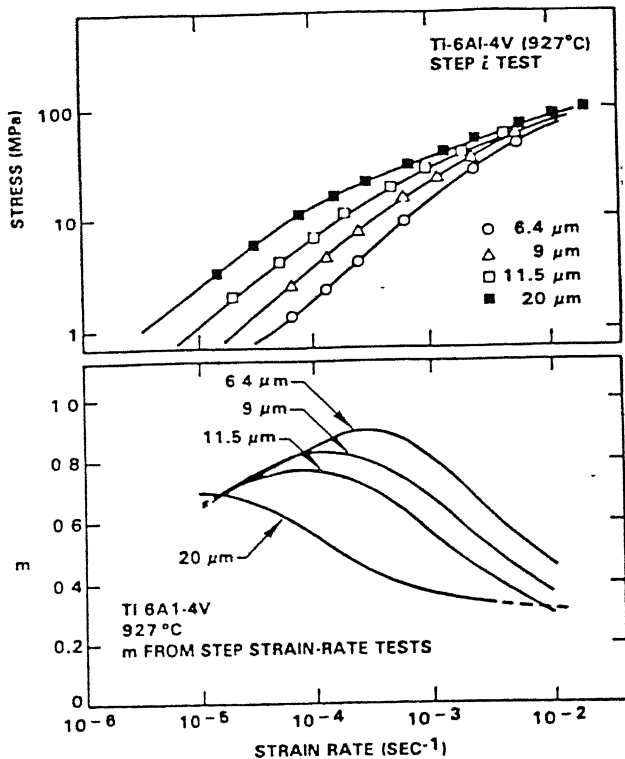


**Figure 2.12** Effect of Average Grain Size on the Flow Stress and Strain Rate Sensitivity for Ti-6Al-4V at 927°C

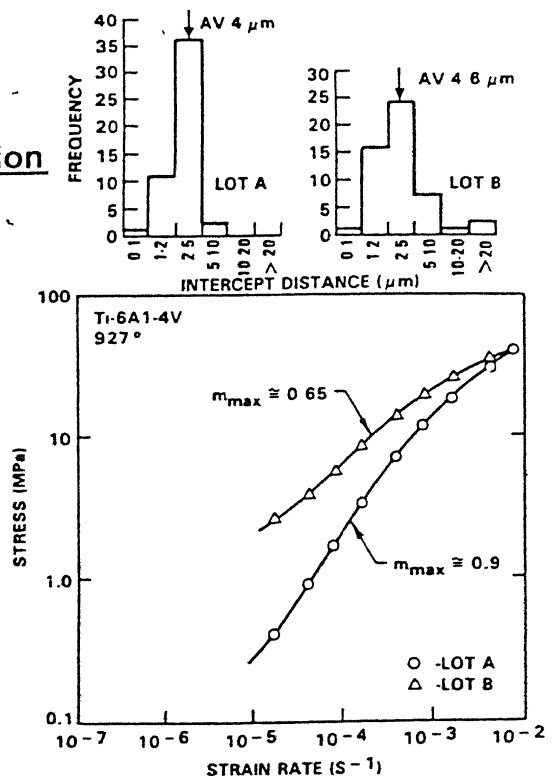


**Figure 2.13** Effect of Grain Size Distribution on The Flow Stress VsStrain-Rate Data for Ti-6Al-4V at 927°C

exhibits significantly lower stresses than the material with larger size distribution. Also the maximum value of  $m$  is much larger for the materials with the smallest size distribution. Even a relatively small number of large grains can have a major effect on the flow stresses and the slope ( $m$ ) of the curve (Figure 2.14) [71].

(3) **Grain Shape** : One of the prerequisites for superplasticity is equiaxed grain structure. Often thermo-mechanically treated materials do not have an equiaxed microstructure initially, the grain aspect ratio decreases during superplastic deformation as the elongated structure evolves towards a near-equiaxed one, eventually stabilizing at the aspect ratio of around 1.2, after about 30 % strain. Hence, mechanical data collected below that strain level does not represent true steady state condition. Usually after achieving an equiaxed condition, the structure remains equiaxed even after several hundred percent elongation, when deformed in superplastic regime[72,73].

(4) **Grain Growth Kinetics** : As flow stress of superplasticity is sensitive to grain size, it is pointed out[74] that grain growth influences and stabilizes the deformation itself. The flow stress increase due to the deformation induced grain growth is distinguished as 'flow hardening' from the usual work hardening. Grain growth not only increases flow stress, but also decreases the  $m$  value. Rate of grain growth is reported to increase with increasing strain rate in Ti-6Al-4V[75]. But occurrence of grain growth at lower strain rate is also reported for this alloy attributing that behaviour to the long holding time, due to low strain rate, at high temperature[76]. Grain growth kinetics is also accelerated by superplastic deformation. The deformation induced grain growth can be estimated approximately by  $(D/D_s)$  where  $D$  and  $D_s$  are average grain sizes after deformation and after static annealing without deformation, respectively[77,78].

(5) **Texture** : Appreciable amount of grain rotations have been observed during superplastic flow. Studies revealed that grains never rotate more than

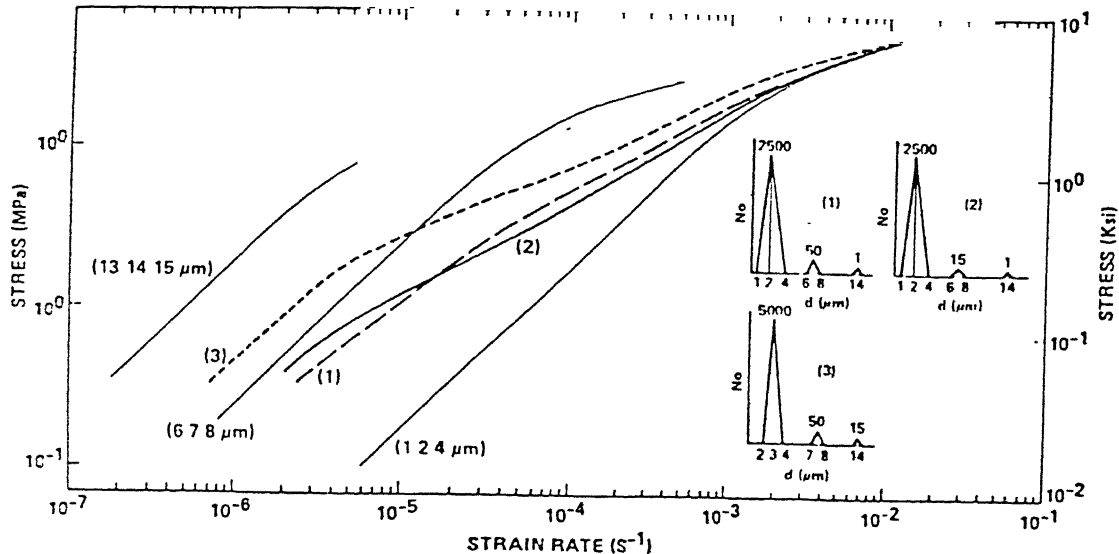


**Figure 2.14** Grain Size Distribution Effect On Flow Stress and Strain Rate for Ti-6Al-4V at 927°C

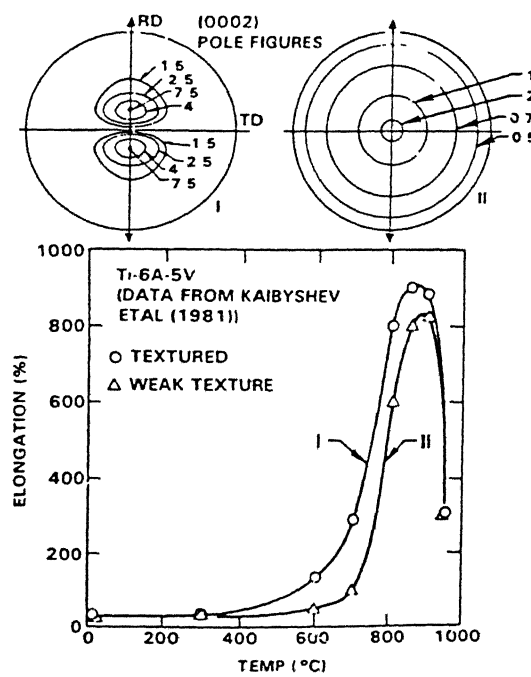


**Figure 2.15** Effect of Texture on Total Elongation for Ti-6Al-5V

45° and that they often change their sense of rotation during the deformation. During deformation, grain rotation alongwith grain boundary sliding will lead to an overall reduction in texture. A systematic study on Ti-6Al-5V alloy shows that significantly higher total elongation can be obtained from a strongly textured alloy than a weakly textured one(Figure 2.15)[79], at intermediate temperatures. This is attributed to the ease of grain boundary sliding in a textured material. For this material, difference in superplastic behaviour is pronounced at tensile test directions along RD and at 45° to RD, but not along ND.

(6) **Phase Ratio** : That the  $\alpha/\beta$  phase ratio strongly influences the superplastic behaviour of titanium alloys, is well established and experimentally verified[80-82,62,71]. The researches in this field have proved that the minima in flow stress and maxima in  $m$  value lies in a phase ratio range of 40 to 60 %  $\beta$ . This phase ratio can be changed either by changing temperature or by changing the alloy composition. The effect of phase ratio is shown in Figure 2.16, which shows maxima and minima in  $m$  and flow stress value respectively, at around 65 %  $\alpha$ . This behaviour is attributed to a balance between moderated grain growth ( due to the presence of  $\alpha$ ) and enhanced diffusivity (due to the presence of  $\beta$ ). Not only the phase ratio of  $\alpha$  and  $\beta$ , but also relative content and distribution of the orthorhombic martensite ( $\alpha''$ ) phase, produced by proper heat treatments, also affect superplasticity, lowering the superplastic temperature[83].

(7) **Diffusivity** : It is widely accepted that diffusion is an important process in the superplastic flow of fine-grained alloys including Ti alloys. This is well explained by the activation energy, which is determined from the change in strain rate with changes in temperature as expressed by the equation

$$Q = \delta \ln \dot{\varepsilon} / \delta (-1/RT)$$

Where Q is the activation energy, R is the gas constant.

Activation energy data for some common Ti alloys are given in Table 2.8[62].

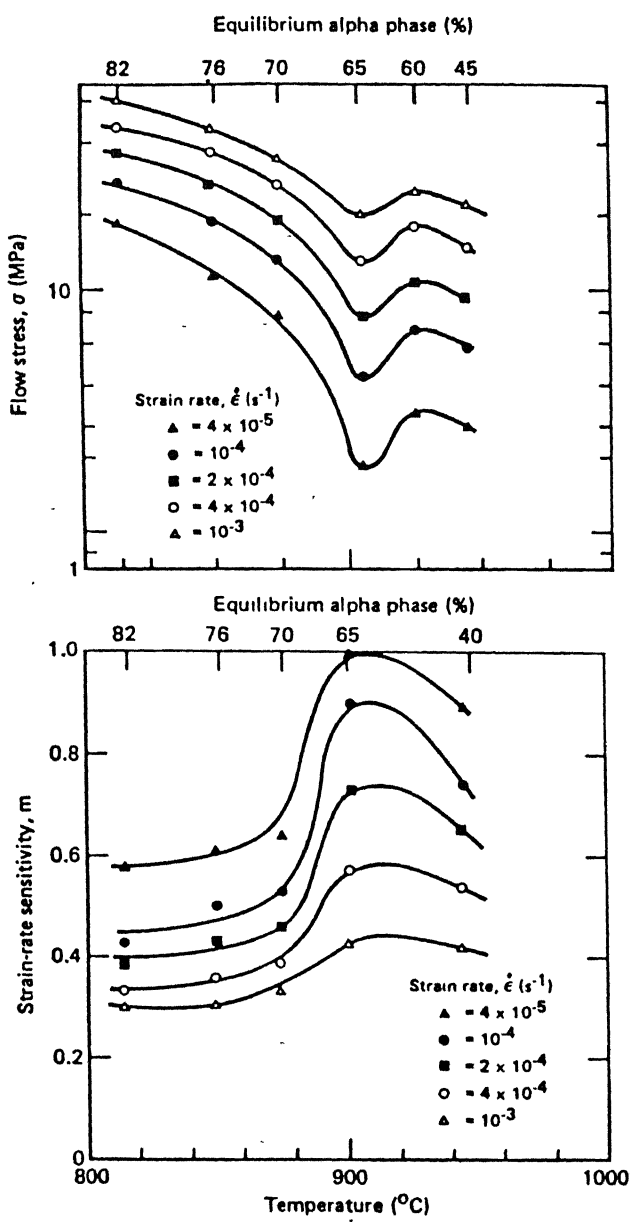


**Figure 2.16 Flow Stress and  $m$  as Functions of Temperature and  $\alpha$  Phase Content for Ti-6Al-4V**

**Table 2.8 : Activation Energies for Superplastic Deformation and Self-Diffusion in Titanium alloys**

Alloy	Temp. Range (°C)	Q (kCal/mole)
Ti-5Al-2.5Sn	800-950	50-65
Ti-6Al-4V	800-950	45
Ti-6Al-4V	850-910	45-99
Ti-6Al-4V	815-927	45-52
Ti-6Al-2Sn-4Zr-2Mo	843-900	38-58
Self Diffusion, alpha phase		40.4
Self Diffusion, beta phase		36.5
Self Diffusion, beta phase		31.3

(8) **Specimen Geometry** : The importance of specimen geometry on strain to failure is first recognized by Morrison[84] who formulated a relation between elongation to failure and initial diameter and gauge length of a rounded specimen. An empirical relation for failure strain in sheet specimens has been proposed for Ti-6Al-4V[85] :

$\varepsilon_f = B m(\varepsilon_f) / (w/t)$  where w and t are the width and thickness of the specimen, respectively,  $m(\varepsilon_f)$  is the strain rate sensitivity measured just before the failure and the constant  $B \approx 32$  for this alloy.

(9) **Initial Microstructure** : Very little attention has been paid to the effect of the initial microstructure in the studies of superplasticity. Materials having the same nominal chemical composition and initial grain size, but undergoing different thermo-mechanical treatments prior to superplastic deformation, show striking variations in flow stress and ductility[70]. When the starting microstructure is slightly elongated, a decrease in flow stress occurs in the early stages of deformation due to the evolution of the grain structure toward an equiaxed condition.

(10) **Internal Stress** : The elevated temperature deformation of crystalline materials is often discussed in terms of initial and effective stresses. The dislocation is driven by the effective stress, which is the difference between the externally applied stress and the internal or back stress. Experiments showed that the high strain rate sensitivity associated with superplasticity is largely caused by the effective stress, which was thought to be responsible for grain boundary sliding, rather than the internal stress, which was associated with a value of m closer to 0.2[70].

#### 2.4.5 Superplasticity and Ti-Alloys

As already stated in this chapter, many titanium alloys have been investigated successfully for their superplastic behaviour. Maximum of these works were on Ti-64 alloy, while some works on alloys like Ti-6242[86-92]. For the alloy Ti-64, it was found that maximum elongation is obtained in the temperature range 880-920°C at a strain rate near about  $10^{-4}$  sec<sup>-1</sup>. It was

also observed that the cold formable titanium alloys are not superplastically formable. Many attempts have been made to reduce the superplastic forming temperature by addition of elements like Fe, Co, Ni to the  $(\alpha+\beta)$  alloys or to the cold formable alloys. These researches have led to the development of new alloys, like  $\beta$ -CEZ[93], which shows superplastic properties at a temperature as low as 725°C and SP-35[94], which shows good cold workability as well as good superplasticity at 700-750°C.

Researches to enhance the superplasticity of the titanium alloys have led to development of new processing routes to obtain an ultra fine  $(\alpha+\beta)$  structure. Such an attempt has produced a total elongation of 2100% at 850°C even at a high strain rate of  $10^{-2}$  sec<sup>-1</sup>[86] in Ti-64 alloy. In a previous work carried out in this laboratory[5], elongation as large as 900% was found in Ti-6.8Al-3.2Mo-1.8Zr-0.3Si alloy, which is also quite good for this alloy. From the study of mechanism of enhanced superplasticity in  $(\alpha+\beta)$  titanium alloys, it was concluded that deformation within thin  $\beta$  phase films is the origin of the large superplasticity.

## CHAPTER 3

### EXPERIMENTAL PROCEDURE

#### 3.1 Starting Material

Ti-6Al-4V alloy (hence after referred to as Ti-64 alloy) used in this study was supplied by DMSRDE. The supplied material was in the form of a rolled plate of 15 mm. thickness. It was a (170×170) mm<sup>2</sup> plate. Chemical composition of the supplied material has been shown in Table 3.1.

**Table 3.1 Chemical composition of the material**

Alloying Elements	Al	V	O	H	C	N
Composition (Wt%)	5.94	4.07	0.05	0.021	0.014	0.012

#### 3.2 $\beta$ -Transus Determination

As we were interested in  $\beta$ -processing of the material, it was very important to know the exact  $\beta$ -transus temperature of the supplied material. Theoretically the  $\beta$ -transus temperature of Ti-64 alloy is 980°C[55]. Keeping this in mind, six small samples of dimension (4×4×5) mm<sup>3</sup> were taken, which were then heated at different temperatures for 15 minutes for temperature homogenization and directly quenched in water to arrest the phases present at respective temperatures. The six temperatures were 920, 940, 960, 980, 1000 and 1020°C respectively. Optical microscopy was done, later, on these samples to identify the phases present in them and hence, to determine the exact  $\beta$ -transus temperature.

#### 3.3 Thermo-Mechanical Treatment

Thermo-mechanical processing done in the present investigation involved homogenizing, followed by with or without hot rolling at different temperatures.

### **3.3.1 Equipments for Thermo-Mechanical Processing**

Heating and soaking of the samples was done in a specially designed high temperature furnace, kept very close to the rolling mill. The design of the furnace was done in such a manner that it was capable of maintaining protective atmosphere. During heating and soaking, grade I pure Ar gas was continuously passed through the furnace to protect the material from oxygen absorption. The furnace was having a constant temperature zone of 7 inch in length and was heated by silicon carbide rods. Muffle of the furnace consisted of an inconel tube and was closed from one end. Gas was introduced into the furnace through a 4 mm. Internal diameter stainless steel tube passing through the closed end of the chamber. The furnace was mounted on wheels so as to bring it very close to the rolling mill.

Hot rolling was done in a 2 high rolling mill which had 135 mm. diameter of the rolls. Speed of rotation for the rolling mill was kept at 55 rpm in all the experiments. No prior heating of the rolls was done before hot rolling of the specimens and they were maintained at room temperature.

Prior to the thermal treatment, the samples were placed on a small perforated inconel tray fitted with a long handle and then pushed carefully into the hot zone of the furnace.

Hot rolling was multipass in nature. In between every pass, 2 minutes soaking time was given to nullify the temperature drop effect. For hot rolling, the samples were taken out and quickly fed to the feeding end of the rolling mill. There was a very little temperature drop till the time the samples could get rolled, due to quickness of feeding and taking out of the samples from rolls (within 4-5 seconds). After rolling, the samples were quickly quenched into water.

The surface of the rolled samples were ground and subjected to pickling in 10 %  $\text{HNO}_3 + 5\%$  HF solution for nearly 3 hours at room temperature to remove the  $\alpha$ -casing layer formed due to oxygen diffusion. These samples were further subjected to belt grinding and emery paper polishing before being investigated further.

### **3.3.2 Working Schedule**

The thermo-mechanical processing schedule followed in this work were divided into two stages – stage I, consisting of the thermo-mechanical treatment in the  $\beta$ -phase region and stage II consisting of the thermo-mechanical treatment in the  $(\alpha+\beta)$  region. In the stage I, 5 different routes were followed. Schematic representation of the schedules are shown in Figure 3.2, whereas the flow charts are given in Figure 3.1, samples were ground to different initial thickness values so that after stage I the thickness becomes 6 mm.

#### **Stage I**

##### **Route I**

The specimen was to be heated in the  $\beta$ -phase field. To take care of the grain growth at higher temperature in the  $\beta$ -phase field, a temperature  $30^{\circ}\text{C}$  above the  $\beta$ -transus was selected. The sample was soaked at that temperature for 20 minutes for homogenization of temperature and then furnace cooled to room temperature.

##### **Route II**

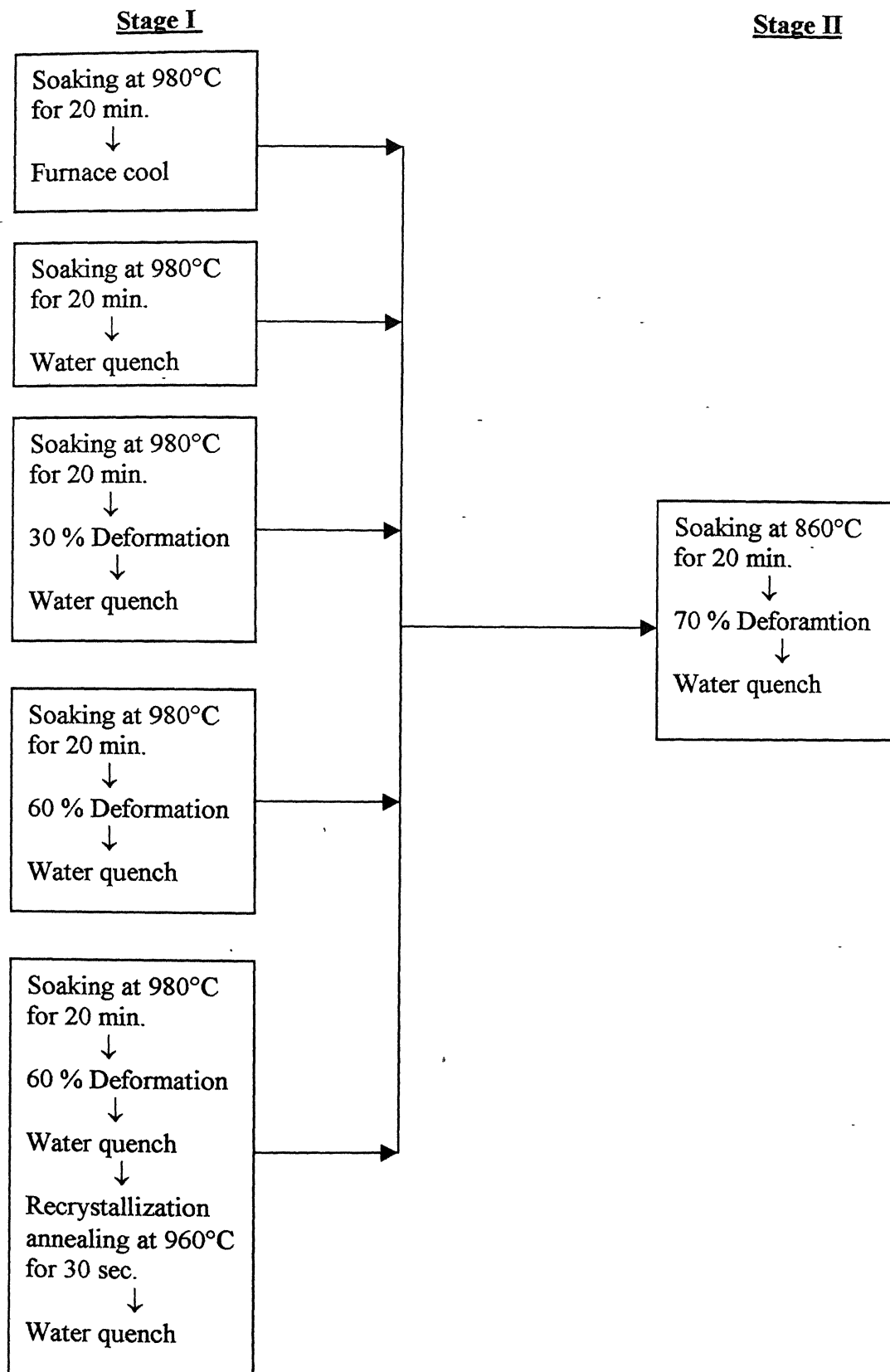
The specimen was heated at the same temperature for route 1, soaked there for 20 minutes followed by direct water quenching.

##### **Route III**

The specimen was heated at the same temperature for route 1, soaked there for 20 minutes, rolled at that temperature in 2 passes giving 30% deformation followed by water quenching.

##### **Route IV**

The specimen was heated at the same temperature for route 1, soaked there for 20 minutes, rolled at that temperature in 4 passes giving 60% deformation followed by water quenching.

Figure 3.1 Flowsheet of the Thermo-mechanical Process.

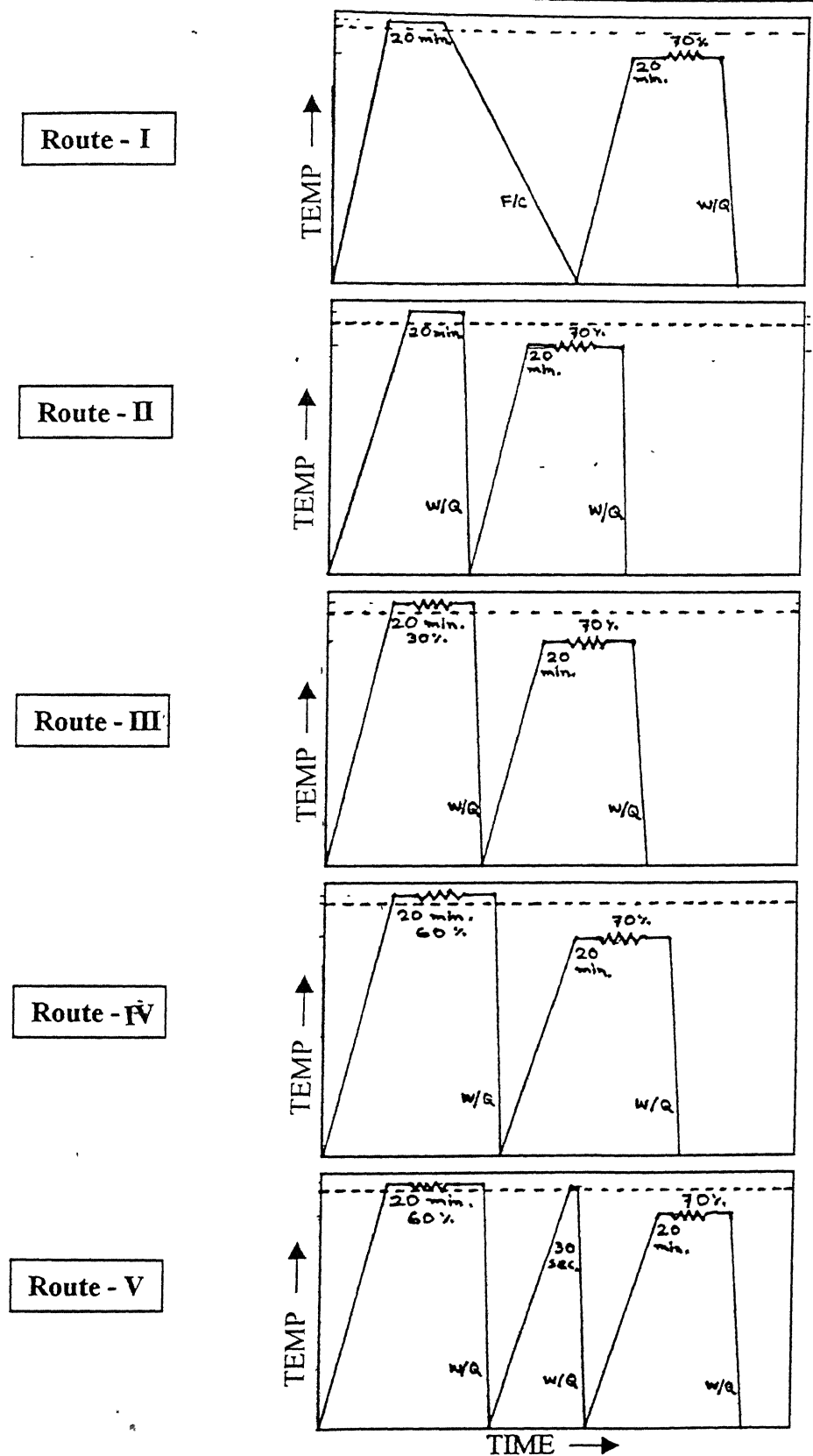


Fig.3.2 : Schematic Representation of Thermomechanical Processes Studies

### **Route V**

The specimen was heated at the same temperature for Route I, soaked there for 20 minutes, rolled at that temperature in 4 passes to give 60% deformation, followed by water quenching. The sample was then further recrystallized in the  $\beta$ -phase field, just  $10^{\circ}\text{C}$  above the  $\beta$ -transus, soaked there for 30 seconds followed by water quenching.

Small samples for microstructural studies were cut out from each of the specimens.

### **Stage II**

All the specimens produced through Route I to route V were given same treatment in the stage II. All of them were soaked at  $860^{\circ}\text{C}$  for 20 minutes, rolled unidirectionally at that temperature in 5 passes giving 70 % deformation followed by water quenching. Care had been taken during the rolling about the previous rolling direction. Small samples for microstructural studies were cut out from each of the specimens. Samples for superplasticity testing were made from each of the specimens.

## **3.4 Characterization**

The characterization techniques used in the present investigation can be classified under three heads : microstructural characterization, phase characterization and mechanical property characterization.

### **3.4.1 Microstructural Characterization**

Microstrctures taken from all the specimens were examined by optical and scanning electron microscopes. Prior to the observations, all the samples were mechanically polished on emery papers ( 0 to 4 grades) followed by wheel polishing with alumina powders of sizes 1 mm., 0.3 mm. and 0.05 mm., respectively. The samples were then etched with Kroll's reagent ( $4\%\text{HF}+2\%\text{HNO}_3$ ). Microstructural observations were, generally,

done on transverse cross sections of the specimens, unless otherwise mentioned.

Optical microscopy was done under a Leitz Wetzlar optical microscope.

Scanning electron microscopy was done under a JEOL-JSM 840A Scanning electron microscope. The samples were observed under the scanning electron microscope, operated at 10 kV using secondary electron radiation (SE mode).

Quantitative analysis on the microstructures was done to measure length, thickness of different structural features. From these measurements, aspect ratio was calculated. Grain size, wherever mentioned, was given as the diameter of the circle having same area with the measured structural feature i.e. if the length and thickness of the grain were 'l' and 't' respectively, then grain size(d) was calculated as

$$d = 2 \times \sqrt{l \cdot t / \pi}$$

### **3.4.2 Phase Characterization**

Phase characterization was done by X-ray to detect the phases formed in the samples after the stage II operation. The processed samples were subjected to X-ray examination using normal Bragg scan. Normal Bragg scan was recorded from polished surface of the sheet plane of the specimens on a Seifert Deby X-ray Diffractometer operated at 30 kV and 20 mA using  $\text{CuK}_\alpha$  radiation. Scanning sped was kept at  $3^\circ/\text{min.}$  in  $2\theta$ , chart speed was kept at 30 mm/min. X-ray diffraction patterns obtained were indexed and identification of the phases was done by matching the 'd' values corresponding to the each peak position of the diffraction pattern with the 'd' values of all possible phases obtained from standard sources and literature[56,57]. In order to have a consistency, all the measurements were done using a fixed beam dimension.

For some samples, quantitative analysis was done from the XRD patterns to get an idea about the percentage volume fraction of different

phases present in the material. The procedure for the volume fraction calculation was based on the following theory.

If the 'x' and 'y' be the two phases present in a material, then from the basic formula for the calculation of the integrated intensity it can be written that[106]

$$I_x/I_y = (R_x \cdot C_x) / (R_y \cdot C_y)$$

$$C_x + C_y = 1$$

Where  $I$  = integrated intensity calculated as area under the curve

$C$  = content of a phase in volume fraction

$$R = 1/v^2 \cdot [ |I|^2 \cdot p \cdot (1 + \cos^2 2\theta) / (\sin^2 \theta \cdot \cos \theta) ] (e^{-2M})$$

Where  $v$  = unit cell volume and the others have their usual meanings.

Intensity measurements were done for the peaks corresponding to only a single phase. As for alloy systems it is difficult to get the value of temperature factor, it was safely neglected in the calculation of the volume fraction[106].

### 3.4.3 Mechanical Property (Superplasticity) Determination

Superplastic testing of processed sheets was done on the MTS machine model : 810.12.

The furnace, attached to the machine, had a heating rate of 200°C/hr. The samples were homogenized for 15 minutes at the desired temperatures before start deforming. Due to the absence of any purging system in the furnace, the heating and tensile deformation was carried out in air. The processed sheets were machined, further ground, pickled and polished to remove the  $\alpha$ -casing formed due to oxygen diffusion during processing. Tests were carried out with samples having no protective coating on the surface to prevent oxidation. Two types of tests were carried out on these samples at different pre-determined temperatures.

- (a) Strain Rate Jump Test : In this test, the strain rate( actually the cross head speed of the machine)was increased in successive steps from

$8.33 \times 10^{-5}$ /sec. To  $3.33 \times 10^{-2}$ /sec. (9 different strain rates were used) and the corresponding flow stress was calculated from the load-elongation plot. This test was done at two different temperatures,  $800^{\circ}\text{C}$ ,  $850^{\circ}\text{C}$ . Utmost care was taken to prevent necking of the samples throughout the testing history. From the steps of the  $\ln \sigma$  -  $\ln \epsilon$  plots, the value of strain rate sensitivity( $m$ ) was determined for a range of strain rates and temperatures.

(b) Elongation to Failure Test : In this test, the samples were strained to failure under different constant strain rates for different samples at  $850^{\circ}\text{C}$ . After failure, the samples were allowed to cool in furnace and then the maximum elongation was measured. The samples, after testing were cut into different sections and microscopically observed.

The samples used in the above mentioned two types of tests had the following dimensions :

Grip length	=	19 mm.
Grip width	=	19 mm.
Hole diameter	=	6.35 mm.
Gauge length	=	6 mm
Gauge width	=	5 mm.
Gauge thickness	=	2 mm.
Radius at corner	=	1 mm.
Total length	=	46 mm.

A schematic diagram of the sample is given in Figure 3.3.

## Chapter 3: Experimental Procedure

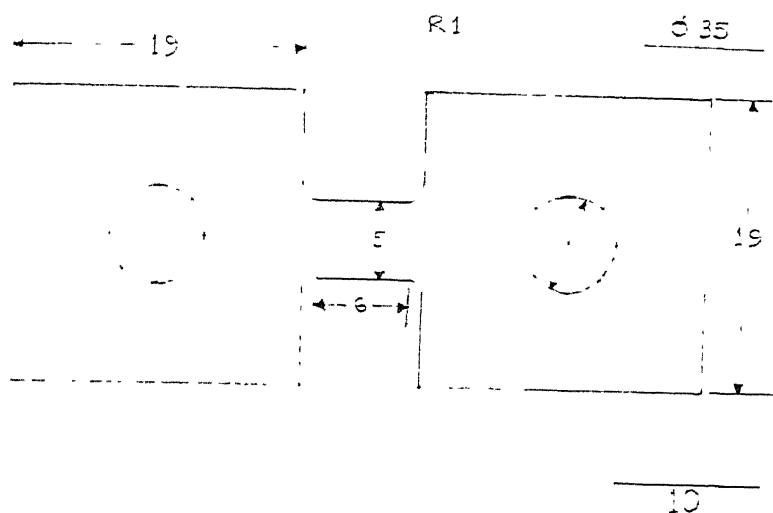


**Figure 3.3 Sketch of the Tensile Sample Used for Superplastic Testing**

(All Dimensions are in mm.)

# CHAPTER 4

## RESULTS AND DISCUSSION

The alloy Ti-6Al-4V is an important member of the family of two phase ( $\alpha+\beta$ ) titanium alloys with both the bcc ( $\beta$ ) and hcp ( $\alpha$ ) phases being stabilized at room temperature. Control of  $\alpha$  morphology is essential in this alloy as far as superplastic forming is concerned. An equiaxed primary  $\alpha$  morphology with grain size less than  $10\mu\text{m}$  is generally necessary for such applications. Lamellar or Widmanstatten primary  $\alpha$  transforms to equiaxed primary  $\alpha$  morphology on hot working of the material in ( $\alpha+\beta$ ) phase field. During hot working the lamellar  $\alpha$  breaks down into small parts and finally results into near equiaxed or equiaxed  $\alpha$  structure either during the hot working itself or during post deformation recrystallization annealing.

While the conventional thermo-mechanical processing of ( $\alpha+\beta$ ) titanium alloys involves forging/rolling/extrusion through the  $\beta$ -transus of the alloy with a minimum specified reduction in the two-phase field, the present study involved with unconventional processing routes incorporating

- (1) conditioning of prior  $\beta$  grains and
- (2) conditioning of lamellar  $\alpha$  prior to working in the ( $\alpha+\beta$ ) phase field.

### 4.1 CHARACTERIZATION OF THE AS-RECEIVED Ti-6Al-4V ALLOY

#### 4.1.1 Structure of the As-Received Alloy

Microstructure and X-ray diffraction pattern obtained from the as-received material are shown in Figure 4.1 and 4.2 respectively. As shown in Figure 4.1, the as-received microstructure consisted of (a) small volume fraction of fine elongated  $\alpha$ , (b) a relatively larger volume fraction of coarser

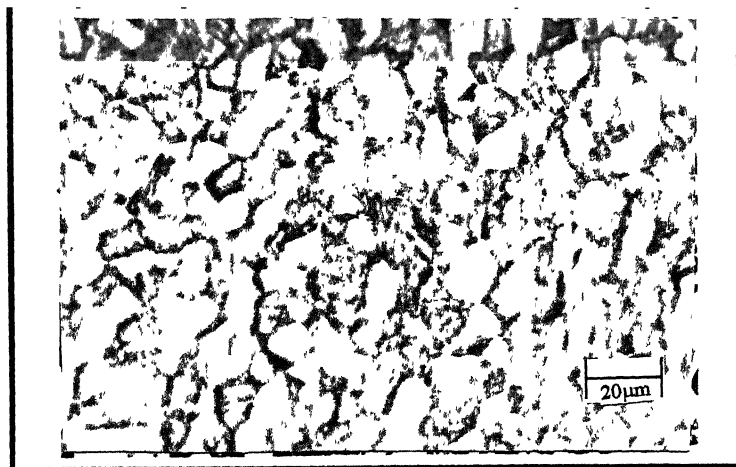


**Figure 4.1 Microstructure of The As Received Material**

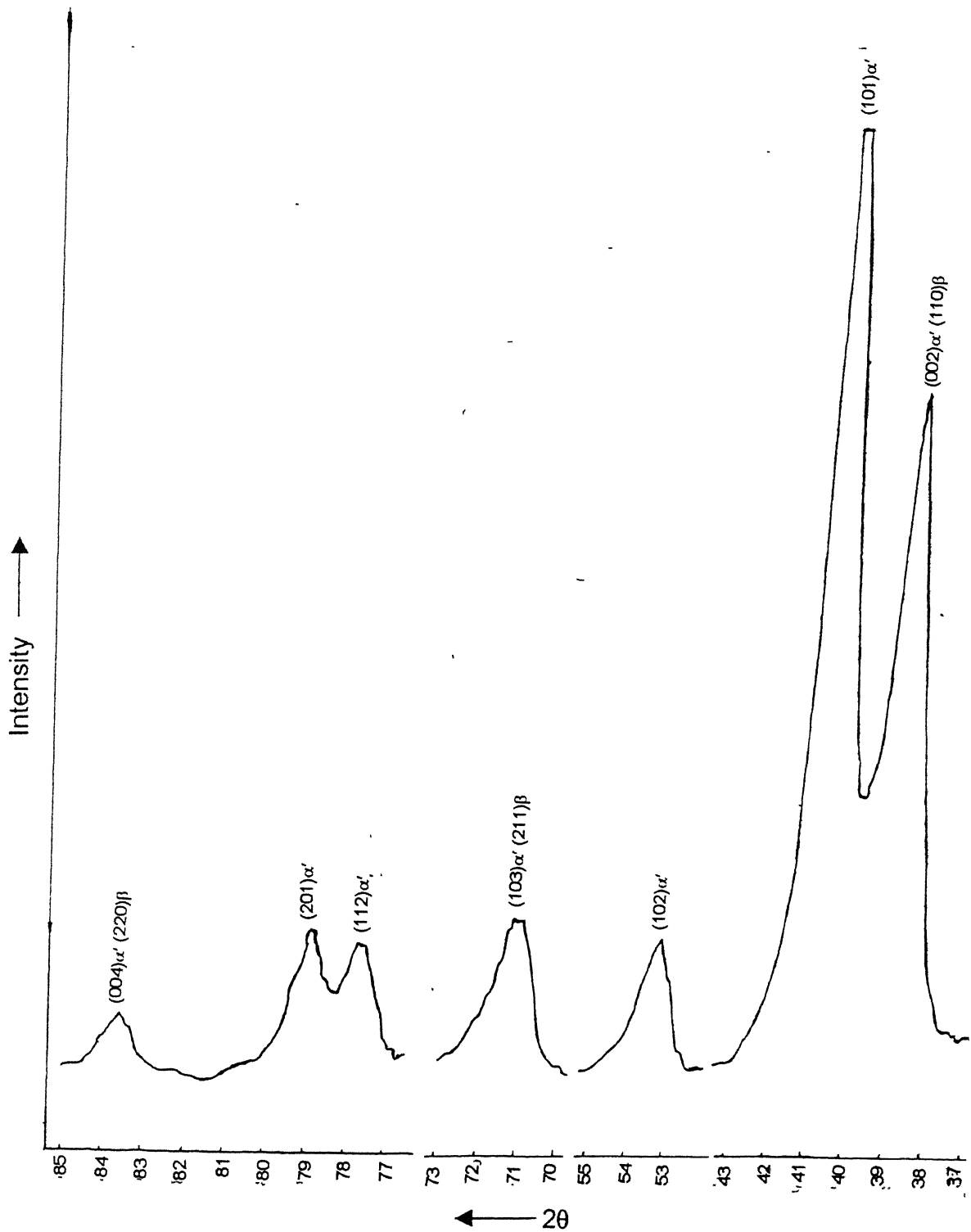


**Figure 4.2 XRD Pattern of the As Received Material**

equiaxed  $\alpha$  and (c)  $\beta$  as matrix. The coarse equiaxed  $\alpha$  grains were found to have the size range between 11.5-31.7  $\mu\text{m}$ . The X-ray diffraction pattern taken from the as-received alloy also confirmed the presence of  $\alpha$  and  $\beta$  phases only in the microstructure.

#### **4.1.2 $\beta$ -Transus of the Alloy**

Sub-transus working of ( $\alpha+\beta$ ) titanium alloys plays an important role in refining their microstructures. However, the  $\beta$ -transus temperature of titanium alloys is known to depend on their exact chemistry and must be determined for each heat. Therefore, the  $\beta$ -transus of the as-received alloy was determined by the metallographic technique. Microstructures of samples quenched from different temperatures ranging between 920°C and 1020°C, raised by an increment of 20°C, were observed to identify phases present in the alloy. While samples quenched from 960°C and above showed full  $\beta$  those quenched from 940°C and below showed presence of both  $\alpha$  as well as  $\beta$  phases. The sample quenched from 940°C showed grains of the  $\alpha$  phase in about 6% in volume fraction [Fig 4.3]. So, the  $\beta$ -transus of the given alloy was taken to be  $950 \pm 5^\circ\text{C}$ . This is somewhat lower than the typical  $\beta$ -transus temperature of Ti-6Al-4V alloy [55]. However, this lower value of the  $\beta$ -transus temperature can be explained by the lower oxygen content of the alloy which has been shown in Table 3.1.

#### **4.1.3 Effect of $\beta$ Annealing Temperature on $\beta$ Grain Size**

Soaking of Ti-6-4 alloy in the  $\beta$  phase field produces recrystallized equiaxed  $\beta$  grains which are known to undergo a rapid grain growth. Therefore, the soaking temperature above the transus affects the  $\beta$  grain size. Microstructures of the water-quenched alloy soaked for 20 minutes at 960°C, 980°C, 1000°C and 1020°C are shown in Figures 4.3 and 4.4. It was observed that as the soaking temperature increased from 960°C to 1020°C the average grain size increased from about 680  $\mu\text{m}$  to 860  $\mu\text{m}$ . It

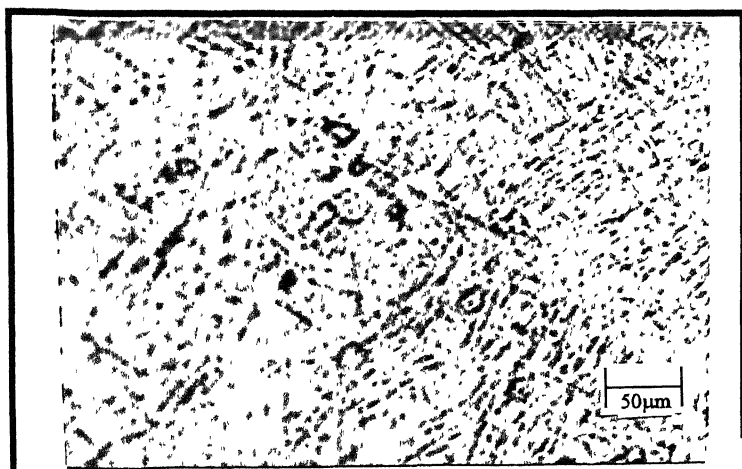


**Figure 4.3 Microstructure of the Sample Water Quenched from**

- (a) 960°C (consisting of martensite with no trace of  $\alpha$ )**
- (b) 940°C (consisting of small islands of  $\alpha$  in martensitic structure)**

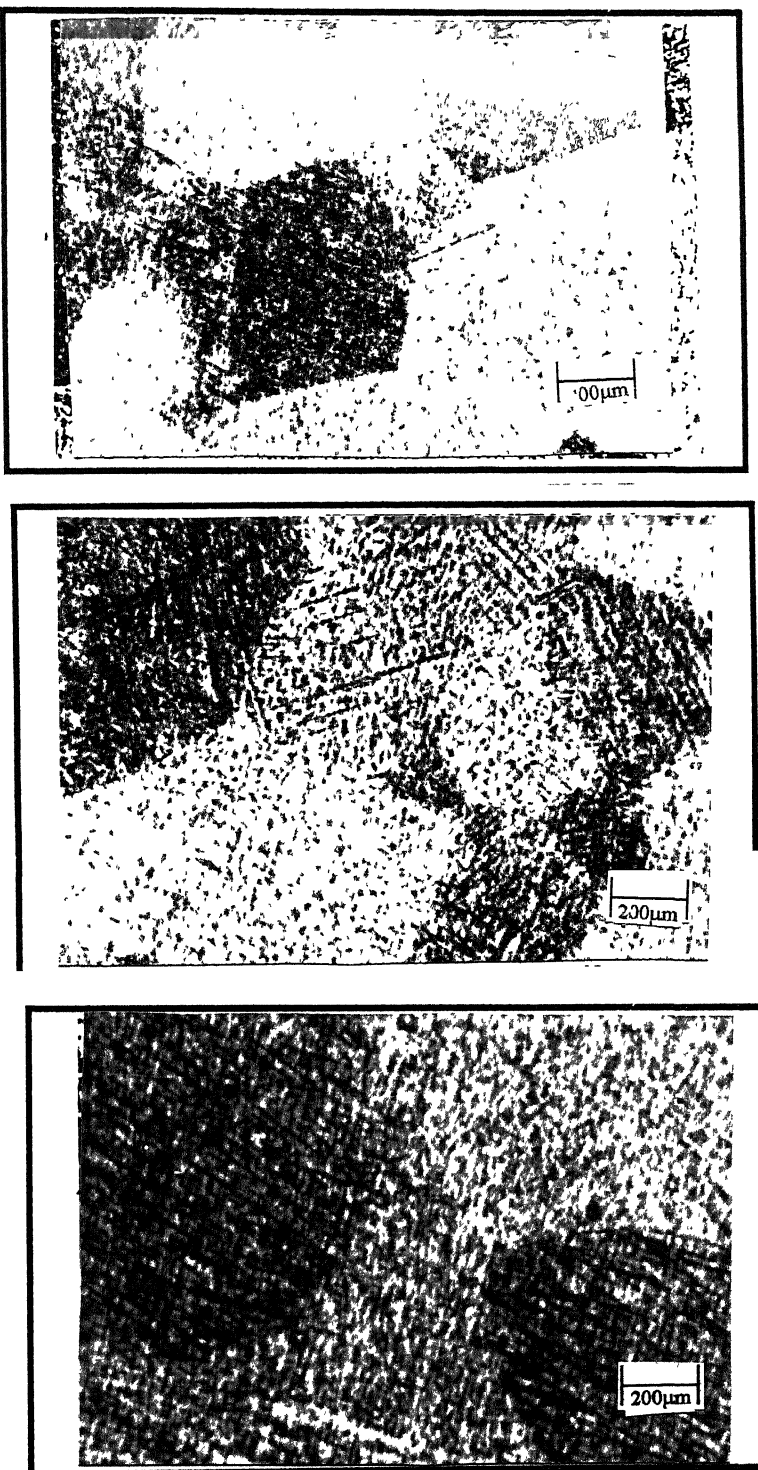


**Figure 4.4 Grain Growth in  $\beta$  Grains as a Function of  $\beta$  Annealing Temperature** (microstructures were observed in water quenched condition)

(a)  $980^{\circ}\text{C}$       (b)  $1000^{\circ}\text{C}$       (c)  $1020^{\circ}\text{C}$

was thus seen that  $\beta$  grains in Ti-6-4 alloy undergo a rapid grain growth with respect to temperature when heated in the single phase  $\beta$  region. It is to be noted that this type of behaviour is generally observed for most ( $\alpha+\beta$ ) titanium alloys [6].

#### **4.1.4 Type of Martensite Formed by Water Quenching**

Hexagonal martensite ( $\alpha'$ ) as well as orthorhombic martensite ( $\alpha''$ ) are known to be forming in titanium alloys due to the rapid cooling of the  $\beta$  phase. Since the present study involves unconventional thermo-mechanical processing routes incorporating water-quenching as intermediate steps, it is of interest to know the type(s) of martensite formed by water quenching from the  $\beta$  as well as ( $\alpha+\beta$ ) phase field. To verify this fact, two as received samples were heated to 980°C and 860°C, i.e. the temperatures of treatment in  $\beta$  and ( $\alpha+\beta$ ) phase fields respectively, and were subsequently water quenched. These samples were subjected to XRD. XRD patterns obtained from these samples are shown in Figures 4.5 and 4.6 respectively. It is seen that while Figure 4.5 contains clearly discernible peaks corresponding to orthorhombic as well as hexagonal martensites, i.e. both  $\alpha'$  and  $\alpha''$ , Figure 4.6 contains peaks corresponding to only the hexagonal martensite  $\alpha'$ . It is also to be noted that weak overlapping peaks corresponding to the  $\beta$  phase are also present in both XRD patterns indicating that the martensitic transformation is not 100% complete and some amount of  $\beta$  is retained at the room temperature. These results show that while  $\alpha''$  is formed in the given Ti-6-4 alloy when quenched from 980°C, i.e.  $\beta$  phase field, but not when the alloy is quenched from 860°C, i.e. ( $\alpha+\beta$ ) phase field. An elementary analysis of volume fractions of  $\alpha'$  and  $\alpha''$  from these results indicates that the orthorhombic phase is the major component in the alloy quenched from the  $\beta$  phase field and its % volume fraction is almost about 90%.

The structure of martensitic needles formed by quenching from different temperatures in the  $\beta$  phase field is shown in Figure 4.7(a) to (e). It is

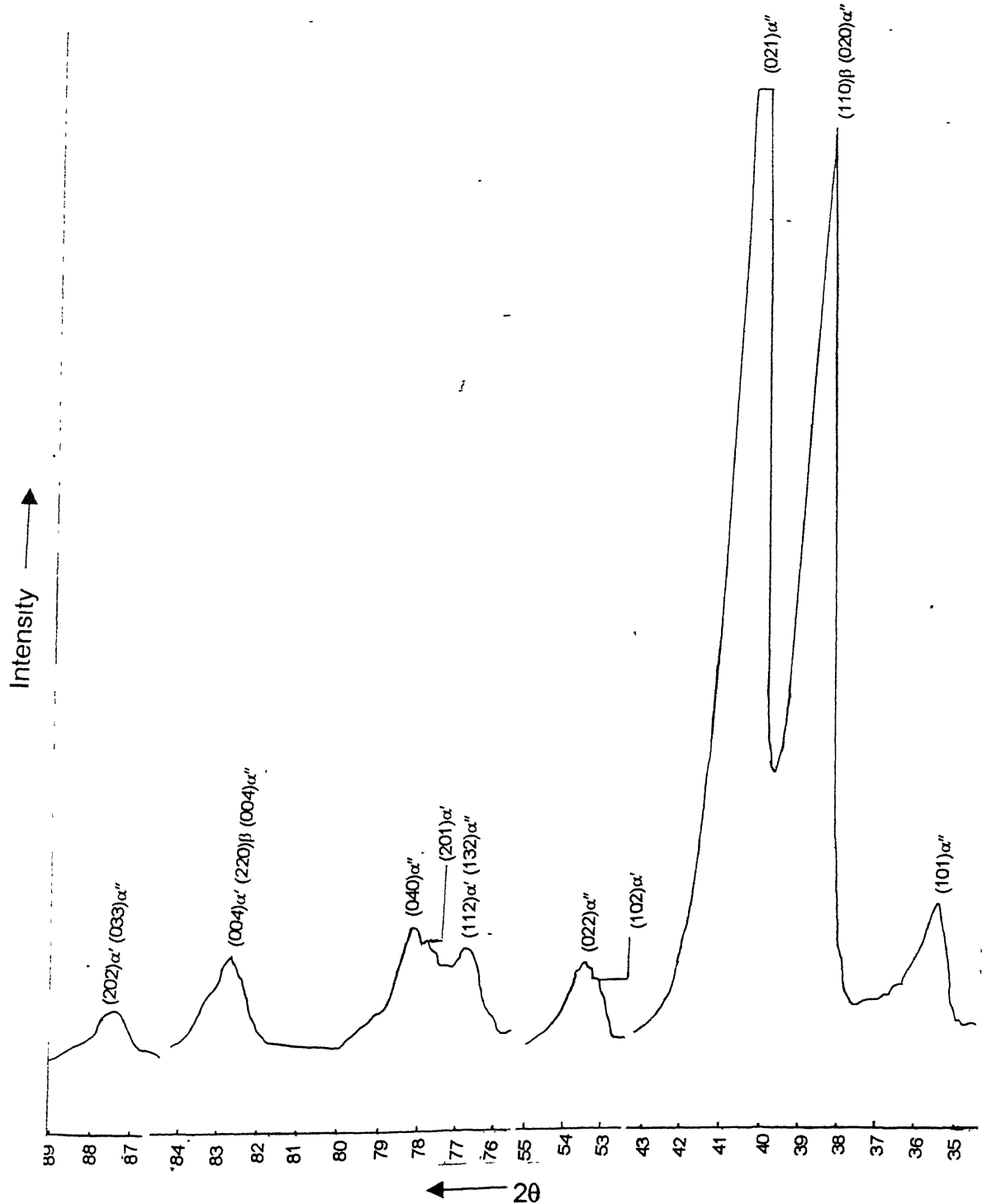


**Figure 4.5** XRD Pattern of the Sample Quenched From  $980^{\circ}\text{C}$

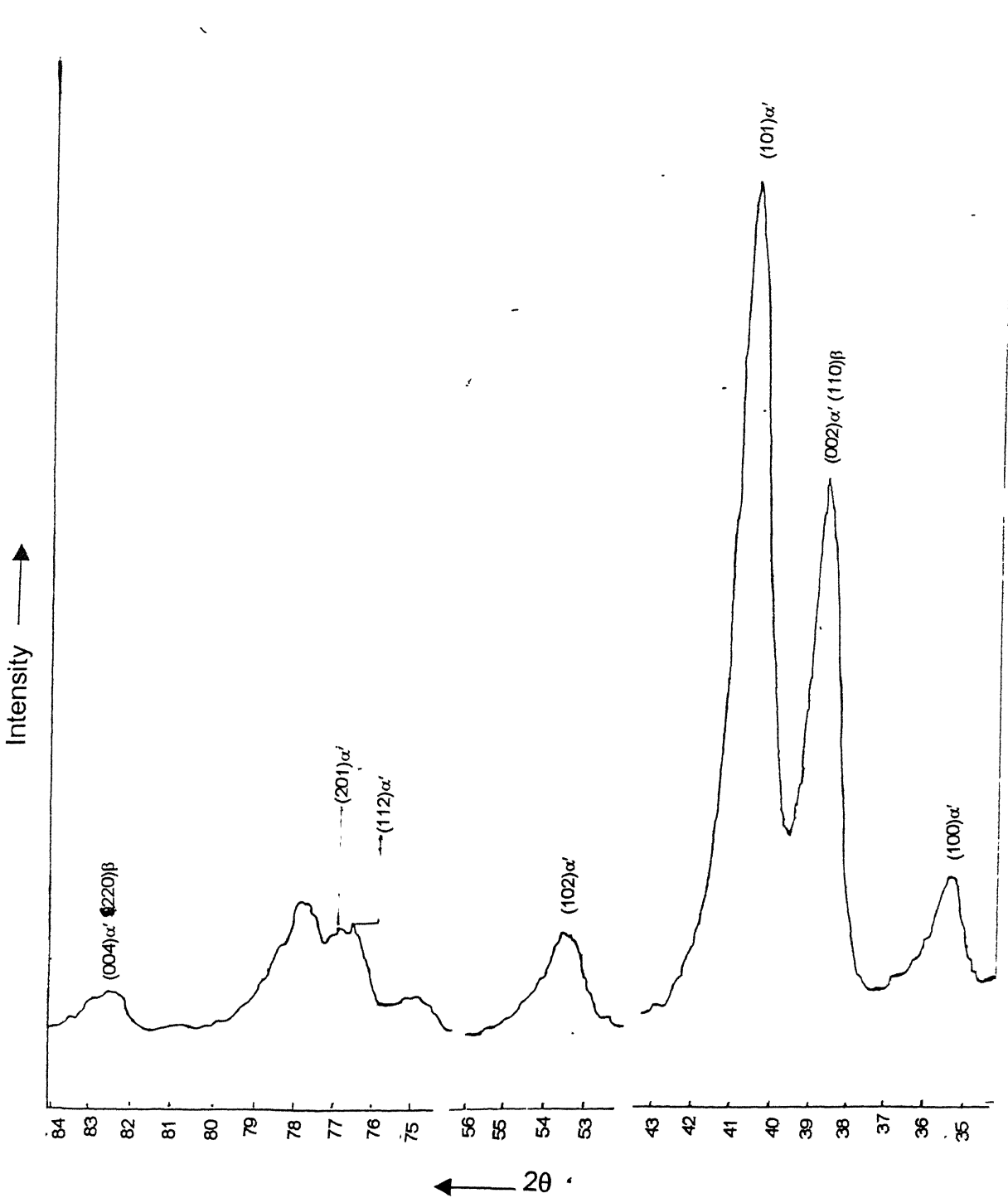


Figure 4.6 XRD Pattern of the Sample Quenched From 860°C

clear that the martensitic needles become somewhat thicker as the soaking temperature increases from 960°C to 1020°C.

#### **4.2 THERMO-MECHANICAL PROCESSING VARIABLES IN THE $\beta$ PHASE FIELD AND THEIR EFFECT ON CONDITIONING OF $\beta$ GRAINS**

Evolution of equiaxed  $\alpha$  and its refinement is the goal of developing new thermo-mechanical processing schedules for two-phase titanium alloys. Since the transformation of lamellar  $\alpha$  to equiaxed  $\alpha$  occurs during working in the  $(\alpha+\beta)$  field, its refinement depends on morphological characteristics of  $\alpha$  lamellae prior to their deformation. Morphological characteristics of  $\alpha$  lamellae, in turn, depend on the conditioning of prior  $\beta$  grains which was affected by thermo-mechanical variables in the  $\beta$  phase field. Details of different thermo-mechanical processing schedules have already been given in chapter 3. In principle, the condition of  $\beta$  grains was affected so as to (a) get coarse as well as fine recrystallized grain structure and (b) get pancaked  $\beta$  grain structure by working the alloy in the temperature field which does not cause dynamic recrystallization. These objectives were fulfilled by changing the following processing variables:

- (a) obtaining coarse  $\beta$  grain structure by annealing at 980°C, i.e. at a temperature of about 30°C above the transus,
- (b) producing pancaked structure of different size and aspect ratio by rolling the alloy with varying deformation at 980°C;
- (c) producing fine recrystallized  $\beta$  grains by subjecting the pancaked structure to recrystallization annealing treatment at 960°C for 30 seconds.

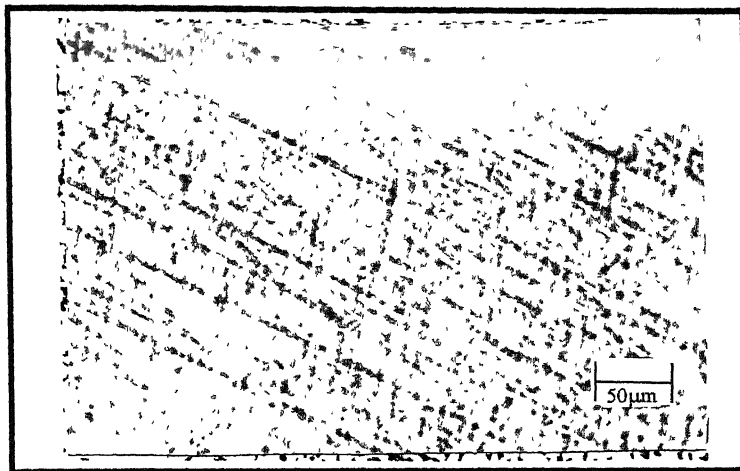


**Figure 4.7(a)**      **Microstructure Obtained from Ti-6-4 Alloy b \ Water**  
**Quenching from 960°C** (optical micrograph)



**Figure 4.7(b)**      **Microstructure Obtained from Ti-6-4 Alloy b \ Water**  
**Quenchin. from 980°C** (optical micrograph)

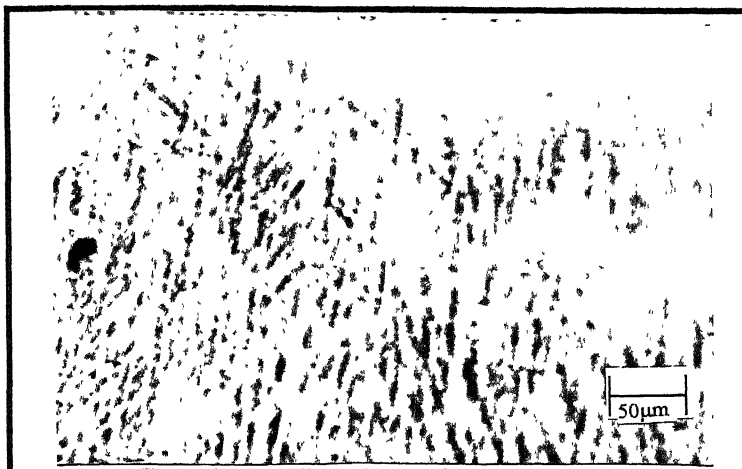


**Figure 4.7(c)**      Microstructure Obtained from Ti-6-4 Alloy by Water Quenching from 1000°C (optical micrograph)

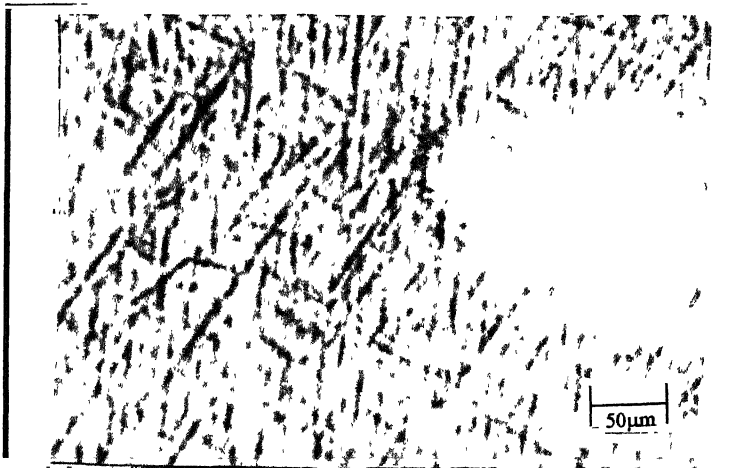


**Figure 4.7(d)**      Microstructure Obtained from Ti-6-4 Alloy by Water Quenching from 1020°C (optical micrograph)

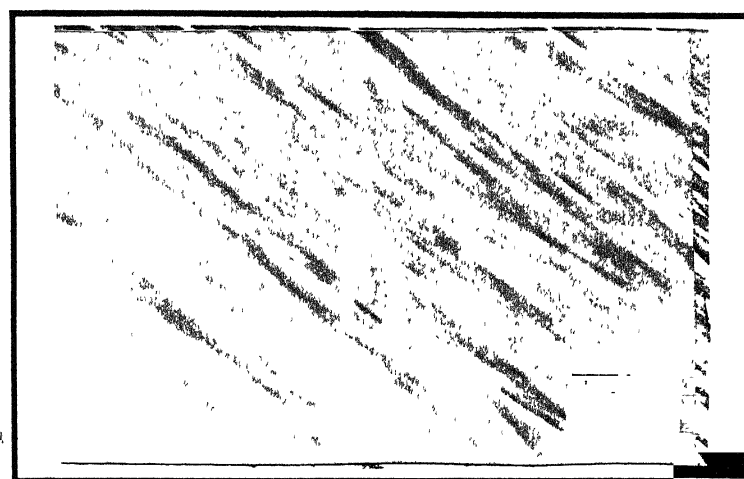


**Figure 4.7(e)**

**Microstructure Obtained from Ti-6-4 Alloy by Water Quenching from 980°C (SEM micrograph)**

#### **4.2.1 Effect of Thickness Reduction on $\beta$ Grain Characteristics**

Stress-strain curves for high-temperature deformation of titanium alloys in the  $\beta$  phase field clearly indicate that the  $\beta$  phase does not undergo dynamic recrystallization [6]. The structure of  $\beta$  grains is well developed and is fairly resistant to recrystallization. However, it may undergo static recovery during deformation. To study the effect of deformation on the  $\beta$  grain characteristics, samples preheated at 980°C for 20 minutes were hot rolled to give 30% and 60% thickness reductions respectively. The hot-rolled samples were water quenched immediately after rolling. The microstructures of Ti-6-4 alloy in these states are presented in Figure 4.8. Pancaked grains of  $\beta$  phase are readily seen in both the cases which clearly indicate that like other ( $\alpha+\beta$ ) titanium alloys, Ti-6-4 alloy also does not undergo dynamic recrystallization during its high temperature deformation at a strain rate of  $10^{-1}$  sec $^{-1}$  (estimated to be typical of rolling conditions prevailing under the present study). The fact that the pancaked grains of  $\beta$  were observed in the material even after 60% thickness reduction supports the above conclusion. It is clear from these micrographs that  $\beta$  grains become increasingly pancaked with increasing amount of deformation.

#### **4.2.2 Effect of Recrystallization Annealing on The Microstructure**

It has already been stated that conditioning of  $\beta$  grains involves obtaining coarse as well as fine recrystallized grains. Coarse recrystallized  $\beta$  grains are formed by heating in the  $\beta$  phase field whereas deformation in the  $\beta$  phase field followed by annealing at a lower temperature in the single phase field produces fine, recrystallized  $\beta$  grains. The effect of recrystallization annealing on the  $\beta$  grain structure is studied by subjecting one 60% deformed sample to recrystallization annealing by soaking at 960°C for only 30 seconds. Annealed specimen was then water quenched to retain  $\beta$  grain boundaries for their subsequent microstructural examination. The microstructure is presented

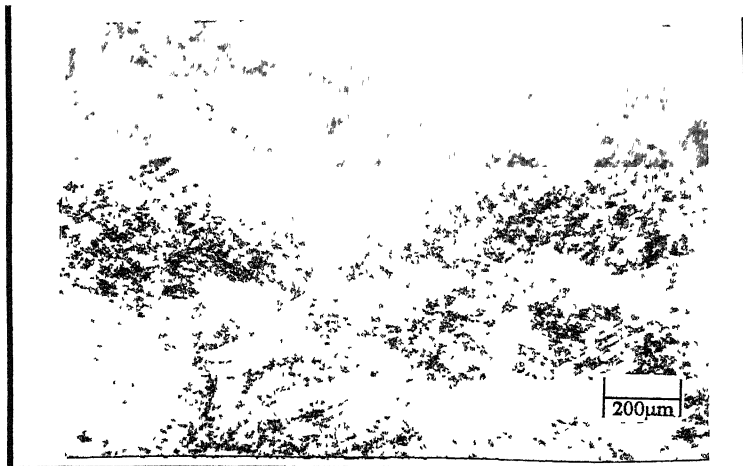


**Figure 4.8 Microstructure Obtained from Ti-6-4 Alloy Deformed at 980°C with Thickness Reductions of**

- (a) 30% and Water Quenched**
- (b) 60% and Water Quenched**

in the Figure 4.9. The heavily deformed structure as presented in Figure 4.8(b) is transformed to a fine equiaxed  $\beta$  structure. A comparison with the microstructure shown in Figure 4.8(b) clearly indicates that the pancaked  $\beta$  grains become equiaxed after annealing at such a low temperature i.e.  $10^{\circ}\text{C}$  above the  $\beta$ -transus temperature for only 30 seconds. Thus it can be seen that considerable refinement of  $\beta$  grains was achieved by the processing route V which involved short-time recrystallization annealing of pancaked  $\beta$  grains.

#### **4.2.3 Morphology of Martensite Formed by Different $\beta$ Processing Routes**

The previous sub-sections have dealt with the microstructural evolution of  $\beta$  grains during different  $\beta$  processing routes followed in the present investigation. As discussed in Chapter 3, Figures 3.1 and 3.2, water quenching from various processing temperatures was an essential step in all the processing routes. Thus martensitic transformation occurred in the alloy after its processing in the  $\beta$  phase field.

Typical martensitic microstructures obtained by water quenching of the alloy after different  $\beta$  processing routes are shown in Figure 4.10. Efforts were made to make quantitative measurements of the distribution of length and thickness of martensitic needles formed after different  $\beta$  processing routes. These length and thickness distributions for various structures are shown in Figure 4.11( f is the % volume fraction of  $\alpha$  lamellae or  $\alpha'$ , whichever is applicable). It can be seen that the length and thickness distributions for martensite are dissimilar for those obtained from (a) recrystallised  $\beta$  grains (Routes II and V) and (b) unrecrystallised pancaked  $\beta$  grains (Routes III and IV). While the martensitic length distribution in both the recrystallized grain  $\beta$  structures is more or less same, the thickness of needles is somewhat higher in fine grain  $\beta$  structure. Similarly, though the martensitic

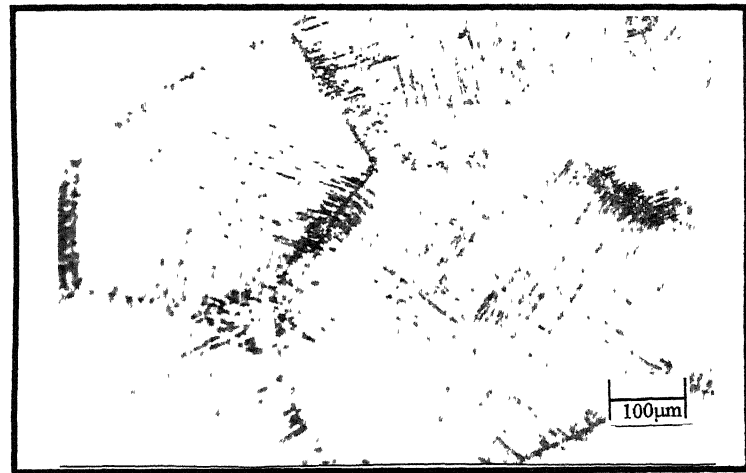


**Figure 4.9** Microstructure of The Sample 60% Deformed at 980°C Followed by Recrystallization Annealing at 960°C for 30 Seconds.

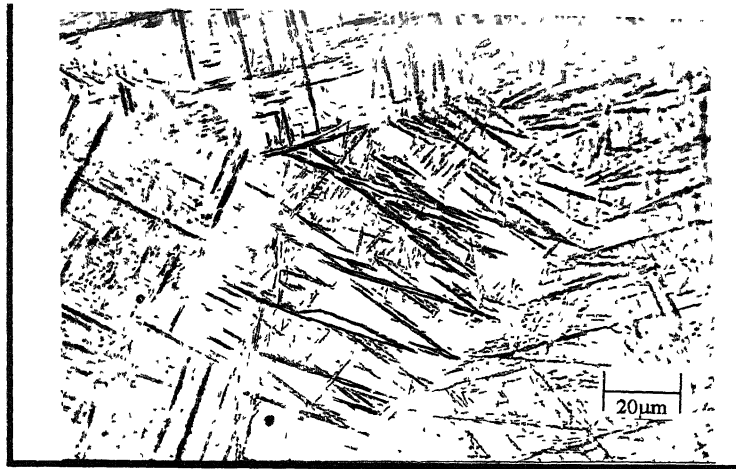


**Figure 4.10(a)** Details of Typical Martensitic Microstructures Obtained After  $\beta$  Processing Through Route II



**Figure 4.10(b)** Details of Typical Martensitic Microstructures Obtained After  $\alpha$  Processing Through Route III



**Figure 4.10(c)** Details of Typical Martensitic Microstructures Obtained After  $\beta$  Processing Through Route IV

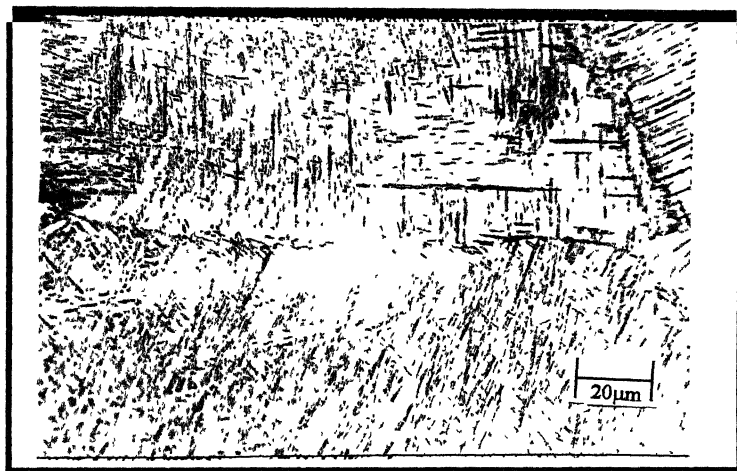


**Figure 4.10(d)** Details of Typical Martensitic Microstructures Obtained After  $\beta$  Processing Through Route V



**Figure 4.10(e)**      Details of Typical Martensitic Microstructures Obtained After  $\beta$  Processing Through Route IV (SEM micrograph)

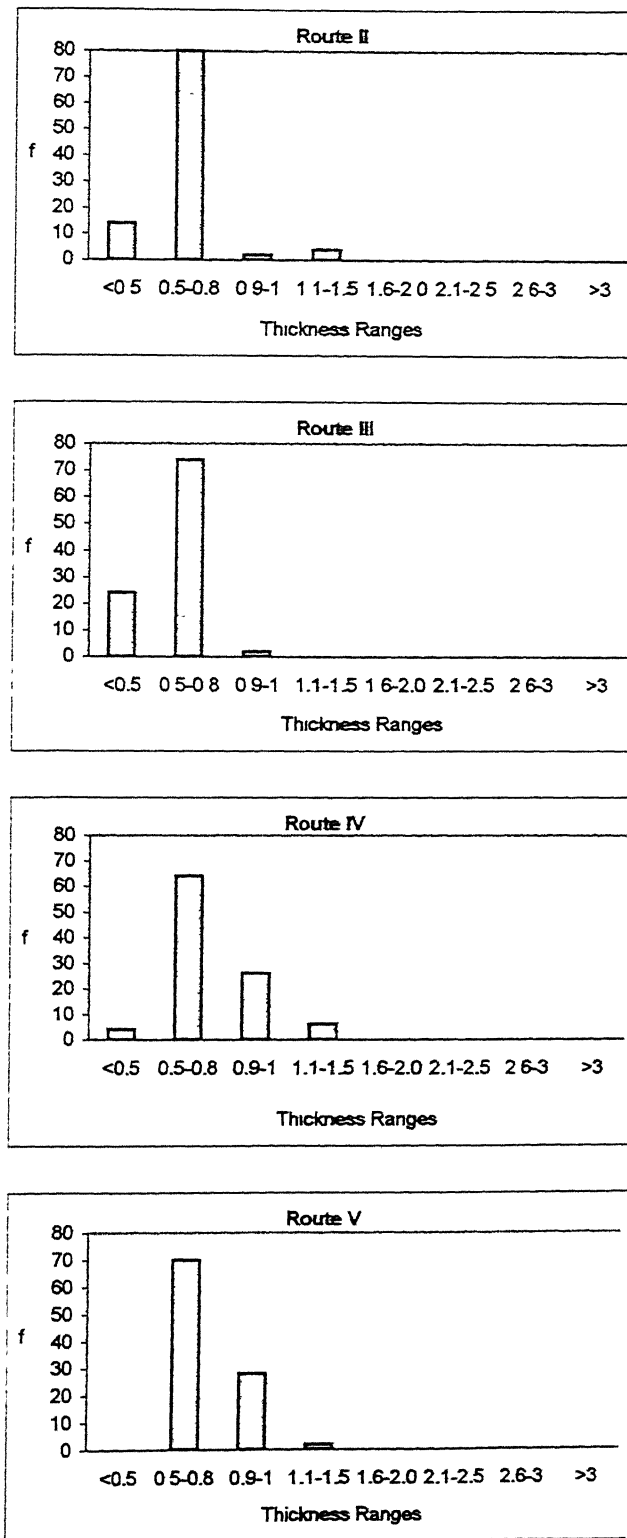


**Figure 4.11(a)      Length Distribution of Martensitic Needles After  $\beta$  Processing for Different Routes**

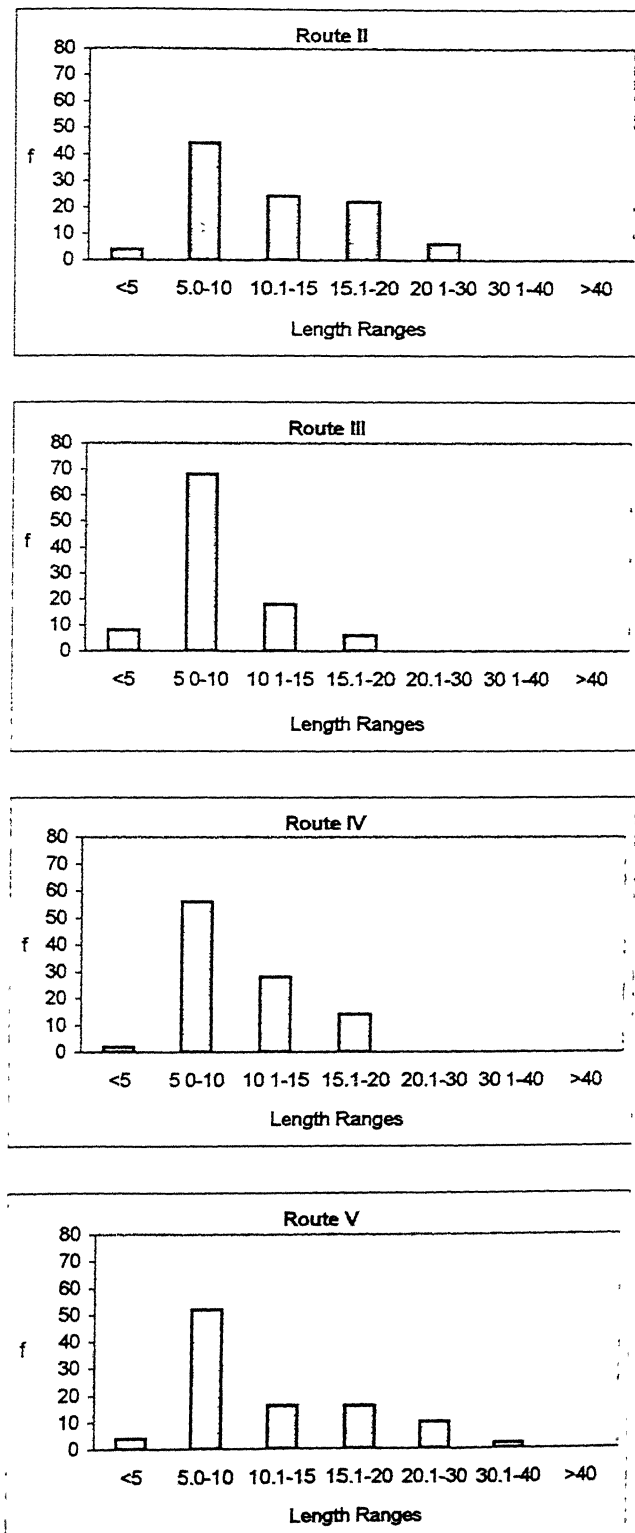


**Figure 4.11(b)** Thickness Distribution of Martensitic Needles After  $\beta$  Processing for Different Routes

length distribution is same for the two pancaked  $\beta$  grain structures, martensitic needles are found to be shorter than those produced in recrystallized  $\beta$  structure. Further, the mean thickness in pancaked  $\beta$  structure is found to be lower for the sample deformed by 30% (Route III), than that deformed by 60% (Route IV).

#### **4.3 EFFECT OF THERMOMECHANICAL PROCESSING IN $(\alpha+\beta)$ PHASE FIELD ON MICROSTRUCTURAL REFINEMENT OF THE ALLOY**

It has already been discussed that the refinement of equiaxed primary  $\alpha$  in  $(\alpha+\beta)$  titanium alloys is essential for their improved superplastic behaviour. As suggested earlier, conditioning of primary  $\alpha$  plates/lamellae in the starting microstructure prior to hot rolling in the  $(\alpha+\beta)$  phase field is of utmost importance. Since primary  $\alpha$  plates/lamellae form as a consequence of transformation of the  $\beta$  phase, their conditioning, in turn, depends on (a) conditioning of  $\beta$  grains, (b) cooling rate during  $\beta$  to  $\alpha$  transformation, (c) cooling rate and temperature of transformation in case  $\beta$  is transformed to  $\alpha'$  or  $\alpha''$  and (d) the temperature of transformation of  $\alpha'$  or  $\alpha''$ , if formed, to  $\alpha$ . Effect of thermo-mechanical processing in altering characteristics of  $\beta$  grains has already been described and discussed in section 4.2. Conventional thermo-mechanical processing routes for  $(\alpha+\beta)$  titanium alloys, involving deformation in the two-phase field, transform  $\beta$  to  $\alpha$  by air cooling. In view of the formation of relatively thick primary  $\alpha$  plates/lamellae under such processing conditions, this approach was not considered in the present study. In contrast, acicular primary  $\alpha$ , which can be obtained by the transformation of  $\alpha'$  or  $\alpha''$  to  $\alpha$  during preheating to hot rolling temperature, is known to be of considerably lower thickness and a higher aspect ratio [96]. However specific morphological features of acicular  $\alpha$  are expected to depend on morphological

## Chapter 4: Results and Discussion

features of  $\alpha'$  or  $\alpha''$ , which, in turn, are expected to depend on conditioning of  $\beta$  grains. Thus, the acicular  $\alpha$  structure, obtained during preheating for hot rolling in specimens differently processed in the  $\beta$  phase field, i.e. by routes I to V, was hot rolled in the  $(\alpha+\beta)$  phase field by giving the thickness reduction of 70% after soaking at 860°C, i.e. about 90°C below the  $\beta$ -transus. The effect of  $(\alpha+\beta)$  working on samples earlier treated by different  $\beta$  processing schedules on the refinement of structure in Ti-6-4 alloy is described and discussed in the present section.

### **4.3.1 Effect of Cooling Rate on The Structure**

In order to compare the effect of cooling rate from above the  $\beta$ -transus, on the structure of the alloy, two sets of samples were soaked at 980°C for 20 minutes and were subsequently (a) furnace cooled and (b) water quenched from the soaking temperature. Martensitic structure of samples water quenched from 980°C has already been shown in Figure 4.7(e). Figure 4.12 shows the microstructures of the furnace-cooled sample. As expected, furnace cooling from above the  $\beta$ -transus produced the equilibrium  $(\alpha+\beta)$  Widmanstatten structure showing the typical basket-weave pattern of the  $\alpha$  and  $\beta$  phases.

### **4.3.2 Type of Martensite Formed As A Function of Processing**

It has been shown in Section 4.1.4 that the water quenching of Ti-6-4 alloy from the  $\beta$  phase field lead to the transformation of the  $\beta$  phase to a mixture of  $\alpha'$  and  $\alpha''$  with  $\alpha''$  being the major constituent. In order to find out whether or not thermo-mechanical processing of the alloy in  $(\alpha+\beta)$  phase field has any effect, samples after the last rolling pass in the  $(\alpha+\beta)$  phase field were quenched in water and were subjected to the XRD test. XRD patterns obtained from Route I to Route V are shown in Figures 4.13 to 4.17. It is to be noted that while samples obtained by Route I ( $\beta$  annealing followed by



**Figure 4.12 Equilibrium ( $\alpha+\beta$ ) Widmanstätten Structure as Obtained From Samples Processed Through Route I After Stage I**

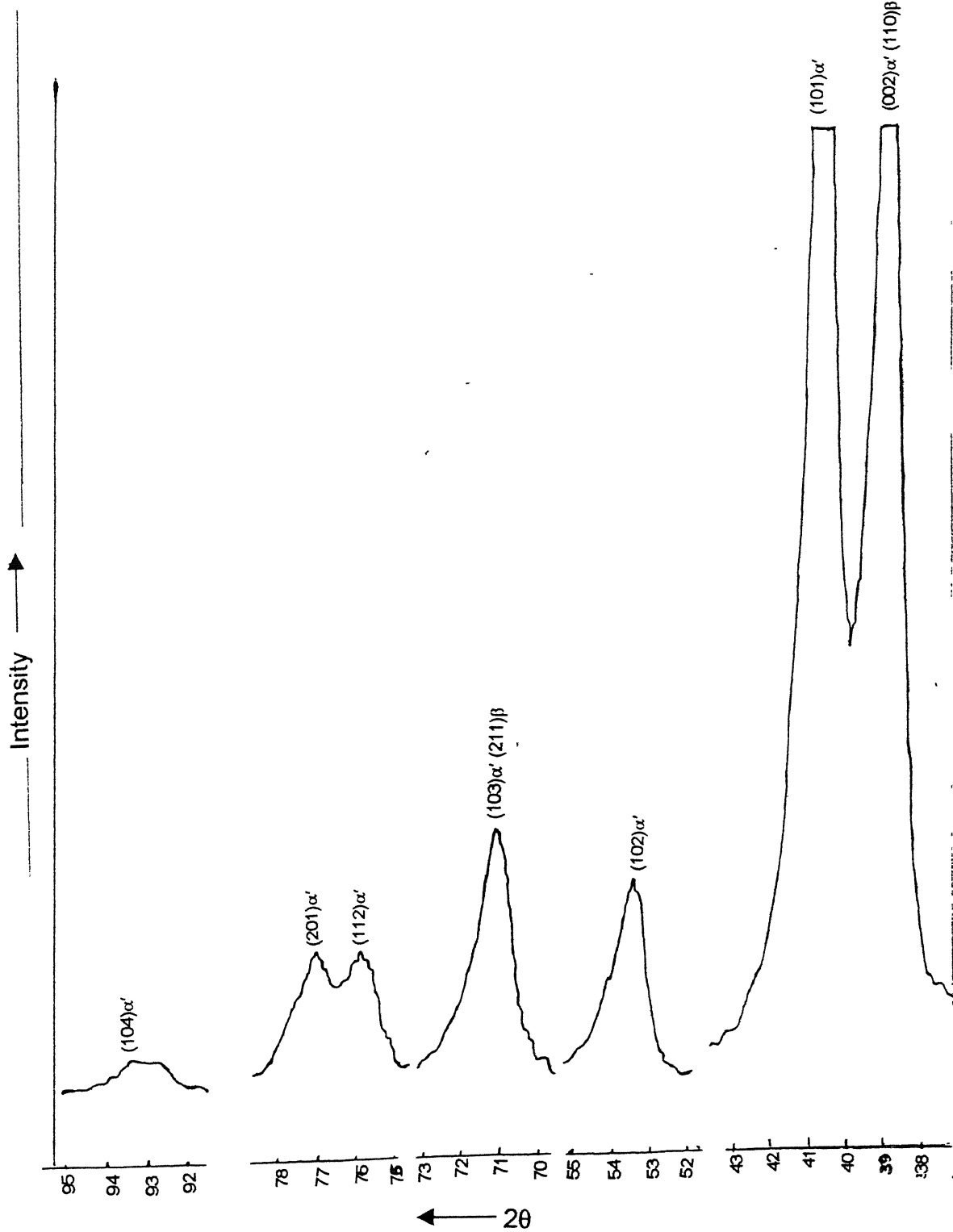


Figure 4.13 XRD Pattern of the Sample Treated Through Route 1

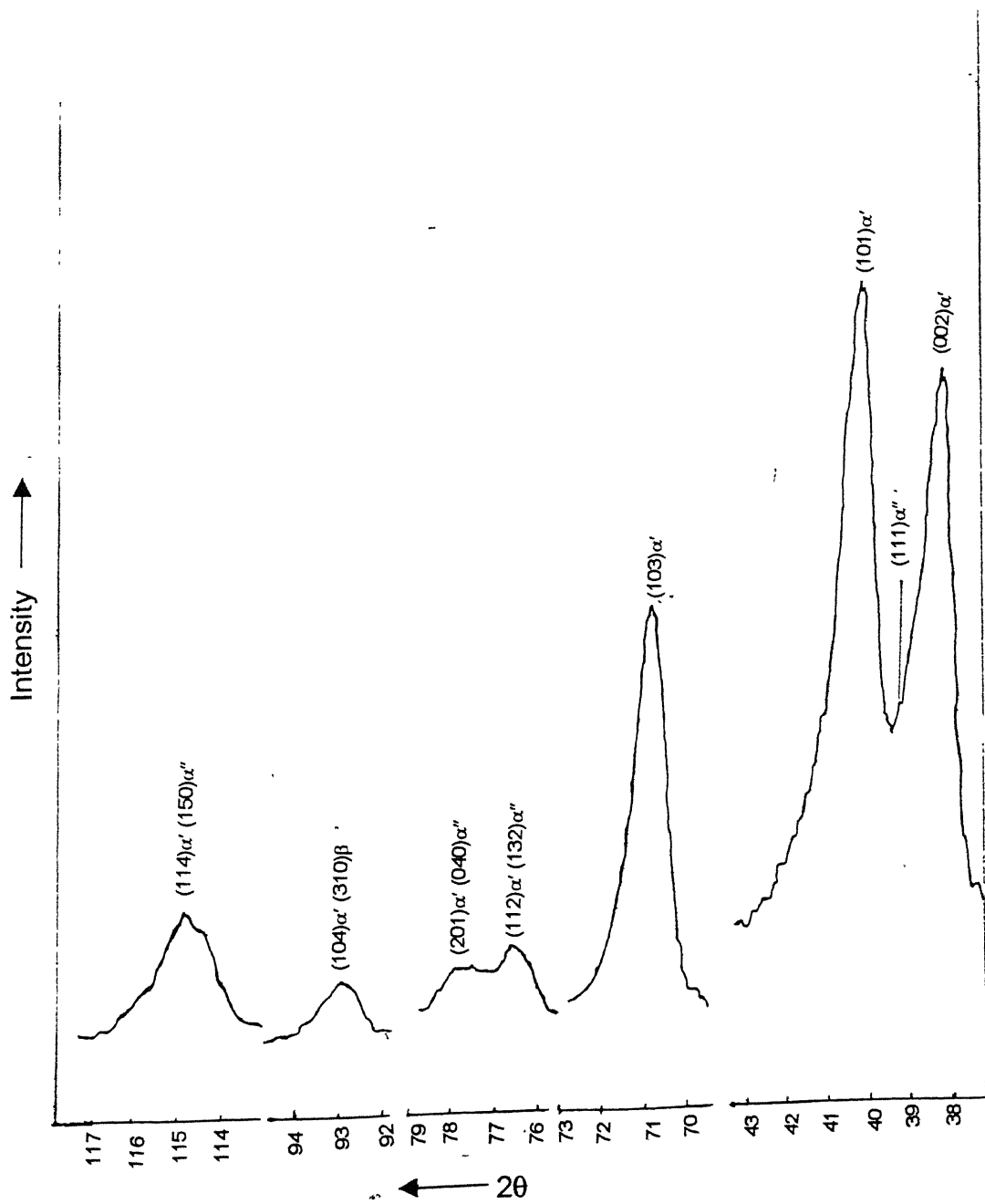


Figure 4.14 XRD Pattern of the Sample Treated Through Route 2

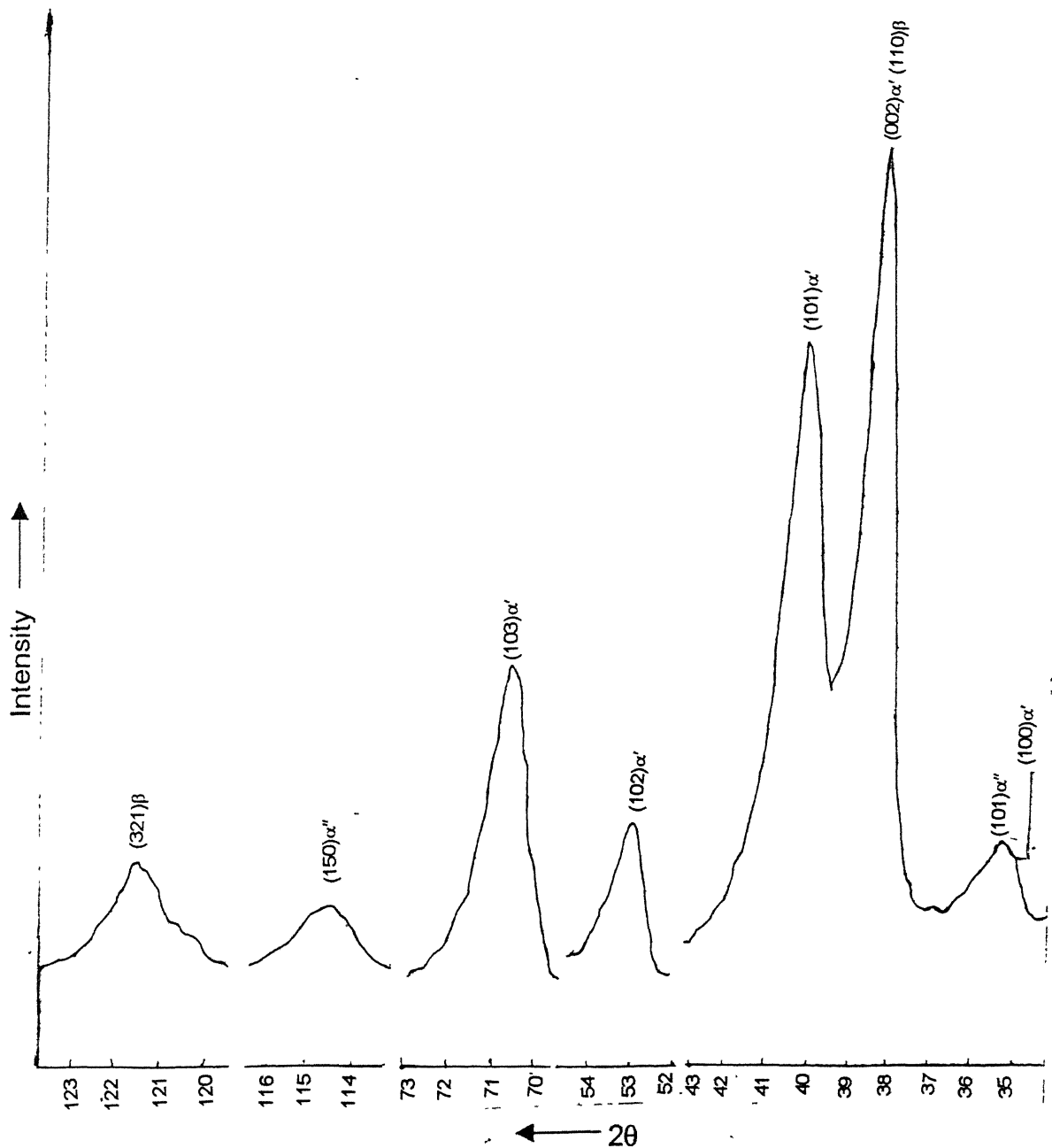


Figure 4.15 XRD Pattern of the Sample Treated Through Route 3

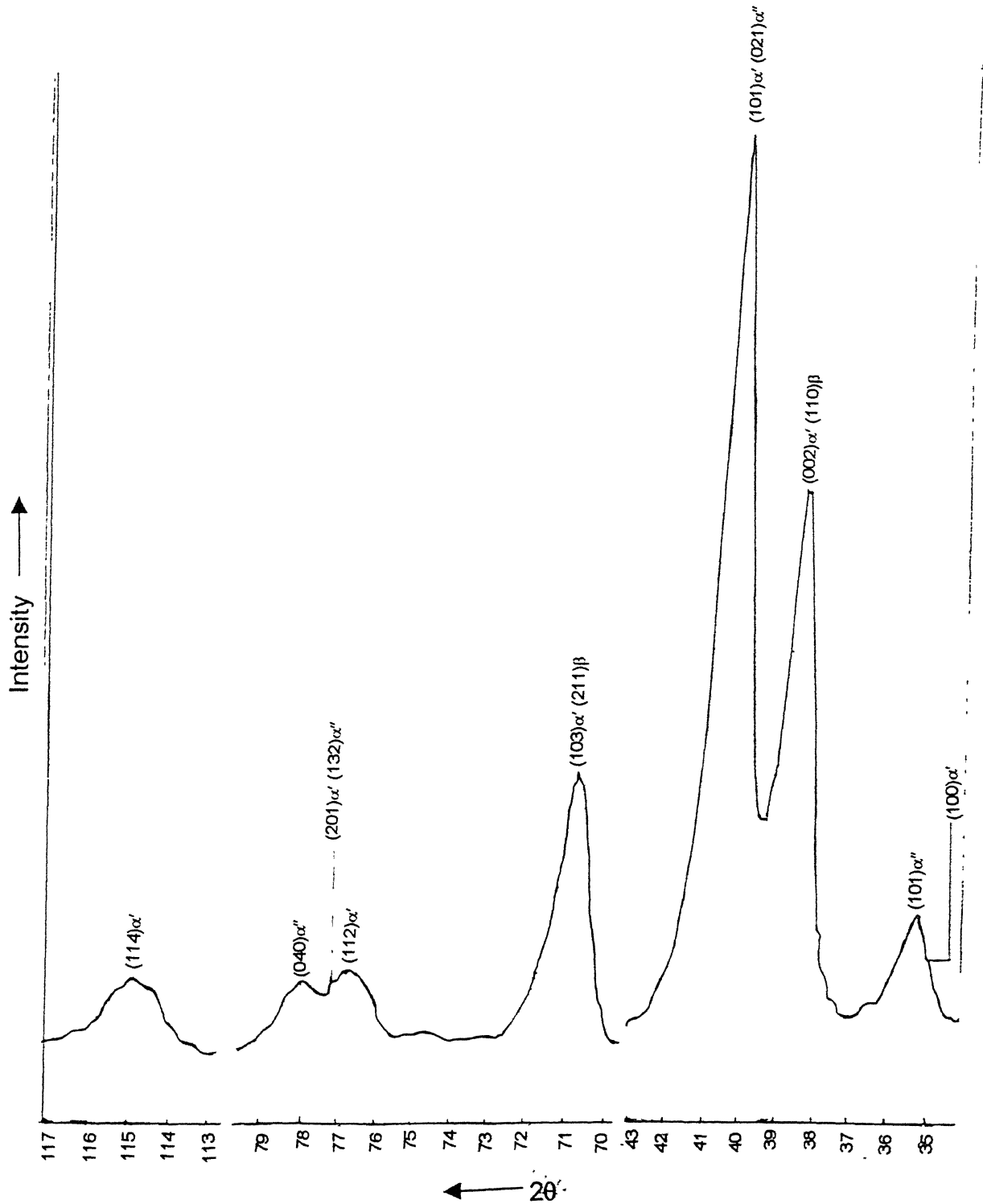


Figure 4.16 XRD Pattern of the Sample Treated Through Route 4

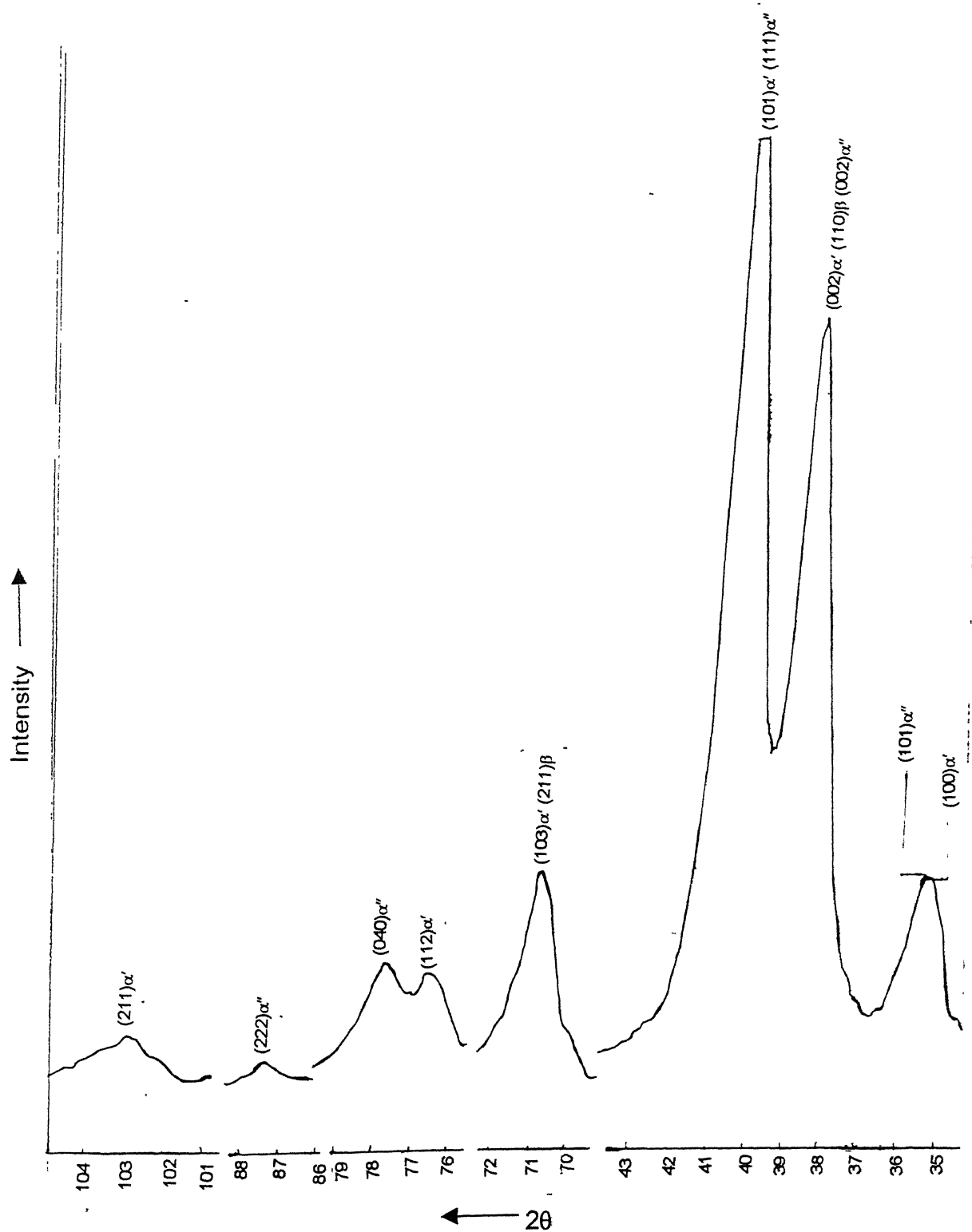


Figure 4.17 XRD Pattern of the Sample Treated Through Route 5

furnace cooling) did not show the orthorhombic martensite, i.e.  $\alpha''$ , in the water-quenched state after working in  $(\alpha+\beta)$  phase field, the samples obtained from all other processing routes, i.e. routes II-V, showed the presence of both orthorhombic as well as hexagonal martensites,  $\alpha'$  and  $\alpha''$ . It is to be noted that while the starting structure in routes II-V before rolling in the  $(\alpha+\beta)$  phase field was obtained by water quenching from the  $\beta$  phase field, that in Route I did not involve with water quenching from the  $\beta$  phase field. The presence of orthorhombic martensite in all the samples rolled by route II-V but not in those processed by Route I, gives an indirect indication that the orthorhombic martensite forms after water quenching from  $\beta$  phase field and not when the Ti-6-4 alloy is quenched from  $(\alpha+\beta)$  phase field.

#### **4.3.3 Effect of Conditioning of $\beta$ Grains on Microstructural Refinements After Rolling in Two-Phase Field**

Microstructures of samples after rolling in the two-phase field are shown in Figure 4.18. It is observed that all the microstructures show very fine  $\alpha$  homogeneously distributed in the  $\beta$  matrix. The variations in length and thickness distributions of the  $\alpha$  lamellae and their mean aspect ratio and length as function of different processing routes are shown in Figures 4.19 - 4.22. It is observed that the minimum aspect ratio is exhibited by the sample processed through route II, but sample processed through route IV exhibits minimum length of  $\alpha$  lamellae. The thickness, on the other hand, is minimum for the sample processed through route V.

#### **4.4 EFFECT OF RECRYSTALLIZATION ANNEALING TREATMENT ON THE EVOLUTION OF EQUIAXED $\alpha$ STRUCTURE ON THERMO-MECHANICALLY PROCESSED Ti-6-4 ALLOY**

Microstructure of two-phase titanium alloys after their working in the  $(\alpha+\beta)$  phase field consists of either fragmented  $\alpha$  plates or  $\alpha$  plates which

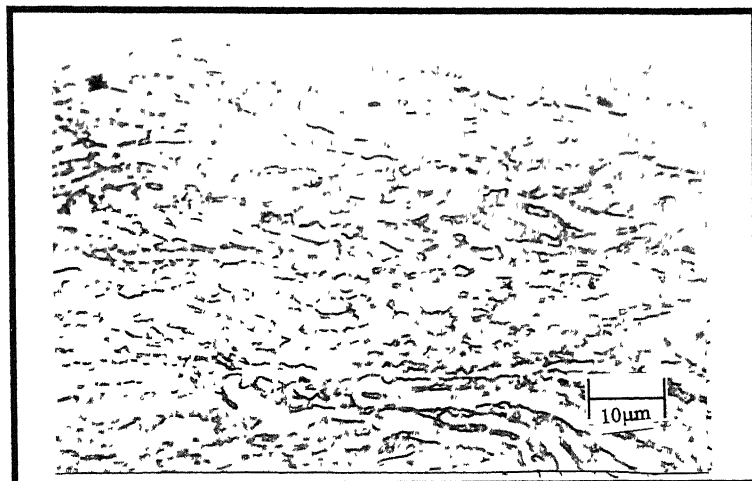


**Figure 4.18(a)** Microstructure of the Sample Processed Through Route I After ( $\alpha+\beta$ ) Rolling

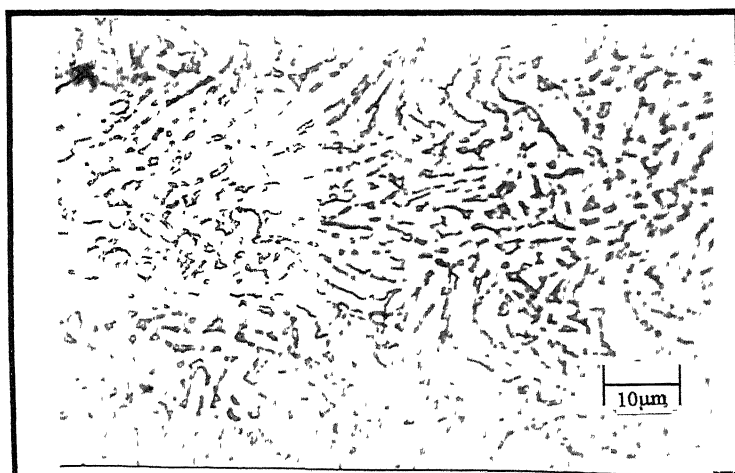


**Figure 4.18(b)** Microstructure of the Sample Processed Through Route II After ( $\alpha+\beta$ ) Rolling



**Figure 4.18(c)** Microstructure of the Sample Processed Through Route III After ( $\alpha+\beta$ ) Rolling

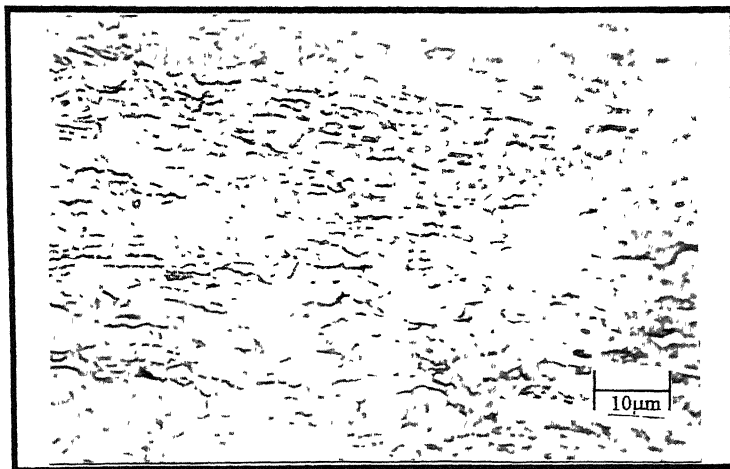


**Figure 4.18(d)** Microstructure of the Sample Processed Through Route IV After  $\alpha+\beta$  Rolling

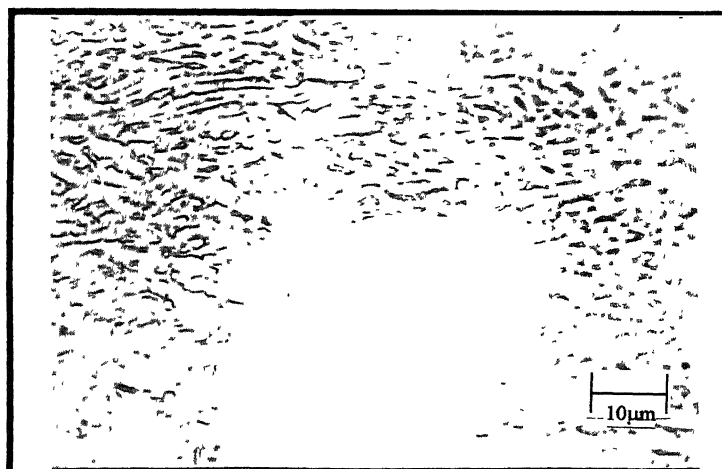


**Figure 4.18(e)** Microstructure of the Sample Processed Through Route V After  $\alpha+\beta$  Rolling

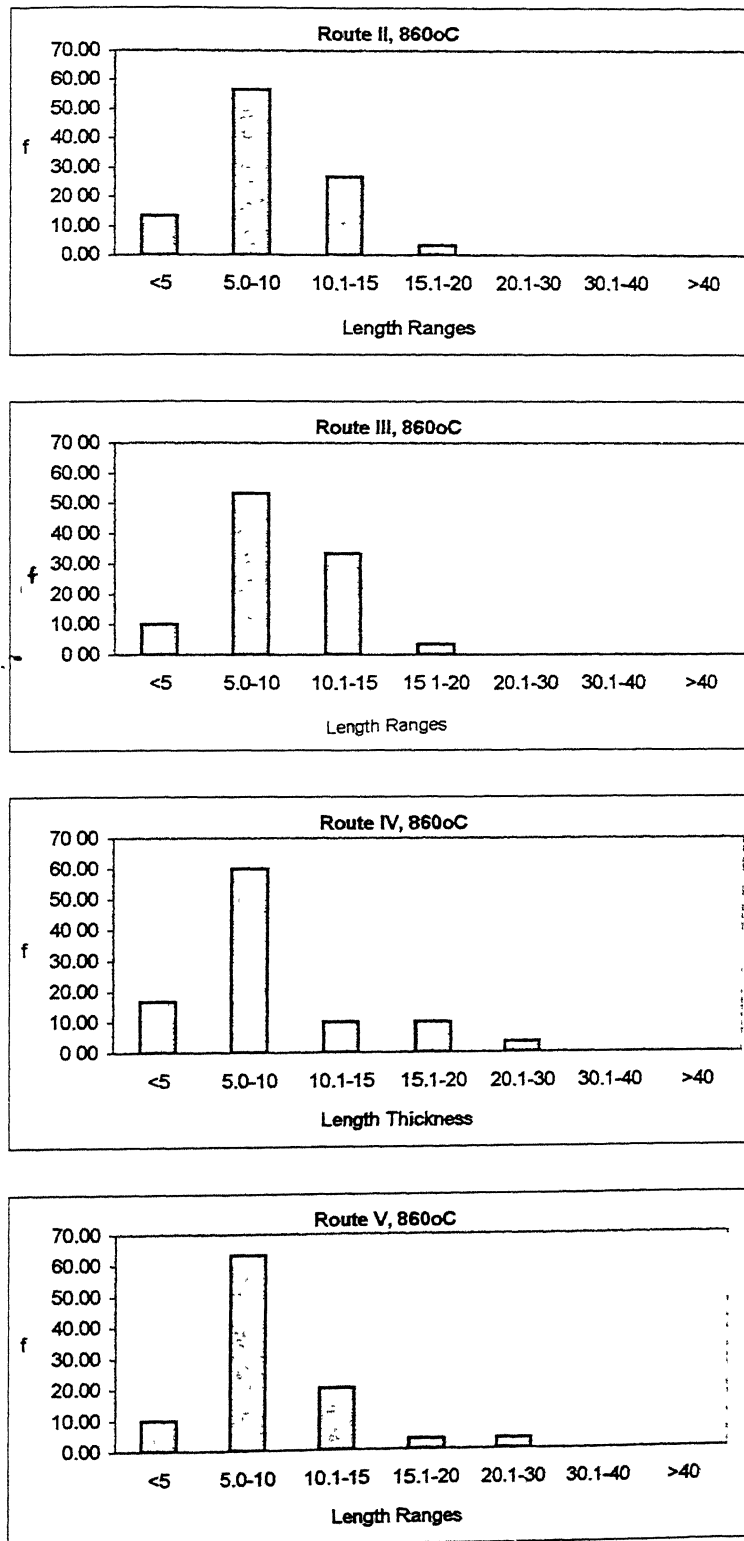


**Figure 4.19 Length Distribution of  $\alpha$  Lamellae After Stage II for Different Routes**

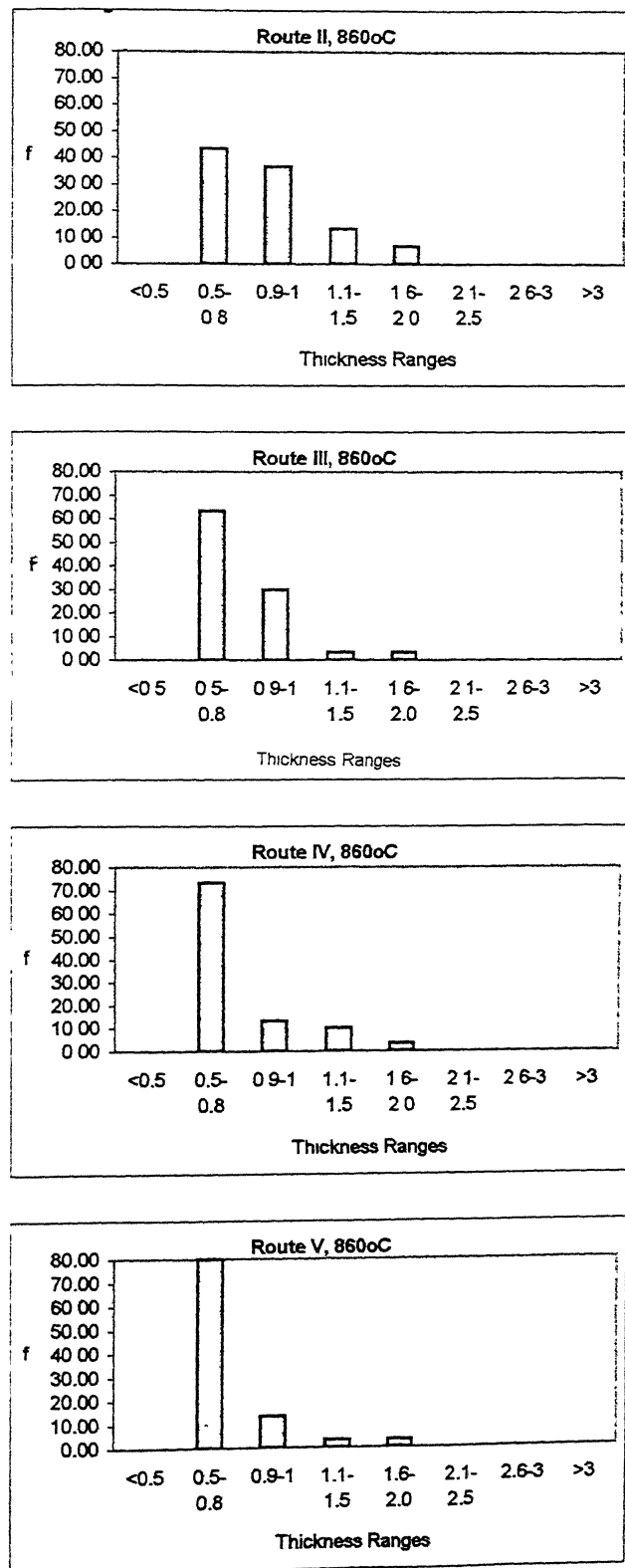


**Figure 4.20 Thickness Distribution of  $\alpha$  Lamellae After Stage II for Different Routes**

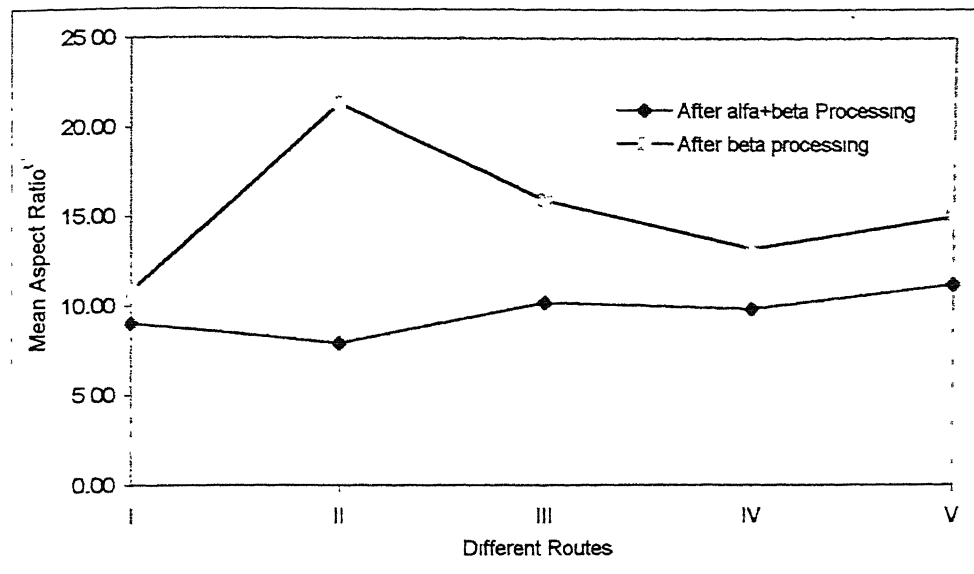


Figure 4.21 Mean Asr ect Ratio of  $\alpha$  Lamellae for Different Routes

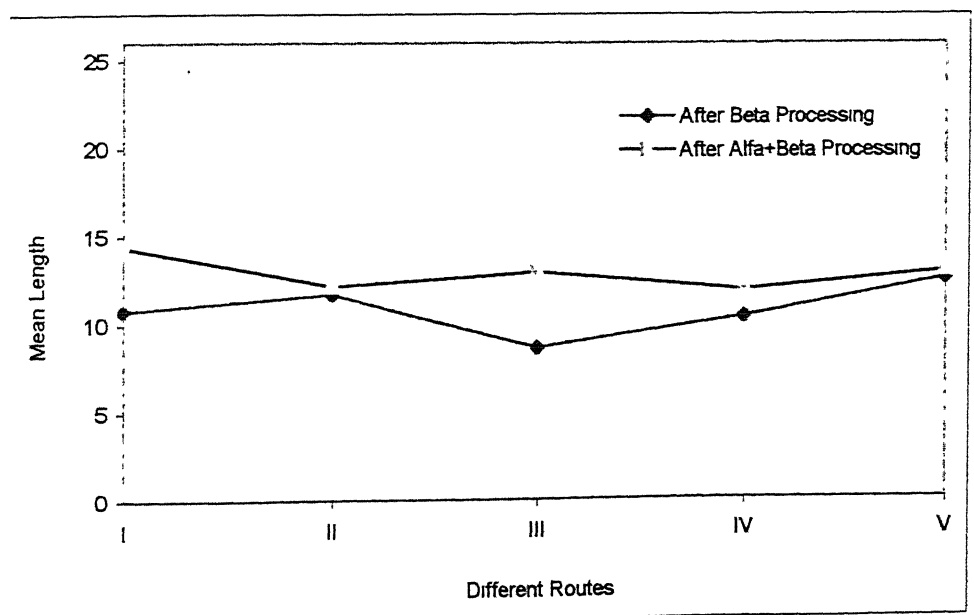


Figure 4.22 Mean Length of  $\alpha$  Lamellae for Different Routes

have undergone moderate-to-high plastic deformation. Many of these plates contain low and high angle  $\alpha/\alpha$  boundaries or shear bands across  $\alpha$  plates/lamellae. The morphology of the  $\alpha$  phase in the as-deformed structure may be altered if the structure is subjected to recrystallization annealing in the  $(\alpha+\beta)$  phase field. It has been proposed that the break-up of  $\alpha$  lamellae into low aspect ratio grains occurs by either of the two processes: (1) penetration of the  $\beta$  phase from the opposite sides to complete the fragmentation of  $\alpha$  phase or (2) formation of fresh high-angle  $\alpha/\alpha$  boundaries by the elimination of low-angle boundaries and sub-structure rotation followed by the penetration of the  $\beta$  phase.

The conventional thermo-mechanical processing of two-phase titanium alloys therefore consists of post-deformation recrystallization annealing in the  $(\alpha+\beta)$  phase field. This treatment essentially transforms the lamellar  $\alpha$  structure to an low-aspect ratio one. In the present study various thermo-mechanically processed samples were subjected to recrystallization annealing at three different temperatures, namely 700°C, 800°C and 850°C i.e. 250°C, 150°C and 100°C below the  $\beta$ -transus respectively for a period of 30 minutes. The effect of recrystallization temperature on the morphology and size of the  $\alpha$  grains are discussed in the present section.

#### **4.4.1 Effect of Recrystallization Temperature on the Evolution of Low Aspect Ratio $\alpha$ Morphology in Ti-6-4 alloy**

Microstructures of the alloy processed through Route III and recrystallized at 700°C, 800°C and 850°C for the annealing time of 30 minutes are shown in Figure 4.23. It is observed from these micrographs that the aspect ratio of  $\alpha$  lamellae decreased and the volume fraction of low aspect  $\alpha$  grains increased as the temperature of recrystallization in the two-phase field increased. Such a trend was observed in all the samples processed through routes I to V after their recrystallization. The aspect ratio distribution for the samples treated through routes I to V after their recrystallization at different

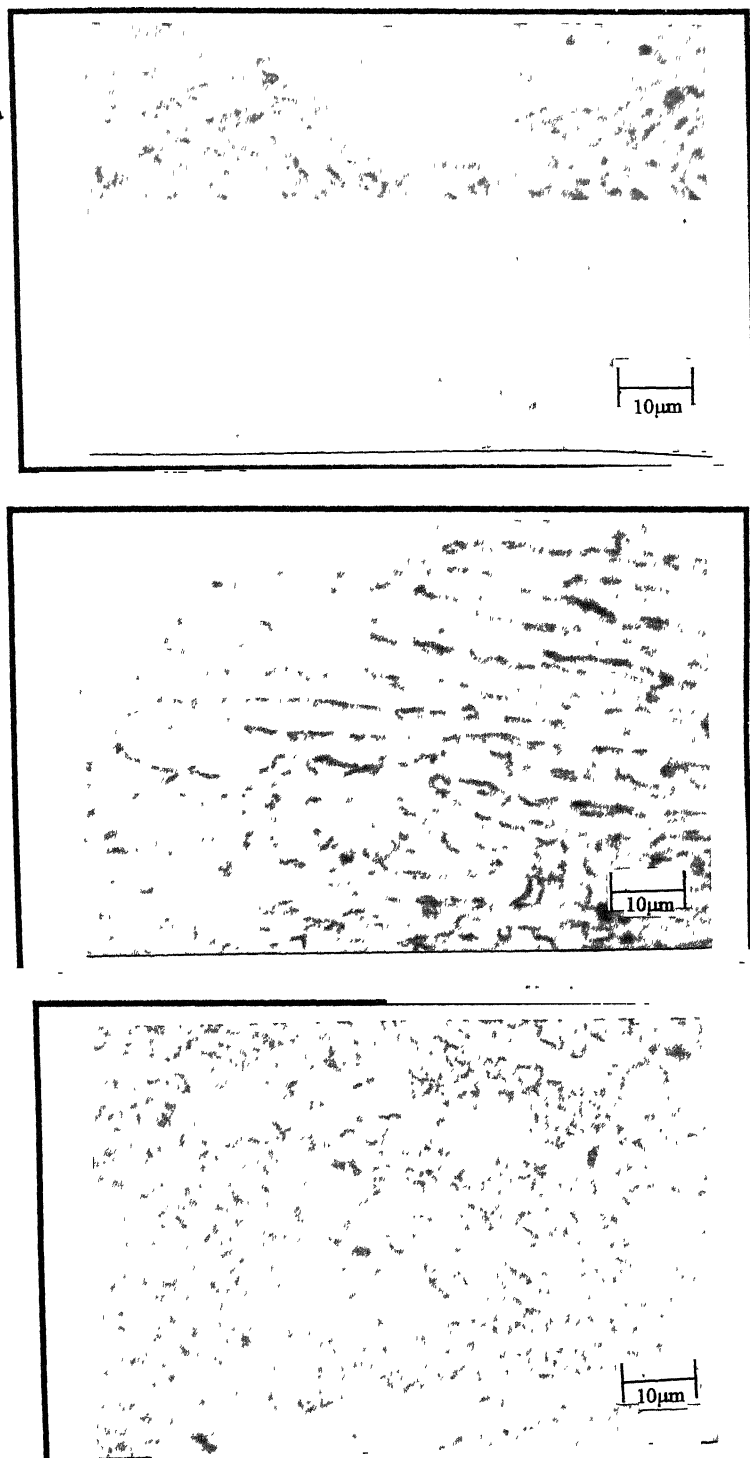


**Figure 4.23 Microstructures of Samples Processed Through Route III and Recrystallized for 30 Minutes at (a) 700°C, (b) 800°C and 850°C**

annealing temperatures are presented in Figure 4.24(a) to (e). These figures clearly indicate that the amount of lower aspect ratio  $\alpha$  grains increased with increasing temperature of recrystallization and was found to be the highest, in all the cases, at 850°C.

#### **4.4.2 Effect of Recrystallization Temperature on the $\alpha$ Grain Size**

The mean size and size distribution of  $\alpha$  grains are known to affect the superplastic behaviour of two-phase titanium alloys. As  $\alpha$  grains present in the alloy after its recrystallization annealing contained some grains of aspect ratio  $> 5$ , the size of  $\alpha$  grains was estimated to be that of equivalent sphere by the projected area diameter method [107]. Figures 4.25(a) to (e) show the grain size distribution of  $\alpha$  grains in Ti-6-4 processed through routes I to V. It is clear that the volume fraction of grains of smaller size increased with increasing the recrystallization temperature.

#### **4.5 SUPERPLASTIC BEHAVIOUR OF THERMO-MECHANICALLY PROCESSED Ti-6-4 ALLOY**

As discussed earlier, for achieving improved superplastic properties in  $(\alpha+\beta)$  titanium alloys, both primary as well as secondary  $\alpha$  phase morphology should be controlled through thermo-mechanical processing. It has been pointed out [59] that not only the deformation mechanism, but also the dynamics of grain boundary dislocation activity get altered, if grains are elongated rather than equiaxed.

As discussed in Section 4.4, the following microstructural states in different processing routes were achieved at different stages.

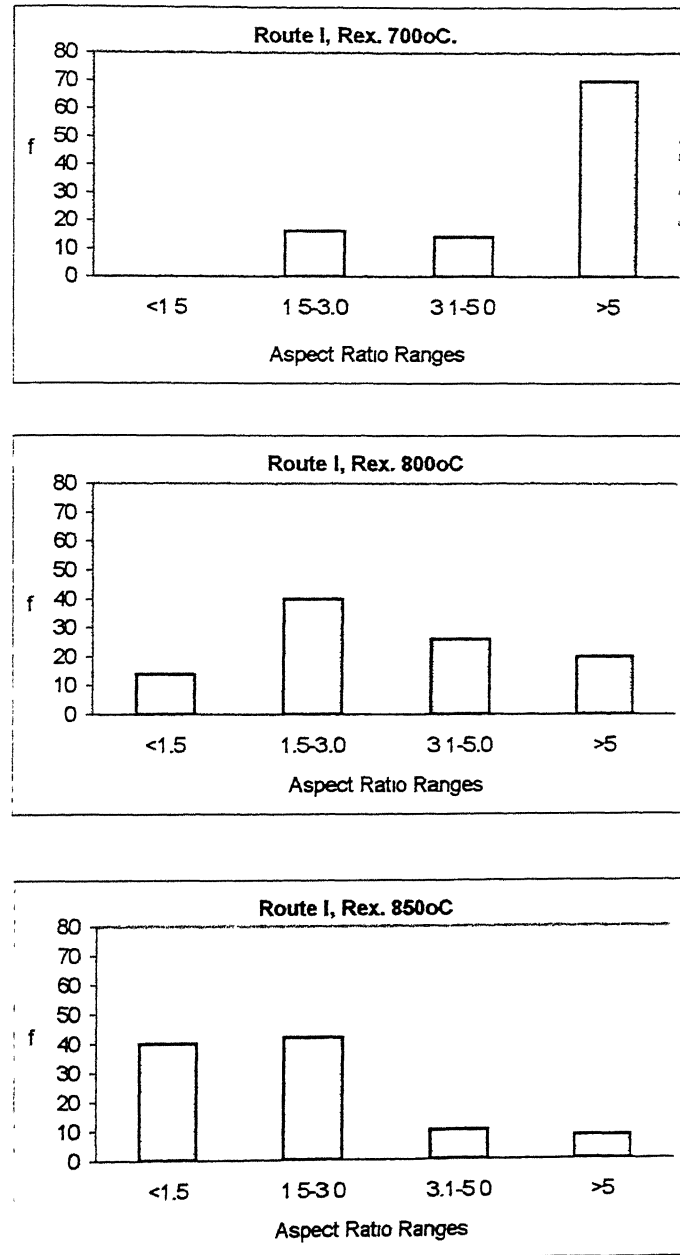


**Figure 4.24(a)      Aspect Ratio Distribution of Samples processed**  
**Through Route I and Recrystallized at Different**  
**Temperatures (as Mentioned In the Figures)**

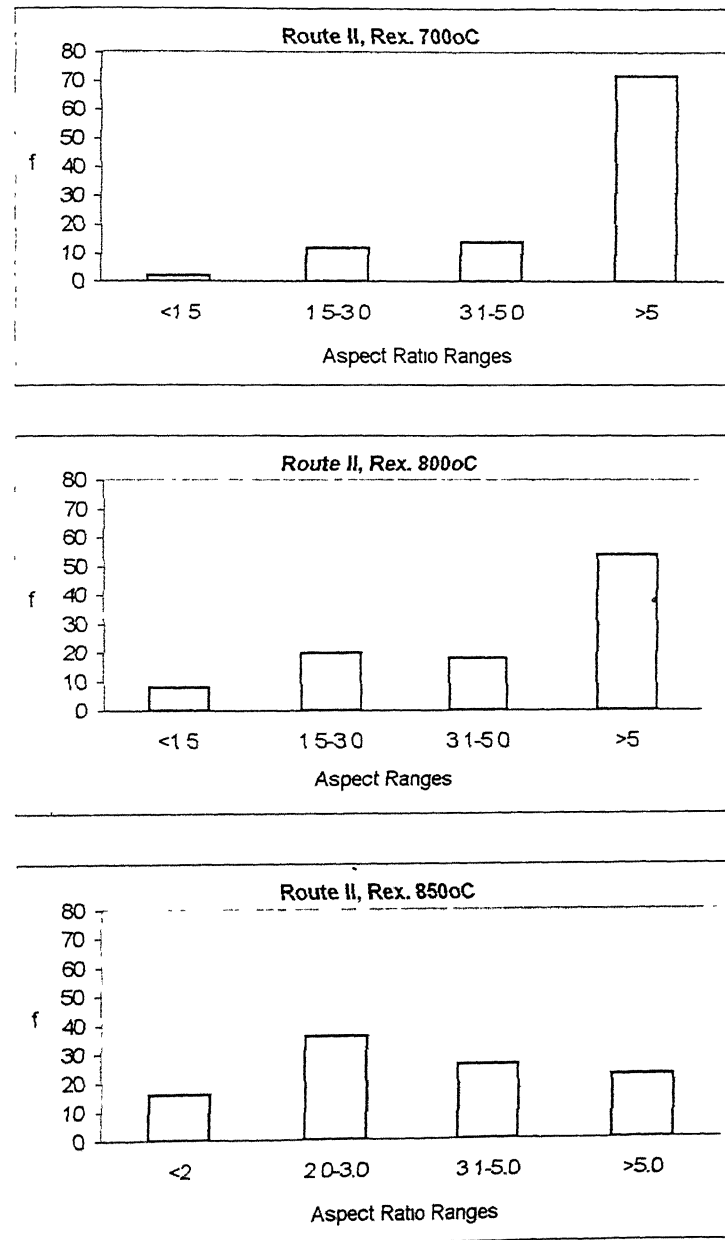


**Figure 4.24(b)      Aspect Ratio Distribution of Samples processed Through Route II and Recrystallized at Different Temperatures (as Mentioned in the Figures).**

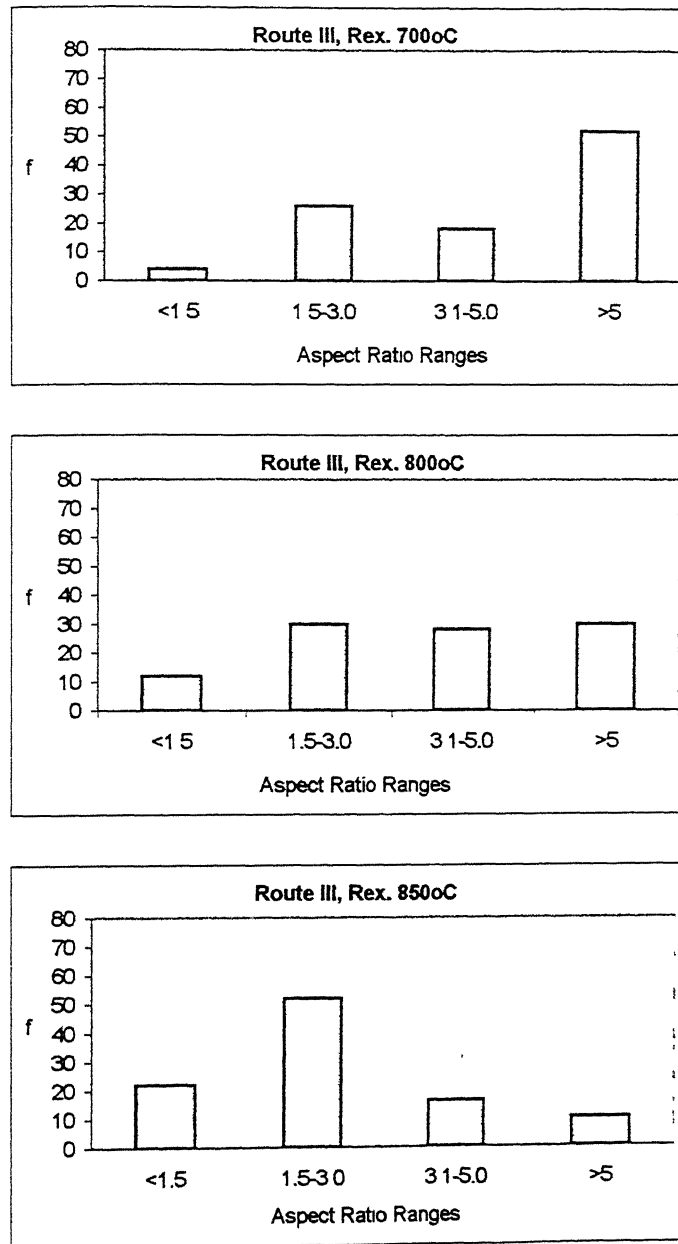


**Figure 4.24(c)      Aspect Ratio Distribution of Samples processed Through Route III and Recrystallized at Different Temperatures (as Mentioned In the Figures)**

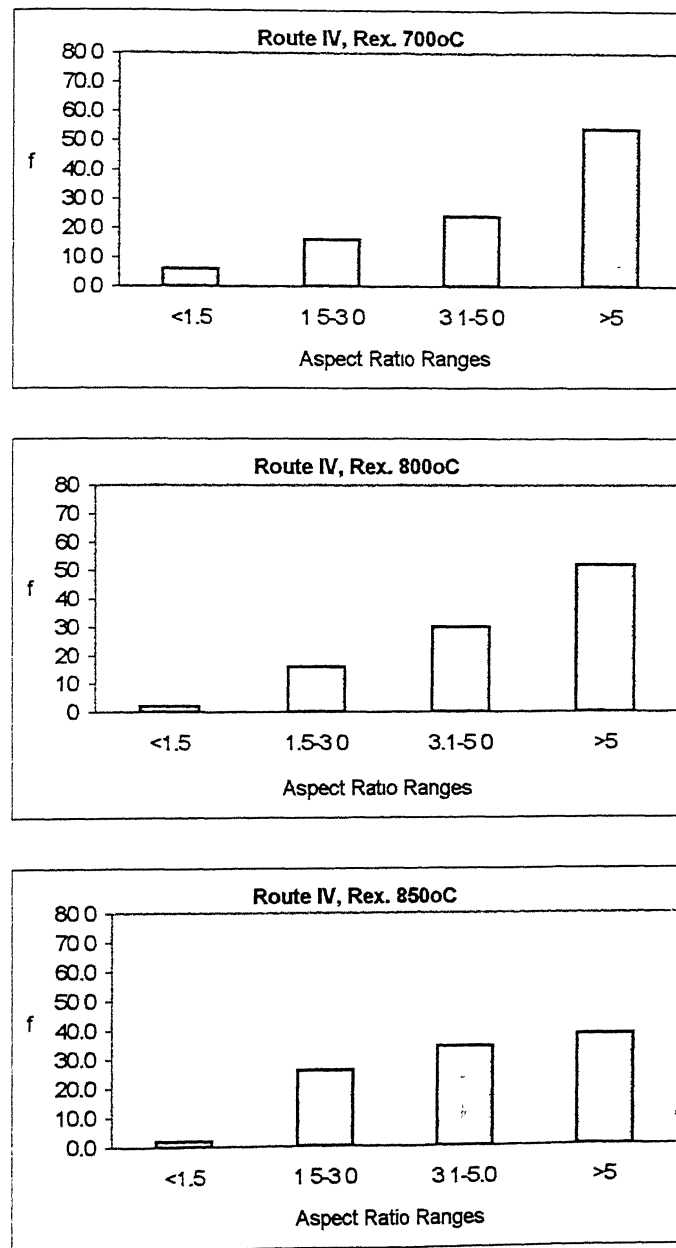


Figure 4.24(d)

Aspect Ratio Distribution of Samples processed Through Route IV and Recrystallized at Different Temperatures (as Mentioned In the Figures)

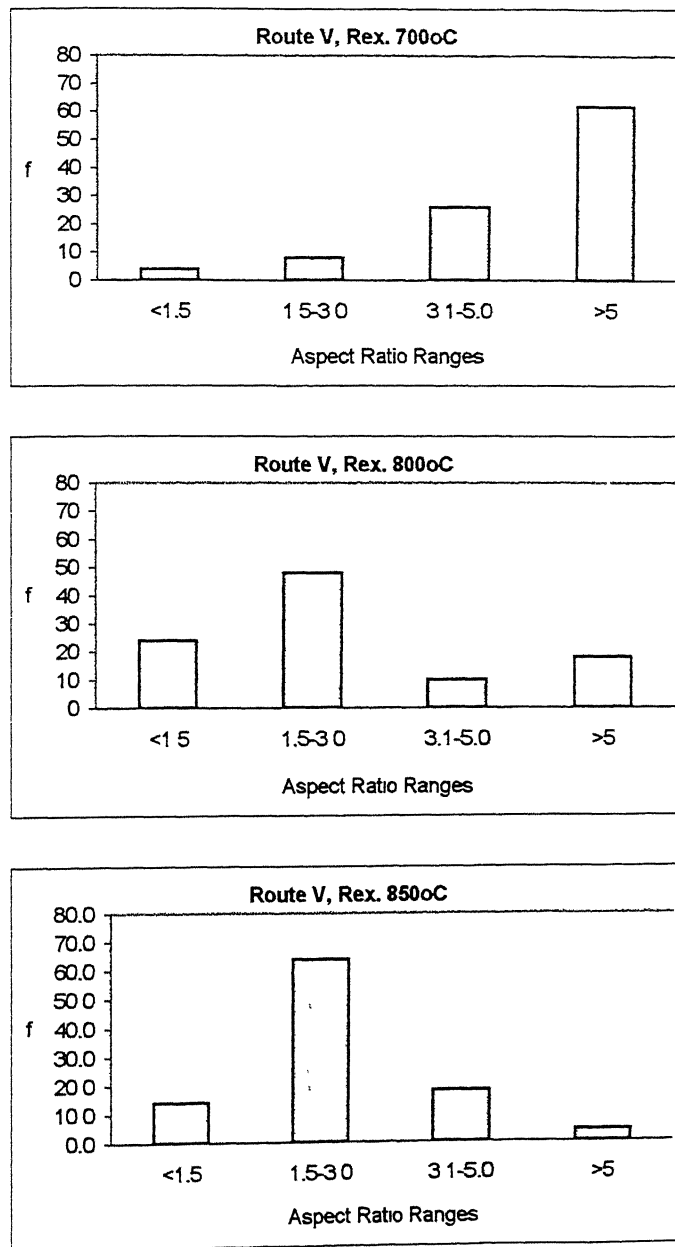
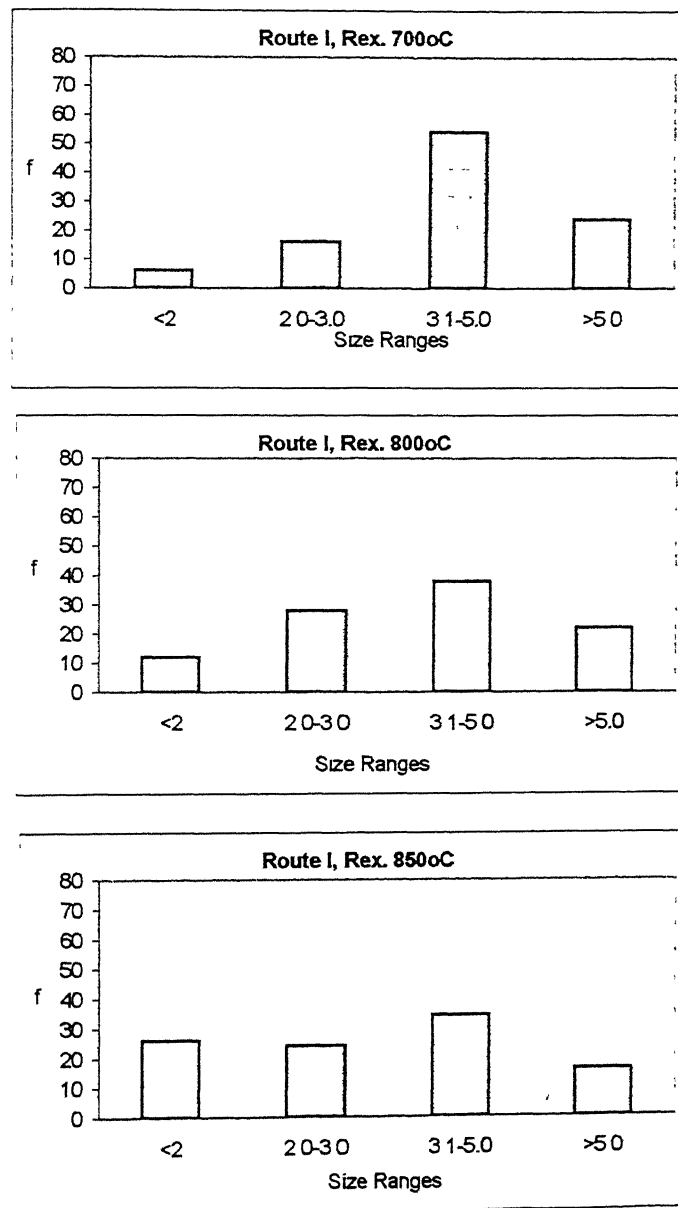
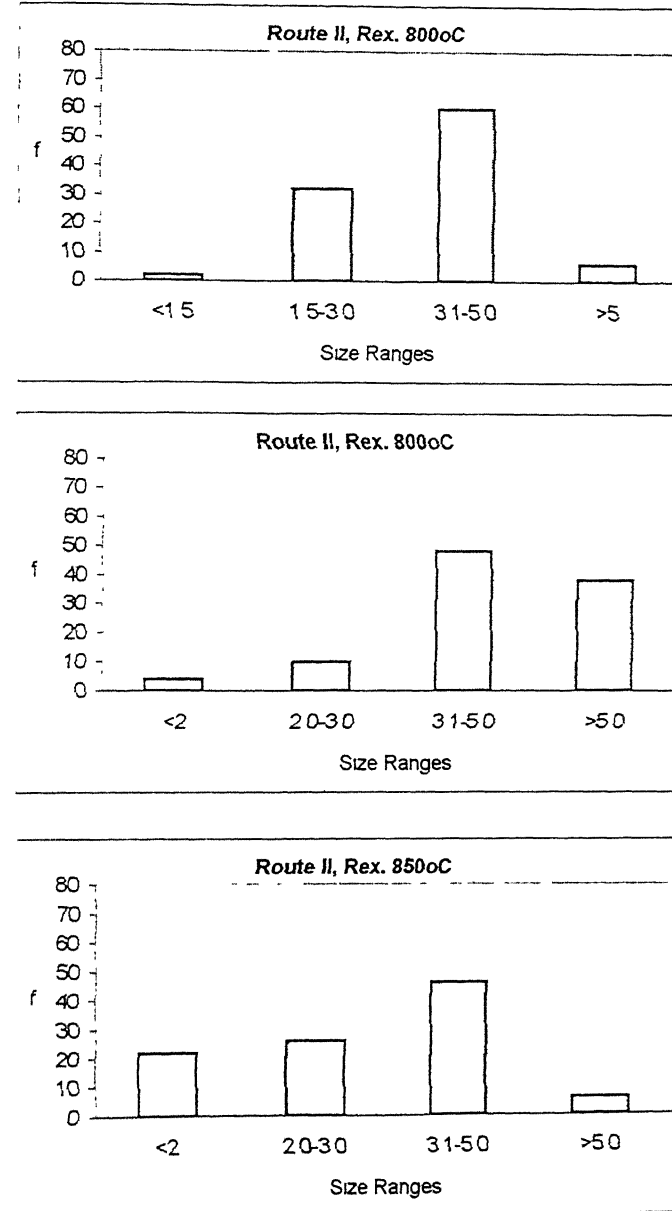


Figure 4.24(e)

**Aspect Ratio Distribution of Samples processed Through Route V and Recrystallized at Different Temperatures (as Mentioned in the Figures)**



**Figure 4.25(a)      Grain Size Distribution of Samples processed  
Through Route I and Recrystallized at Different  
Temperatures (as Mentioned In the Figures)**



**Figure 4.25(b)** Grain Size Distribution of Samples processed Through Route II and Recrystallized at Different Temperatures (as Mentioned In the Figures)

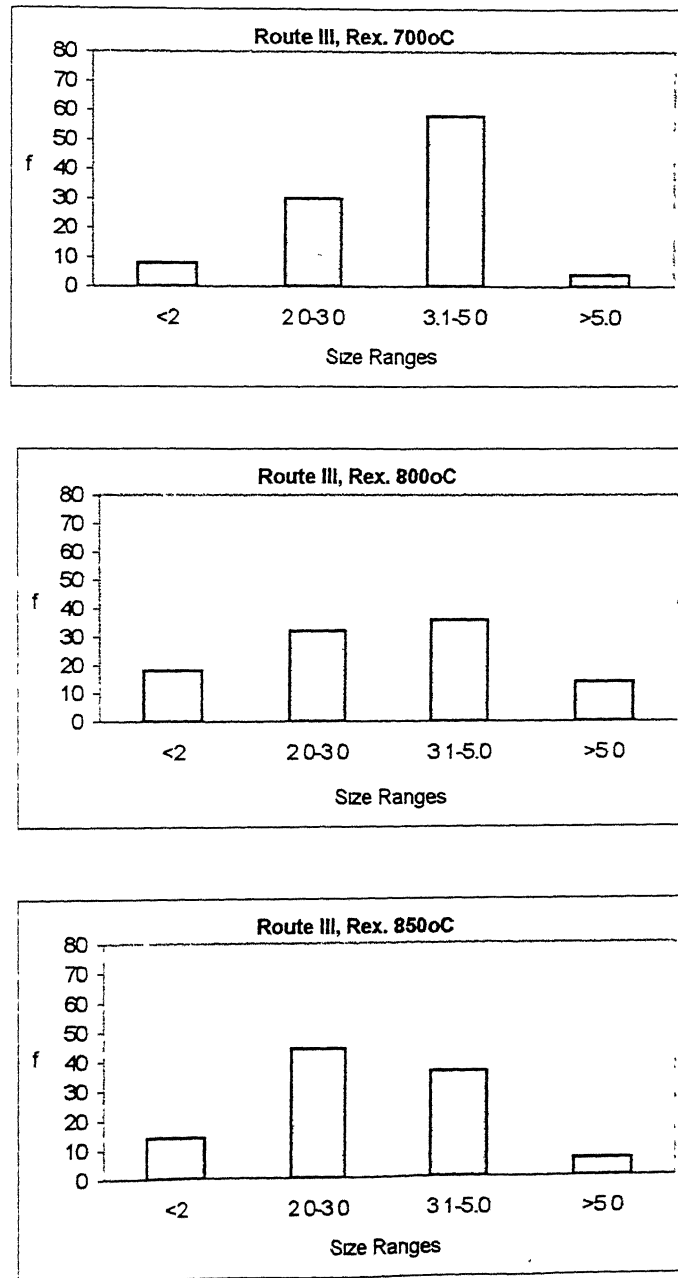


|Figure 4.25(c)      Grain Size Distribution of Samples processed  
Through Route III and Recrystallized at Different  
Temperatures (as Mentioned in the Figures)

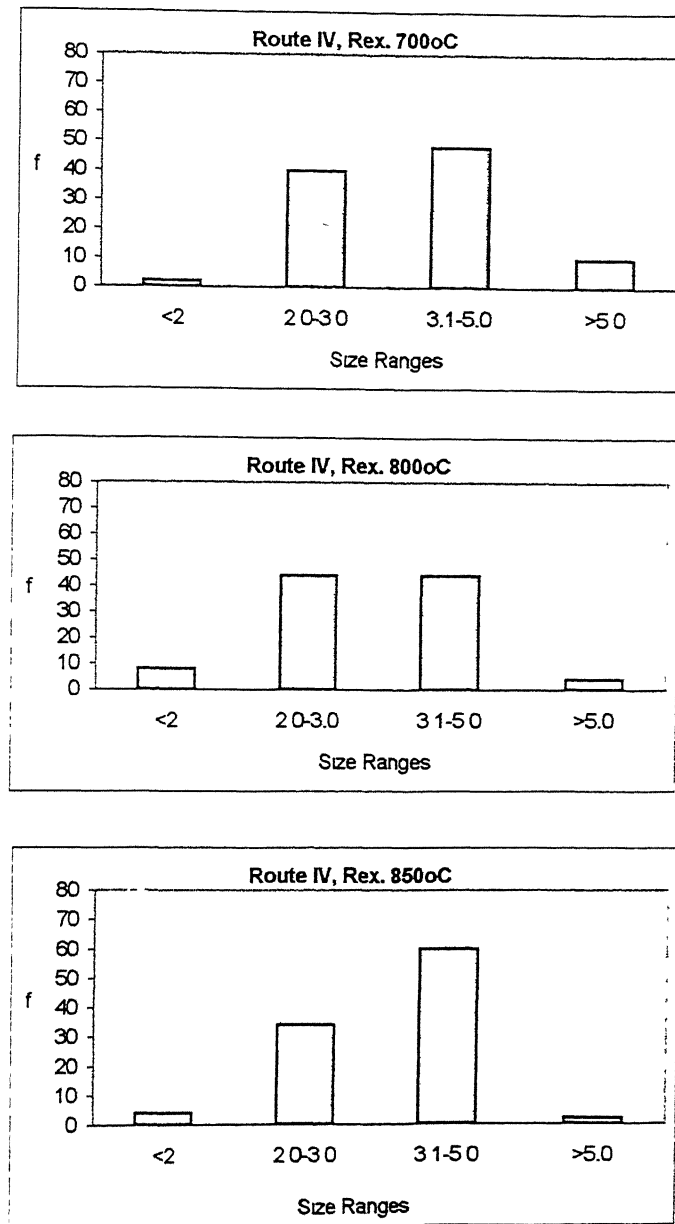


**Figure 4.25(d)      Grain Size Distribution of Samples processed**  
**Through Route IV and Recrystallized at Different**  
**Temperatures (as Mentioned In the Figures)**

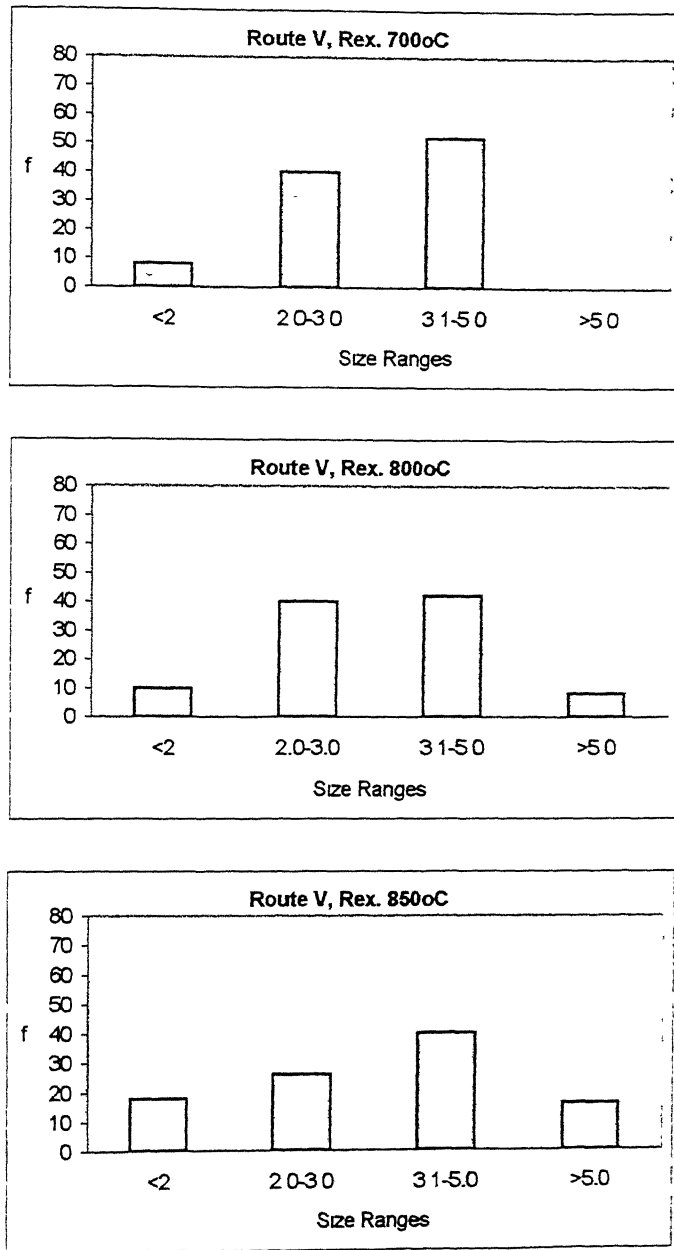


**Figure 4.25(e)      Grain Size Distribution of Samples processed**  
**Through Route V and Recrystallized at Different**  
**Temperatures (as Mentioned in the Figures)**

Route I: Basket-weave ( $\alpha+\beta$ ) structure (on furnace cooling from  $\beta$  phase)  $\Rightarrow$   
 $\alpha$  Lamellae in  $\beta$  matrix (on reheating)  $\Rightarrow$  Acicular  $\alpha$  in  $\beta$  matrix (on  
 $\alpha+\beta$  hot rolling)  $\Rightarrow$  Acicular  $\alpha$  and  $\alpha'$  in  $\beta$  matrix (on water quenching)  
 $\Rightarrow$  Acicular and equiaxed  $\alpha$  and  $\alpha'$  in  $\beta$  matrix (on  
recrystallization).

Route II: Packets of  $\alpha'$  and  $\alpha''$  martensites (on water quenching from  $\beta$  phase)  
 $\Rightarrow$  Acicular  $\alpha$  and  $\alpha''$  in the matrix of  $\beta$  (on reheating)  $\Rightarrow$  Acicular  $\alpha$   
and  $\alpha''$  in  $\beta$  matrix (on  $\alpha+\beta$  hot rolling and quenching)  $\Rightarrow$  Acicular and  
equiaxed  $\alpha$  and  $\alpha'$  in  $\beta$  matrix (on recrystallization).

Route III & IV: Pancaked  $\beta$  grains (on  $\beta$  hot rolling)  $\Rightarrow$  Packets of  $\alpha'$  and  $\alpha''$   
(on water quenching)  $\Rightarrow$  Acicular  $\alpha$  and  $\alpha''$  in  $\beta$  matrix (on  $\alpha+\beta$  hot  
rolling and quenching)  $\Rightarrow$  Acicular and equiaxed  $\alpha$  and  $\alpha'$  in  $\beta$  matrix  
(on recrystallization)

Route V: Pancaked  $\beta$  grains (on  $\beta$  hot rolling)  $\Rightarrow$  Packets of  $\alpha'$  and  $\alpha''$  (on  
water quenching)  $\Rightarrow$  Fine recrystallized  $\beta$  grains (on  $\beta$  recrystallization)  
 $\Rightarrow$  Packets of martensitic  $\alpha'$  and  $\alpha''$  (on water quenching)  $\Rightarrow$  Acicular  
 $\alpha$  in  $\beta$  matrix (on reheating)  $\Rightarrow$  Acicular  $\alpha$ ,  $\alpha'$  and  $\alpha''$  in  $\beta$  matrix (on  
 $\alpha+\beta$  hot rolling and quenching)  $\Rightarrow$  Acicular and equiaxed  $\alpha$  in  $\beta$  matrix  
(on recrystallization)

Microstructural features of Ti-6-4 alloy processed through different routes have already been described in Sections 4.2 – 4.4. Due to the limited availability of the thermo-mechanically processed Ti-6-4 alloy sheets prepared through five different processing routes, few specimens were subjected to tests for the study of their superplastic deformation behaviour. Results obtained from those tests are discussed in the present section.

#### **4.5.1 Flow Curves and the Strain Rate Sensitivity of Thermo-mechanically Processed Ti-6-4 Alloy before Recrystallization Annealing**

The strain rate sensitivity,  $m$  value, of thermo-mechanically processed Ti-6-4 alloy, as a function of their processing, was evaluated from strain rate jump tests. These tests were carried out prior to their recrystallization annealing. Initially these tests were carried out at 800°C by varying the strain rate from  $8 \times 10^{-5}$  to  $2 \times 10^{-2} \text{ sec}^{-1}$ . Figure 4.26(a) to (e) show  $\ln$  (true stress) vs  $\ln$  (true strain rate) curves obtained from the load vs elongation curves for samples tested at 800°C. A comparison of these plots indicates that the unconventional thermo-mechanical processing routes, routes 2-5, lead to a relatively lower flow stress structure in Ti-6-4 alloy than that obtained by the conventional processing route, i.e. route 1. Further, among the unconventional processing routes the flow stress of the material relatively increases as the amount of deformation in the  $\beta$  phase field, during processing in the  $\beta$  phase field, increases from 30% to 60%. However, when the pancaked  $\beta$  grain structure is recrystallized (Route 5), the flow stress of the alloy decreases to some extent. It can also be seen that  $\ln$  (true stress) vs  $\ln$  (true strain rate) curves show a sigmoidal behaviour with three different regimes of deformation, region I and region III at low and high strain rates respectively with region II at intermediate strain rate range.

Strain rate sensitivity,  $m$ , values were obtained at different strain rates from the slopes of  $\ln$  (true stress) vs  $\ln$  (true strain rate) curves. Plots of  $m$  as a function of strain rate are shown in Figure 4.27(a) to (e). It can be observed from these figures that a maximum value of  $m$  (close to about 0.9) was obtained for the sample processed through route III and tested at 800°C with strain rate of  $7.5 \times 10^{-4} \text{ sec}^{-1}$ . The samples processed through route I & II showed lower  $m$  values compared to the other routes. This gives a clear

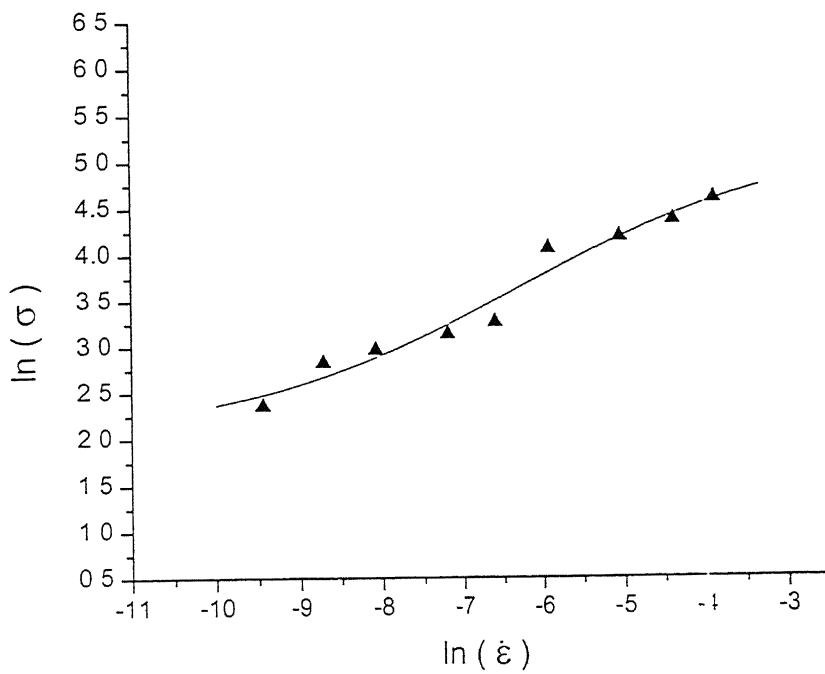


Figure 4.26(a)

True Stress – True Strain Rate Curve for Route I Tested  
at 800°C

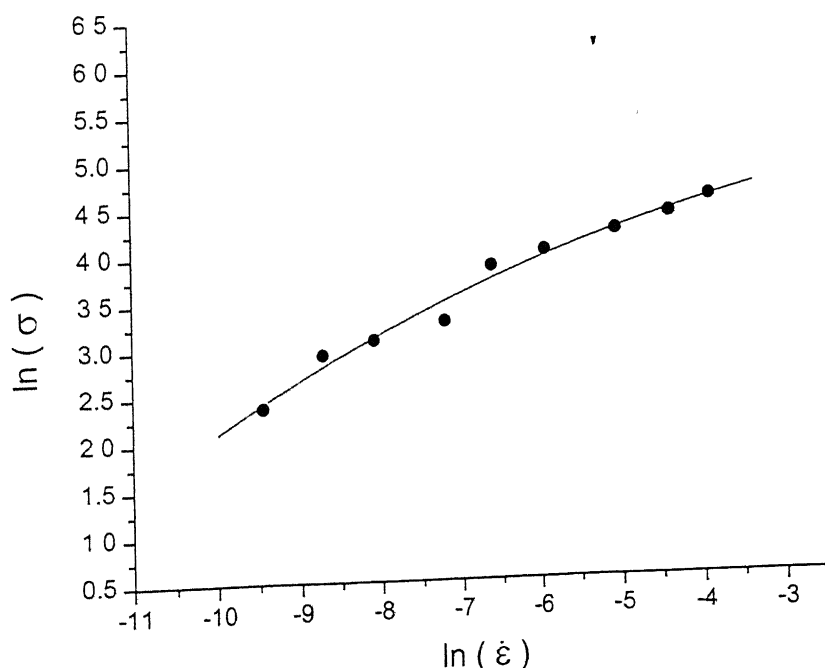


Figure 4.26(b)

True Stress – True Strain Rate Curve for Route II Tested  
at 800°C

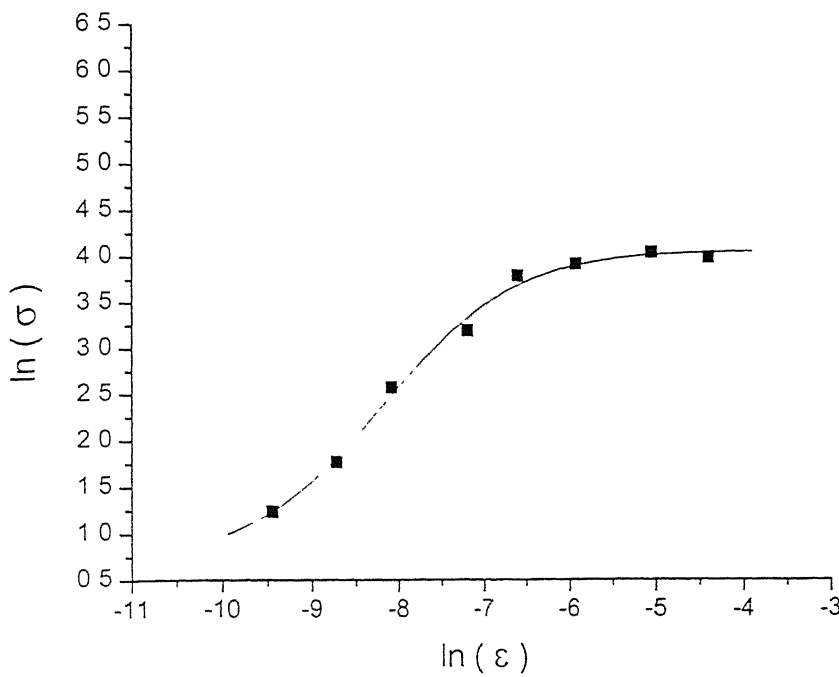


Figure 4.26(c) True Stress – True Strain Rate Curve for Route III  
Tested at 800°C

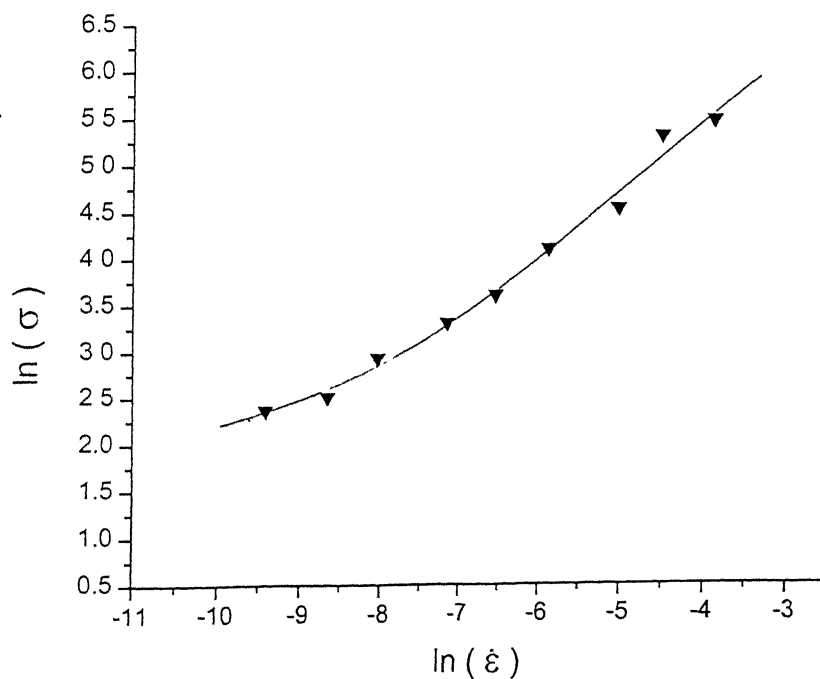
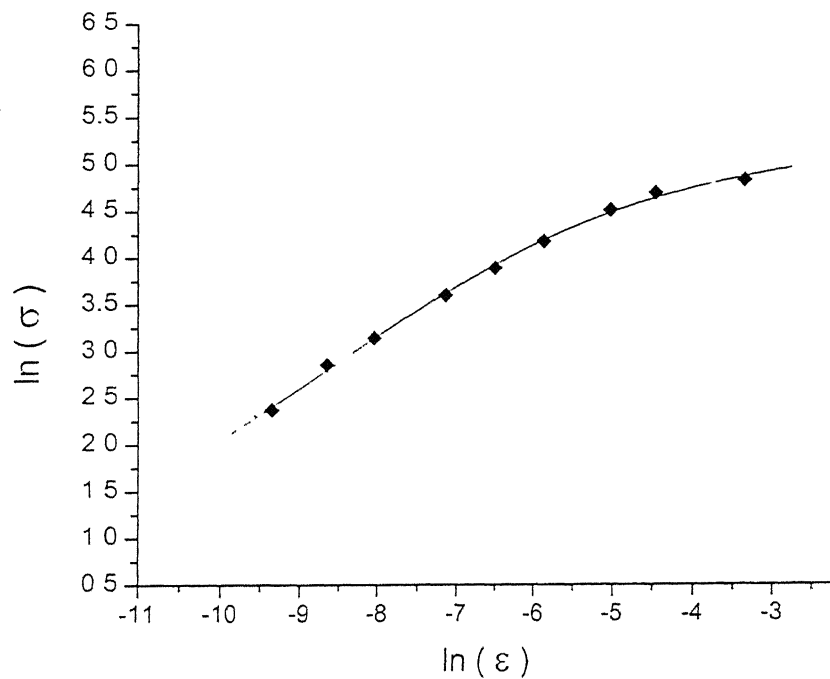


Figure 4.26(d) True Stress – True Strain Rate Curve for Route IV  
Tested at 800°C



**Figure 4.26(e)      True Stress – True Strain Rate Curve for Route V Tested at 800°C**

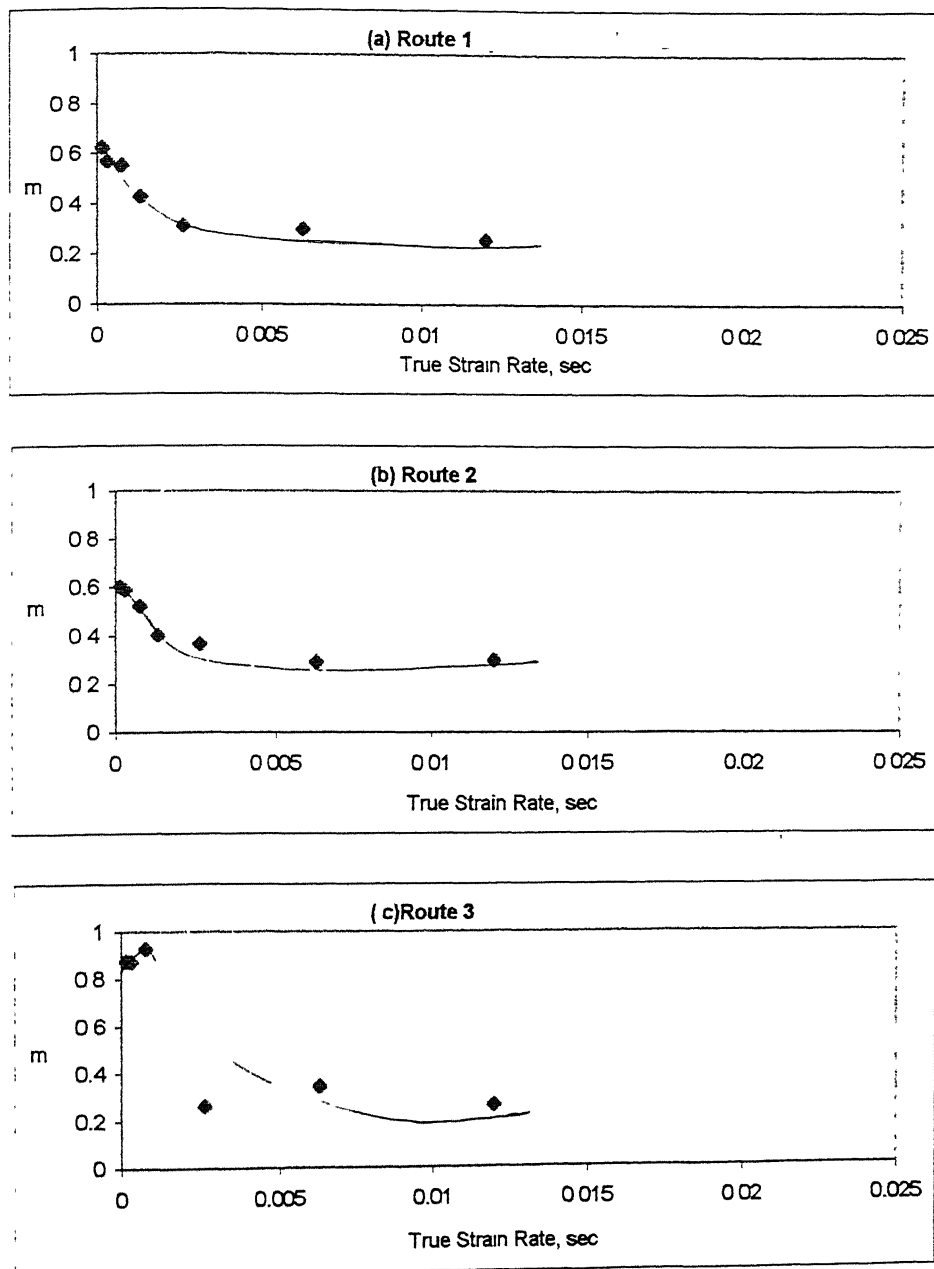


Figure 4.27 (a) – (c)

Strain Rate Sensitivity as a Function of True  
Strain Rate Tested at 800°C

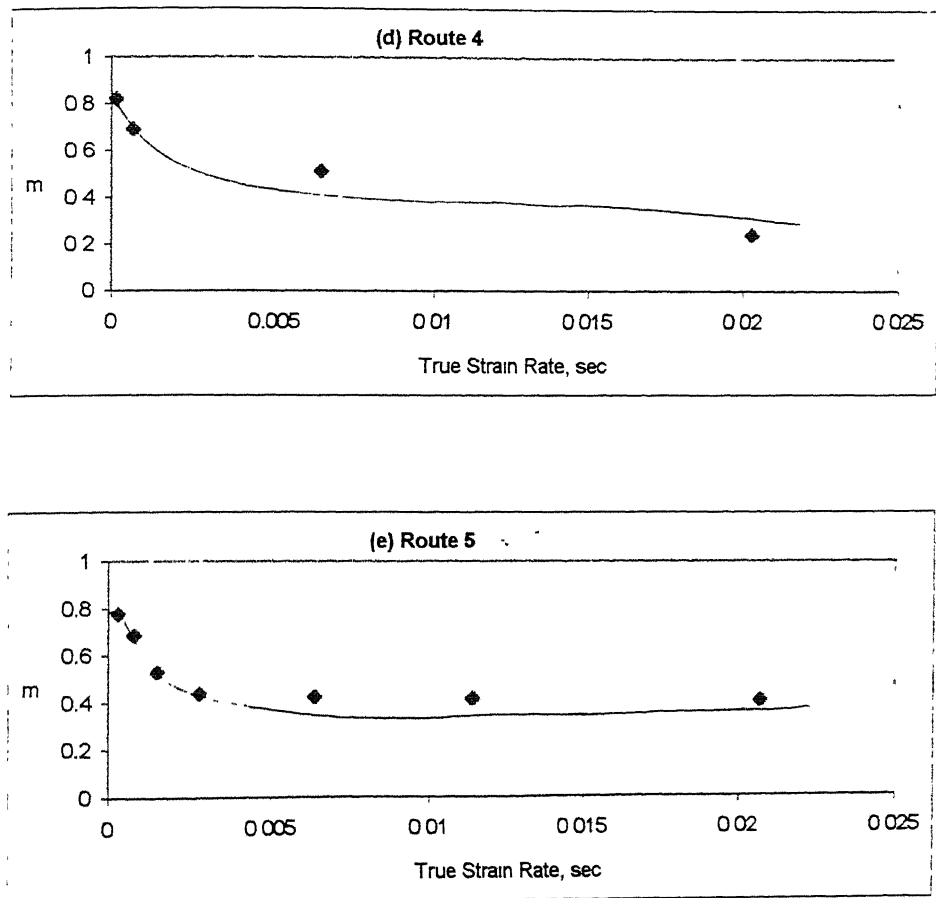


Figure 4.27(d) – (e) **Strain Rate Sensitivity as a Function of True Strain Rate Tested at 800°C**

indication that  $\beta$  processing does improve the superplastic behaviour of the material.

As a few researchers have reported good superplastic properties in as-thermo-mechanically processed condition, i.e. before the recrystallization treatment, a few samples of the Ti-6-4 alloy were subjected to the total elongation test in their as-thermo-mechanically processed state. However, these test results indicated lower ductility. For example, for the sample processed through route IV and tested at 800°C at a strain rate of  $1.7 \times 10^{-4} \text{ sec}^{-1}$  the total elongation at failure was found to be 375%.

#### **4.5.2 Flow Curves and the Strain Rate Sensitivity of Thermo-mechanically Processed Ti-6-4 Alloy after Recrystallization Annealing**

The physical and mechanical properties of  $\alpha$  and  $\beta$  phases are significantly different. For example, the flow properties of the  $\alpha$  and  $\beta$  phases are quite different and also the self-diffusivity of the  $\beta$  phase differs with two orders of magnitude than that of the  $\alpha$  phase. As deformation within thin  $\beta$  phase films is supposed to be the origin of large superplastic deformation[], higher temperature is expected to improve superplastic behaviour of the material.

Fine equiaxed  $\alpha$  grains surrounded by thin  $\beta$  phase films is a prerequisite for the superplastic deformation of Ti-64 alloy. As reported by H. Inagaki[], a fine  $\alpha'$  martensitic structure is fragmented into stringers of deformed  $\alpha'$  particles during hot rolling in two-phase field and decomposed into a very fine and homogeneous distribution of  $\alpha$  and  $\beta$  phases, which is thought to be the origin of enhanced superplasticity in the material, on reheating to the test temperature. The microstructure of an unrecrystallized sample obtained by Route IV and heated to the temperature of 800°C is shown in Figure 4.28 and many  $\alpha$  grains with high aspect ratio may be seen

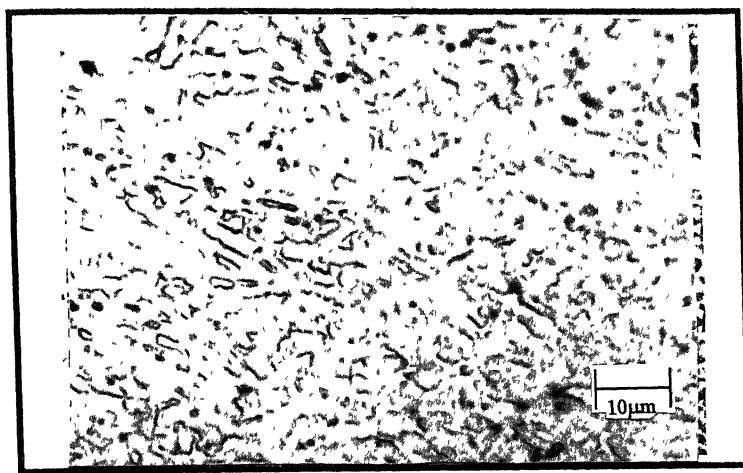


**Figure 4.28 Microstructural Condition of Unrecrystallized Sample  
Treated Through Route IV, Prior to Starting of Deformation  
at 800°C**

in the structure. As mentioned in the previous section, this unrecrystallized sample when tested at the temperature of 800°C at the strain rate of  $1.7 \times 10^{-4}$  sec $^{-1}$  showed only 375% elongation.

As mentioned in Section 4.4., the as-rolled samples, after 15 minutes soaking at the annealing temperature of 800°C did not become equiaxed in nature. Therefore, in order to enhance the superplasticity, all the samples were recrystallized at 850°C for 30 minutes. This temperature and time combination was settled after investigation at different temperature and time combinations. At lower temperatures the structure did not at all form equiaxed grains or the volume fraction of equiaxed grains were very less, whereas, at higher temperatures, the equiaxed grains became coarser. The time was found to have less effect on morphological change or grain growth.

Recrystallized samples of Ti-6-4 alloy were subjected to (1) strain rate jump test and (2) elongation to failure test. The load elongation curves for the strain rate jump test for samples produced from routes I -V, obtained at the test temperature of 850°C, are given in Figure 4.29(a) to (e). An important aspect of load-elongation curves obtained from recrystallized samples was that except for samples processed by route V (fine-grained  $\beta$  grains further hot rolled in the  $(\alpha+\beta)$  phase field) all other samples showed serrated flow in some specific strain rate domains. The strain rate range displaying the serrated flow was found to be widest for samples processed through Route III, i.e. the one involving working of pancaked  $\beta$  grains (deformed by 30% reduction) in the  $(\alpha+\beta)$  phase field. Plots of  $\ln$  (true stress) vs  $\ln$  (true strain rate) were obtained from the load-elongation curves. These plots are shown in Figure 4.30. It can be observed from these curves that the flow stress of the alloy was reduced after the recrystallization treatment and was found to be lower for the condition of the alloy subjected to  $\beta$  processing schedules.

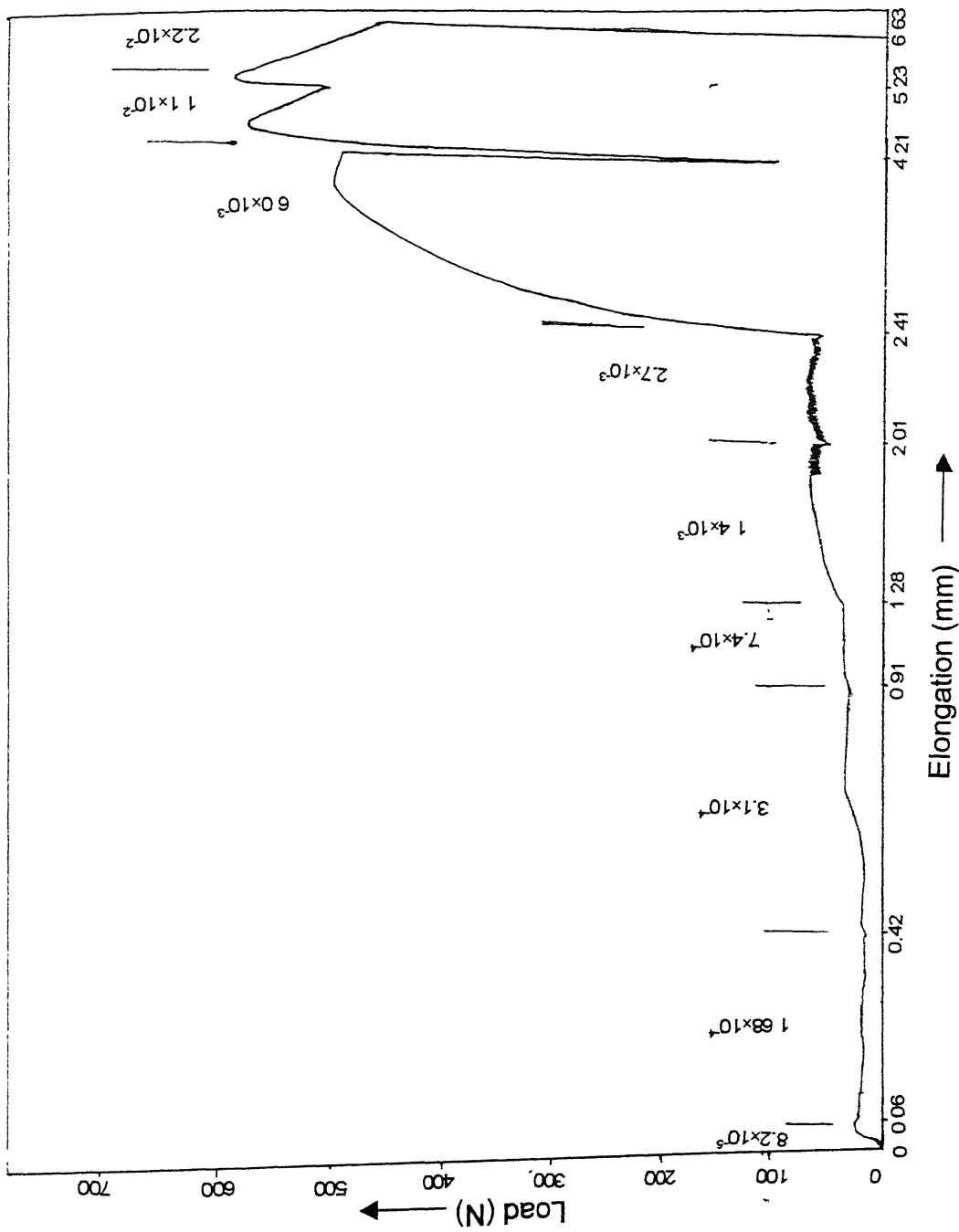
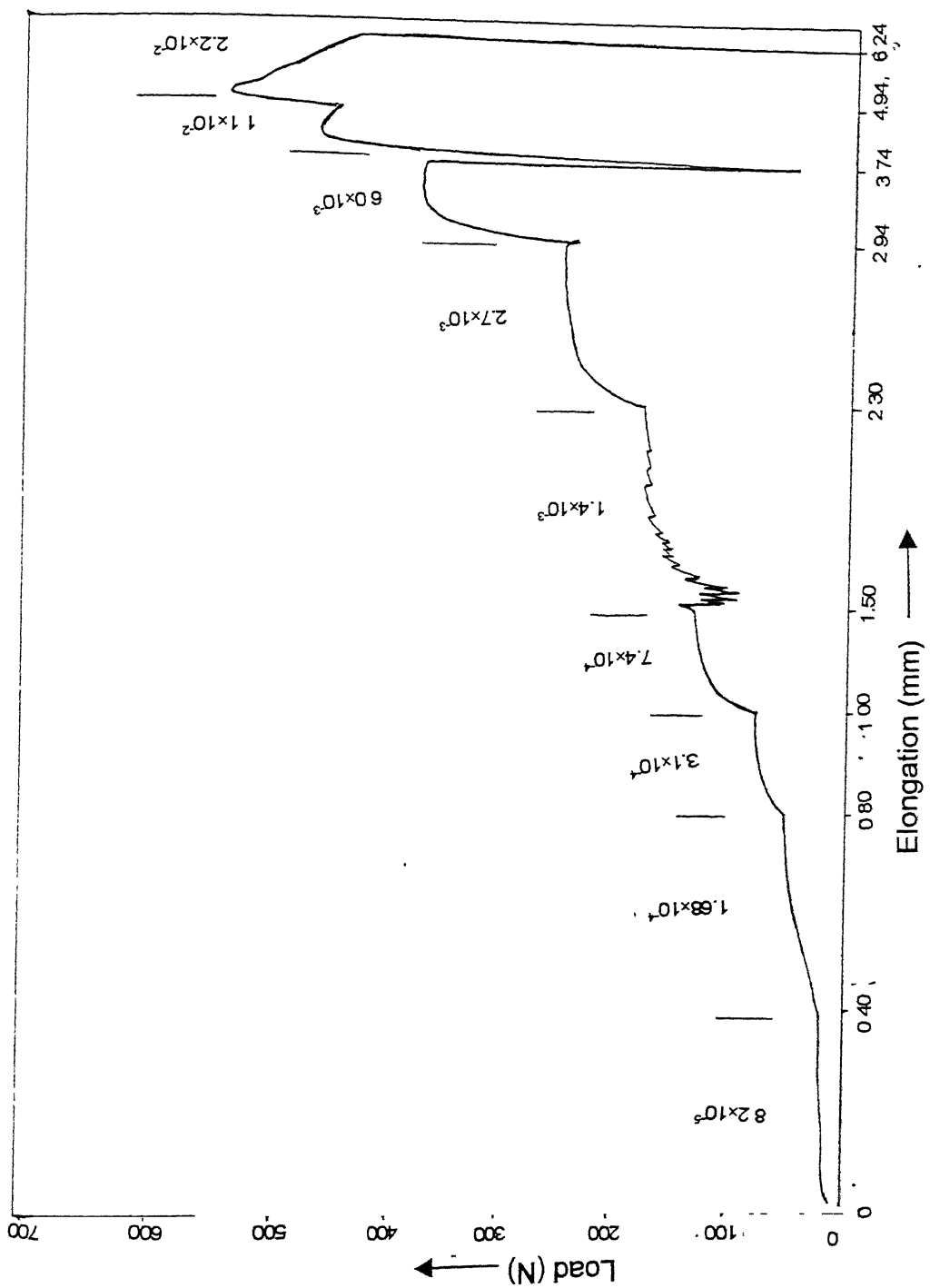


Figure 4.29(a)

Load – Elongation Curve for Route I Tested at 850°C at Different Strain Rates



**Figure 4.29(b)** Load – Elongation Curve for Route II Tested at 850°C at Different Strain Rates

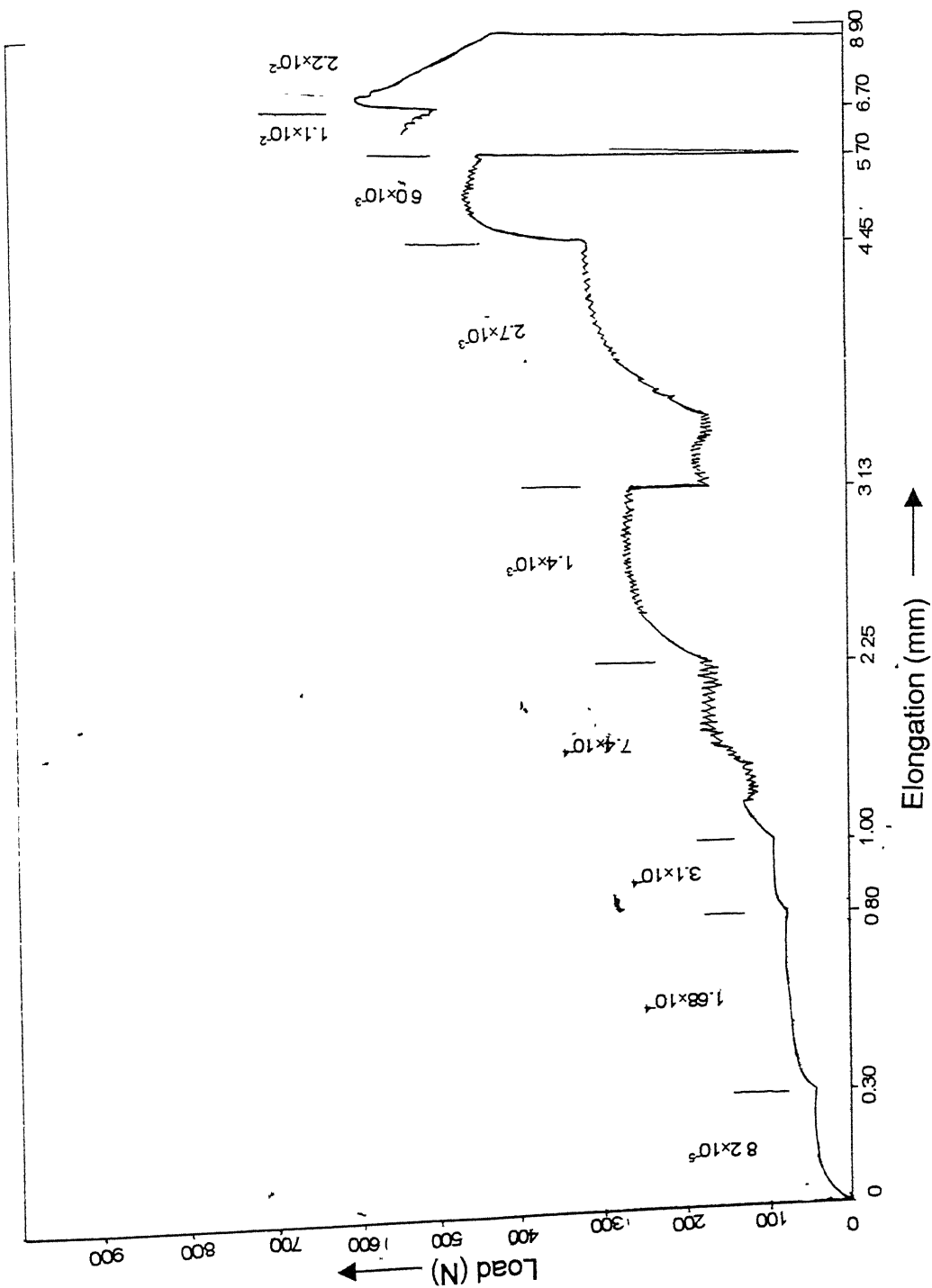
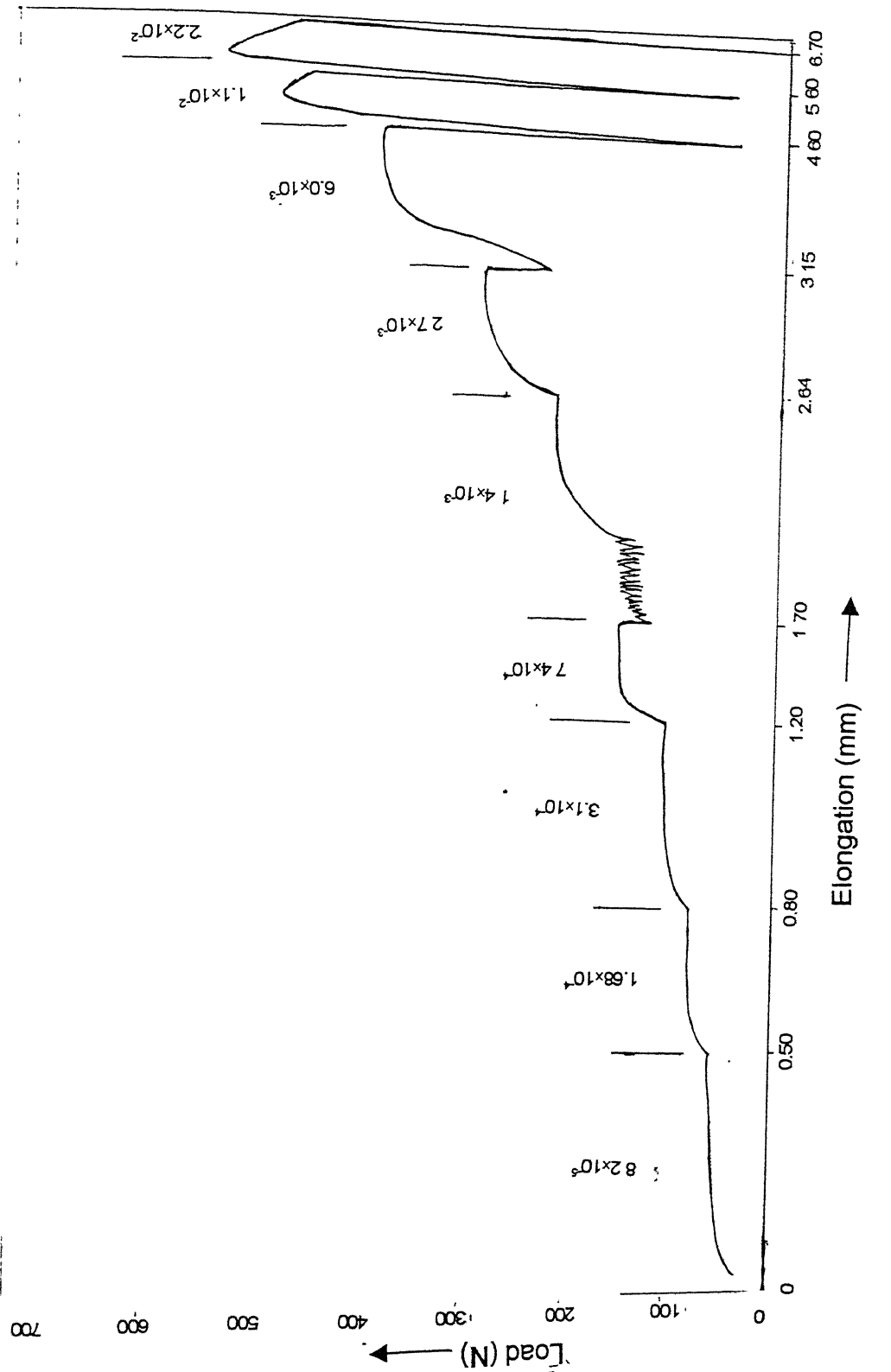


Figure 4.29(c)

Load – Elongation Curve for Route III Tested at 850°C at

Different Strain Rates



**Figure 4.29(d)** Load – Elongation Curve for Route IV Tested at 850°C at Different Strain Rates

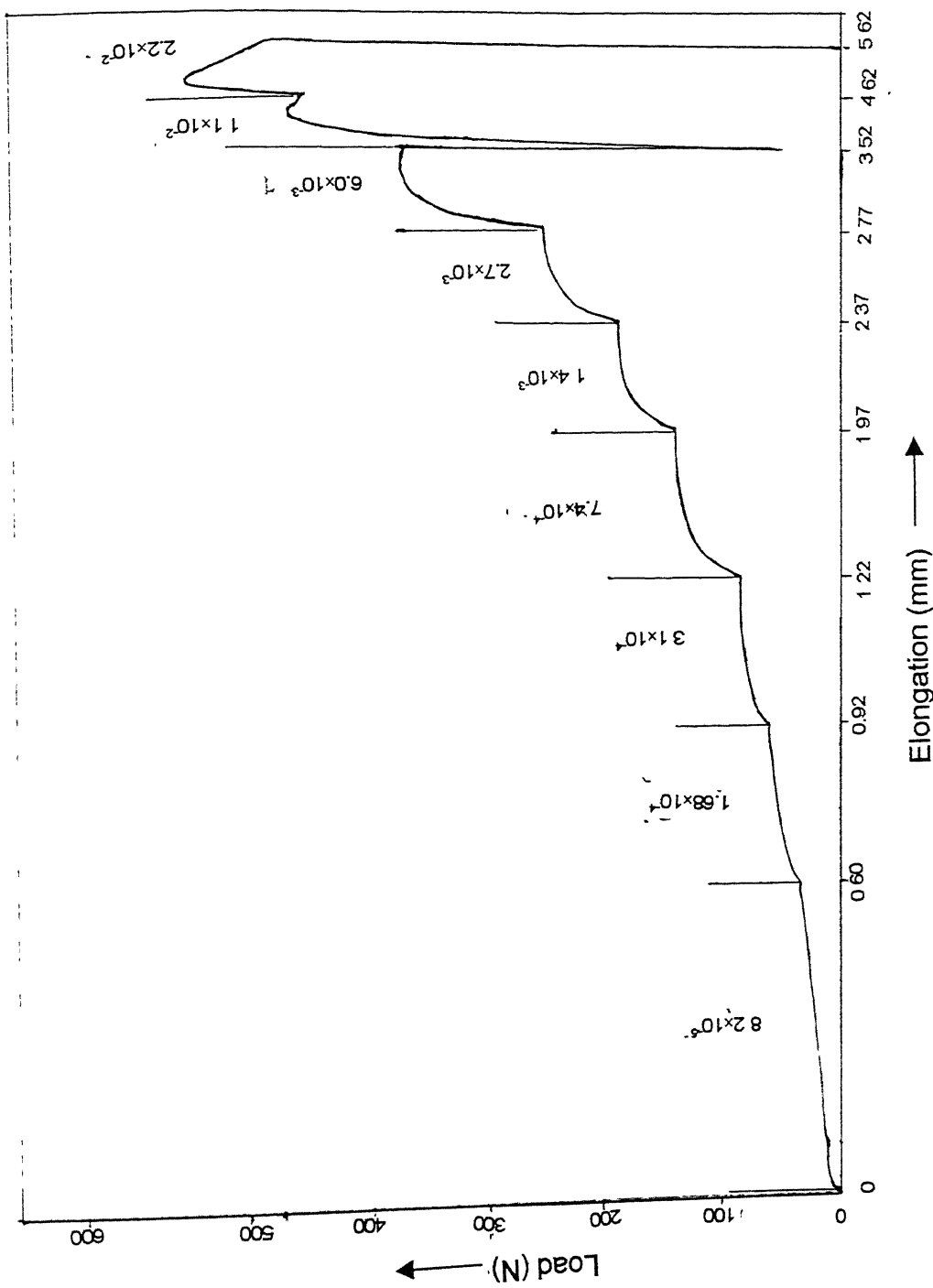
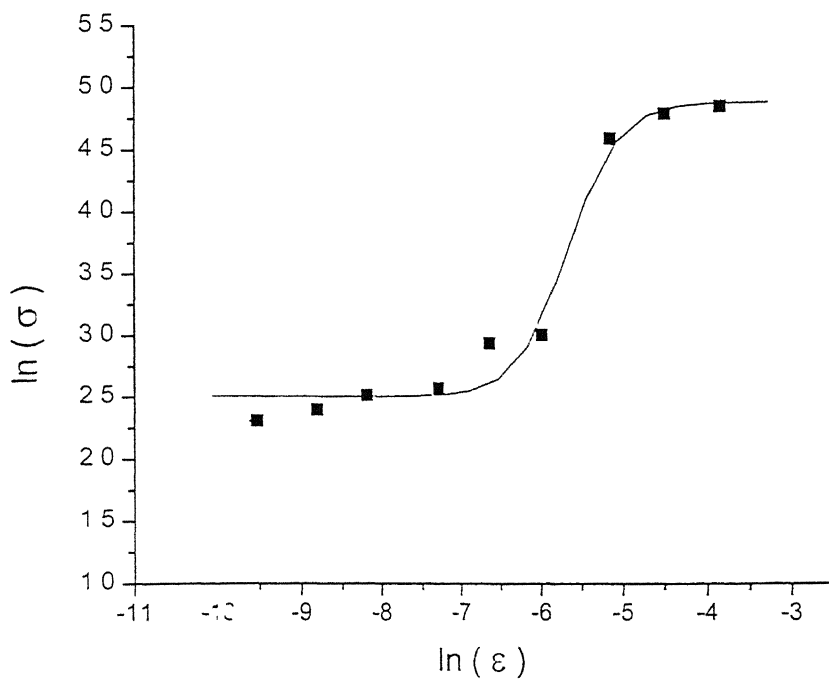
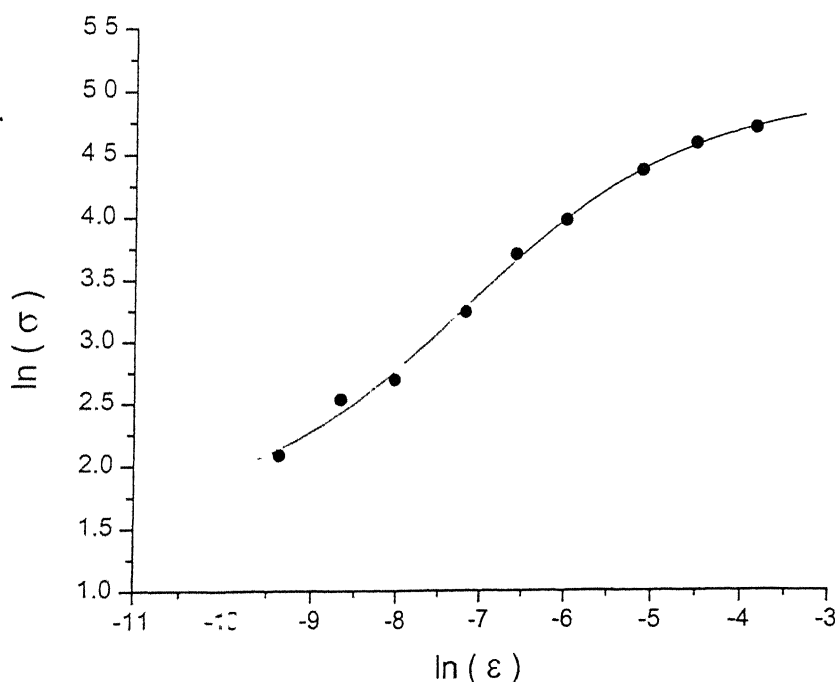


Figure 4.29(e)

Load – Elongation Curve for Route V Tested at 850°C at  
Different Strain Rates



**Figure 4.30(a)      True Stress – True Strain Rate Curve for Route I After Rex. Annealing at 850°C, Tested at 850°C**



**Figure 4.30(b)      True Stress – True Strain Rate Curve for Route II After Rex. Annealing at 850°C, Tested at 850°C**

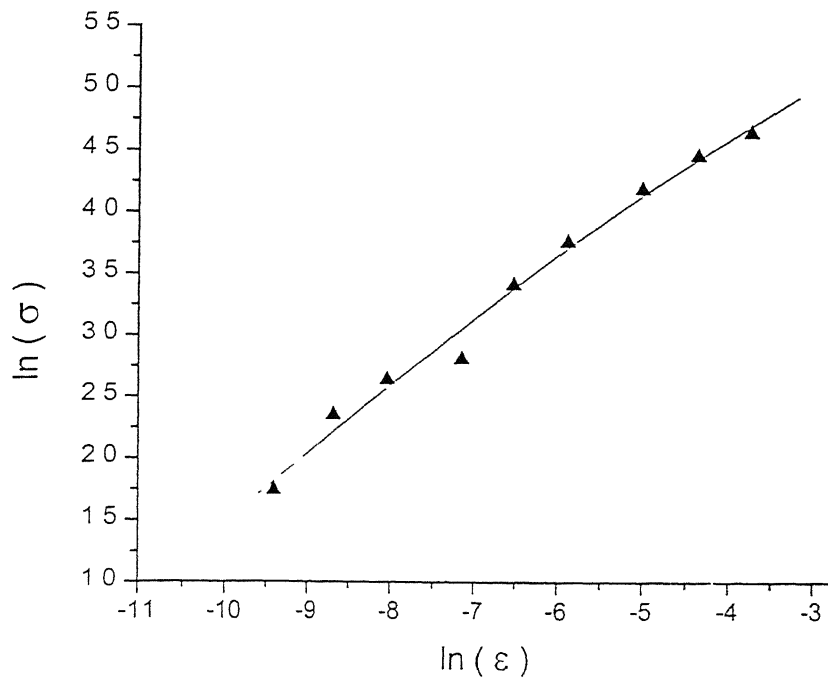


Figure 4.30(c) True Stress – True Strain Rate Curve for Route III After Rex. Annealing at 850°C, Tested at 850°C

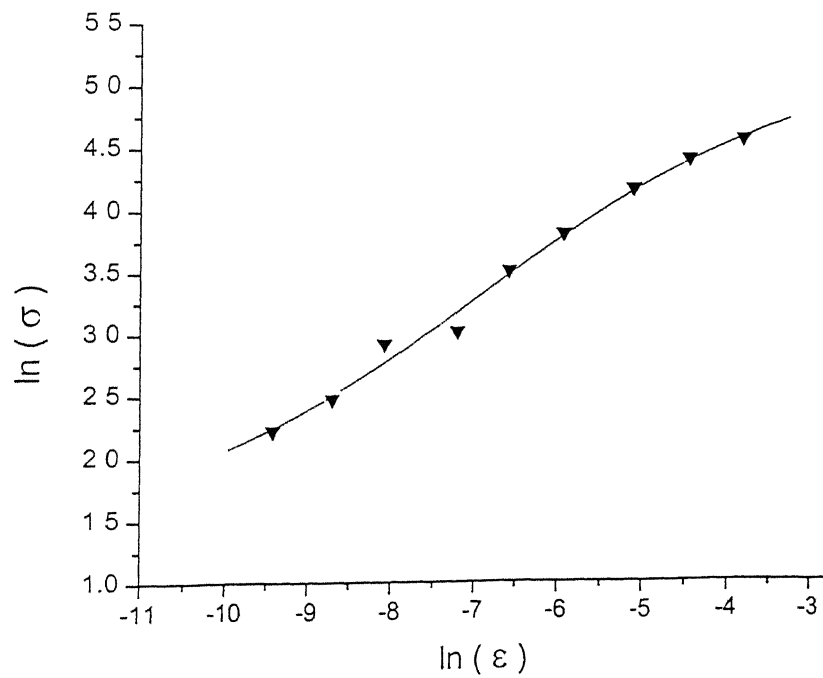


Figure 4.30(d) True Stress – True Strain Rate Curve for Route IV After Rex. Annealing at 850°C, Tested at 850°C

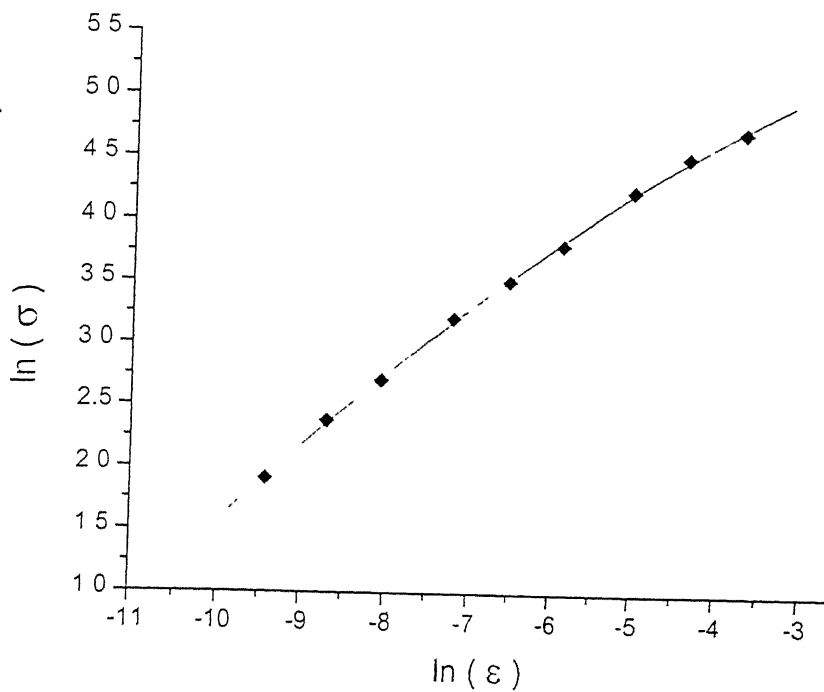


Figure 4.30(e)

True Stress – True Strain Rate Curve for Route V After  
Rex. Annealing at 850°C, Tested at 850°C

The strain rate sensitivity,  $m$ , values were obtained from the slopes of  $\ln$  (true stress) vs  $\ln$  (true strain rate) curves. The variation of  $m$  value with strain rate is shown in Figure 4.31(a) and (b).

Due to the limited amount of differently thermo-mechanically processed Ti-6-4 alloy, elongation to failure tests were carried out at strain rates of maximum  $m$  value for different samples. The load vs elongation curves for the samples are given in Figure 4.32(a) to (e). A highest elongation of 730% was recorded for the material treated through route IV and tested at a strain rate of  $1.5 \times 10^{-3}$  sec $^{-1}$ . Figure 4.33 shows microstructure at different positions of the sample giving highest elongation value. It is to be noted from this figure that considerable grain growth occurred in the sample near the fracture tip. Microstructures of the samples near the fractured region of the sample from each processing steps were examined and the mean size of  $\alpha$  grains was estimated. The starting as well as the final mean grain size of the  $\alpha$  grains in samples obtained by each of the processing route is shown in Table 4.1. It can be seen that the samples processed through routes IV and II underwent the slowest grain growth. It is also observed from figure 4.32 that the sample treated through route V exhibited a relatively lower total elongation of 450%.

A comparison will now be made between results obtained in the present study and those reported in the literature. It is to be noted that an extensive work has been reported by earlier workers on superplastic characteristics of Ti-6Al-4V alloy [62]. However, the following differences between the present study and those undertaken by earlier workers clearly stand out:

- (1) Except for a few exceptions [86,87], the studies undertaken by previous workers are confined to analyse the superplastic behaviour of Ti-6-4 alloy processed by

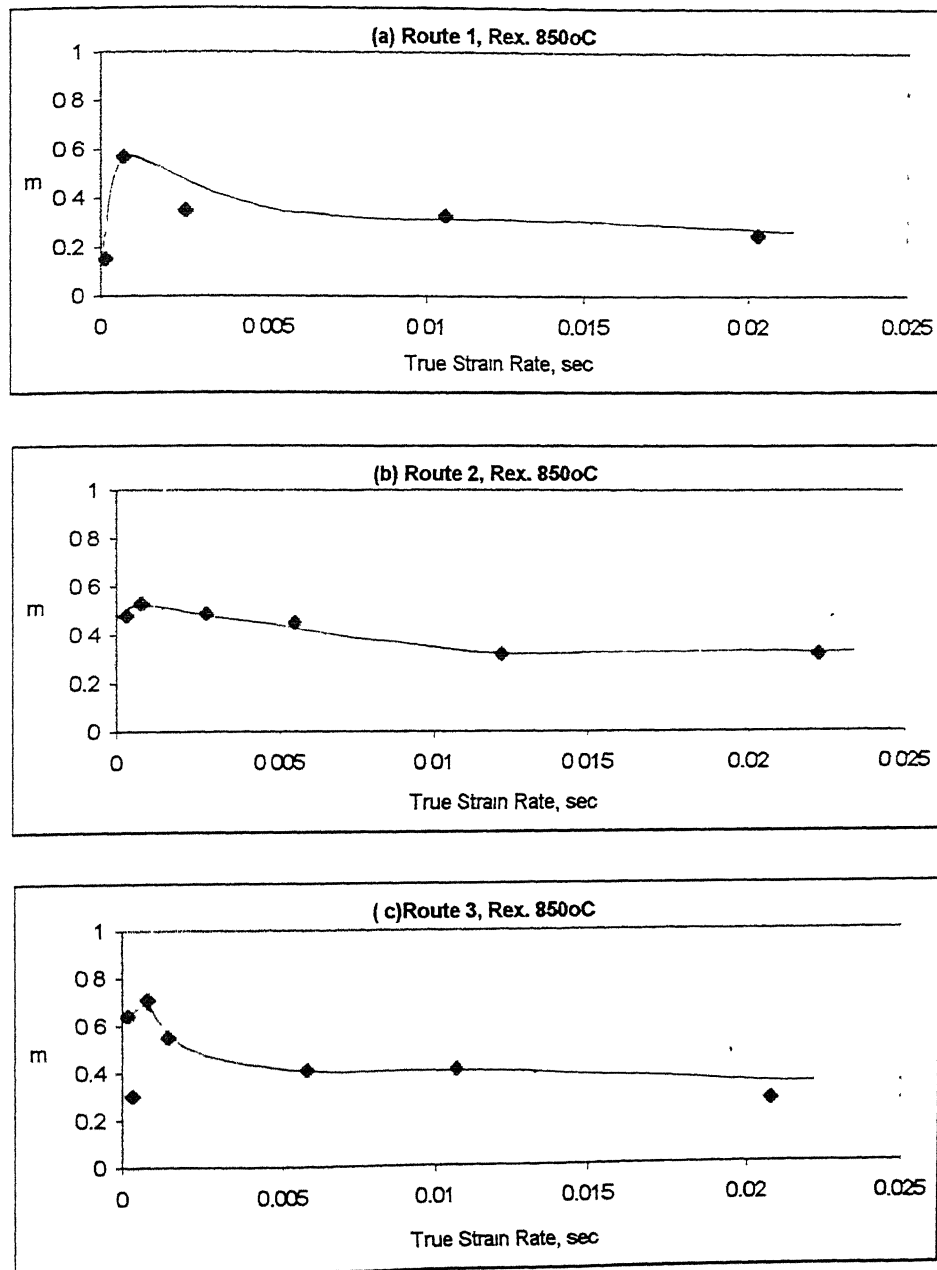


Figure 4.31(a) – (c)

Strain Rate Sensitivity as a Function of True  
Strain Rate for Different Rotes After Rex.  
Annealing at 850°C, Tested at 850°C

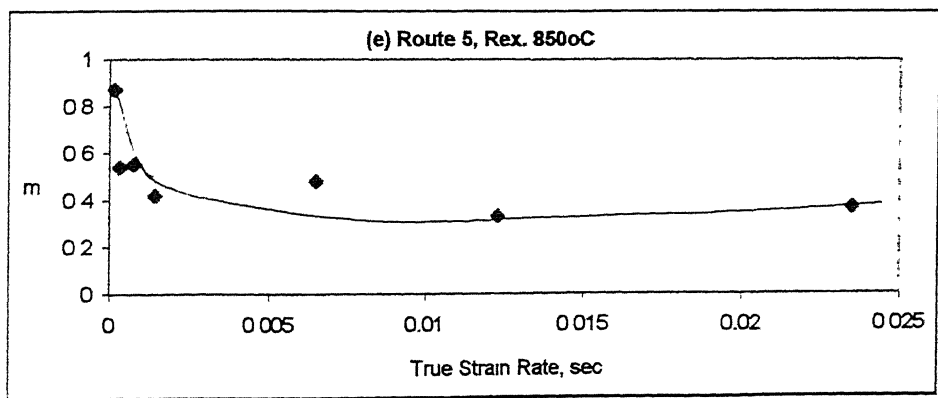
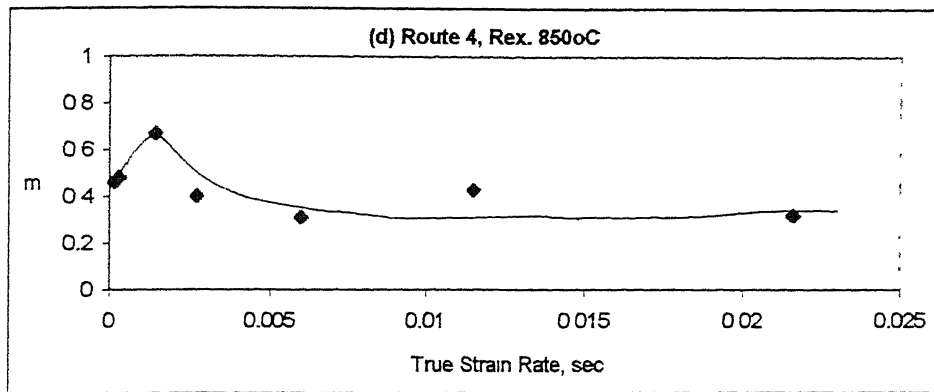


Figure 4.31 (d) – (e)

Strain Rate Sensitivity as a Function of True  
Strain Rate for Different Rotes After Rex.  
Annealing at 850°C, Tested at 850°C

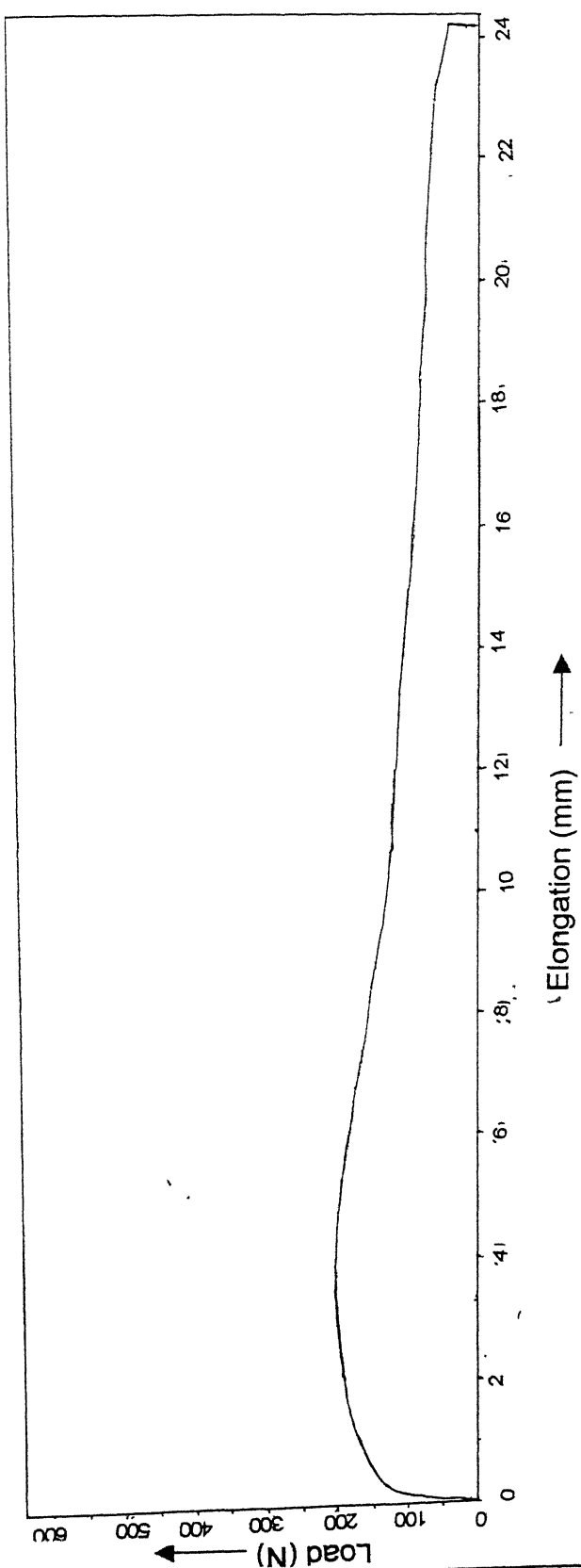


Figure 4.32(a)  
Load – Elongation Curve upto Failure for Route I Tested  
at  $850^{\circ}\text{C}$  at  $\epsilon = 7.4 \times 10^{-4}$

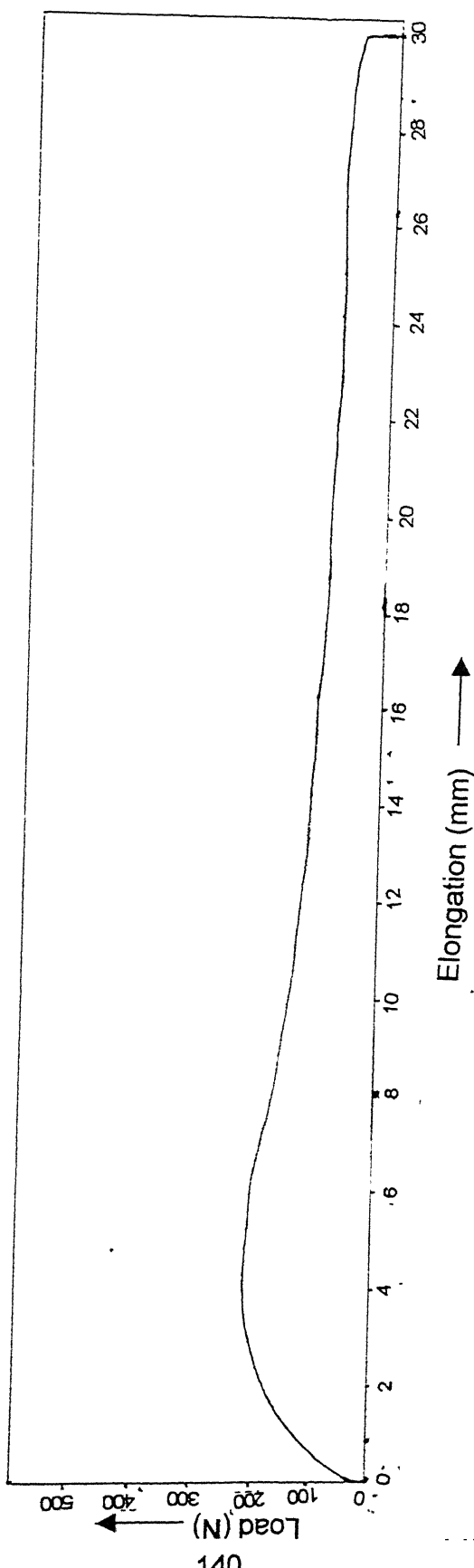


Figure 4.32(b)

Load – Elongation Curve upto Failure for Route II

Tested at 850°C at  $\varepsilon = 7.4 \times 10^{-4}$

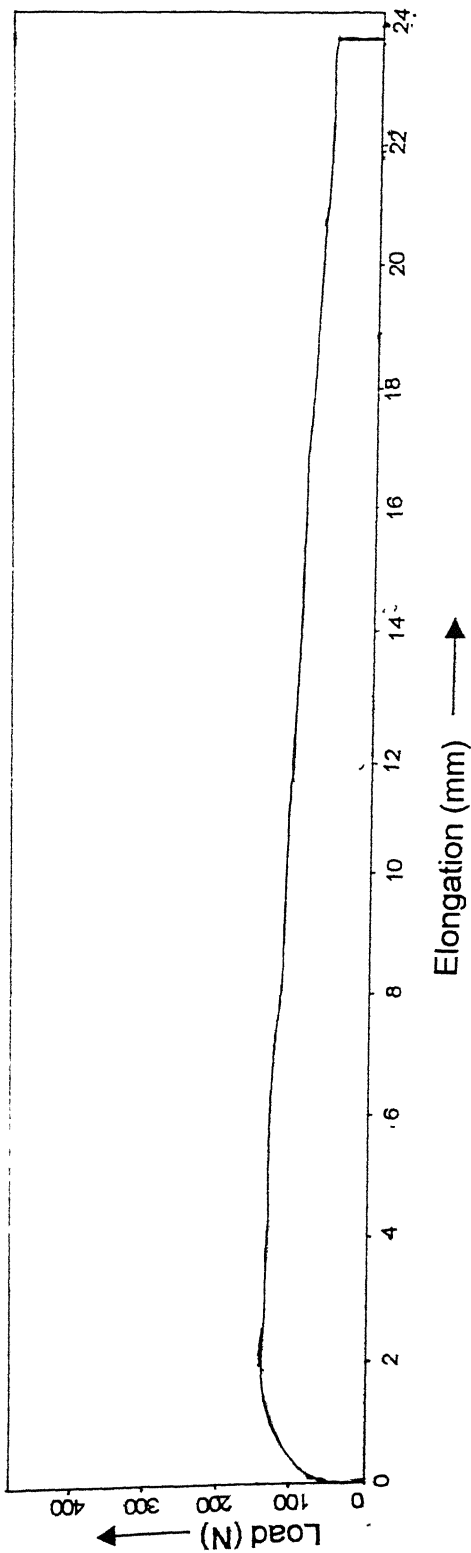
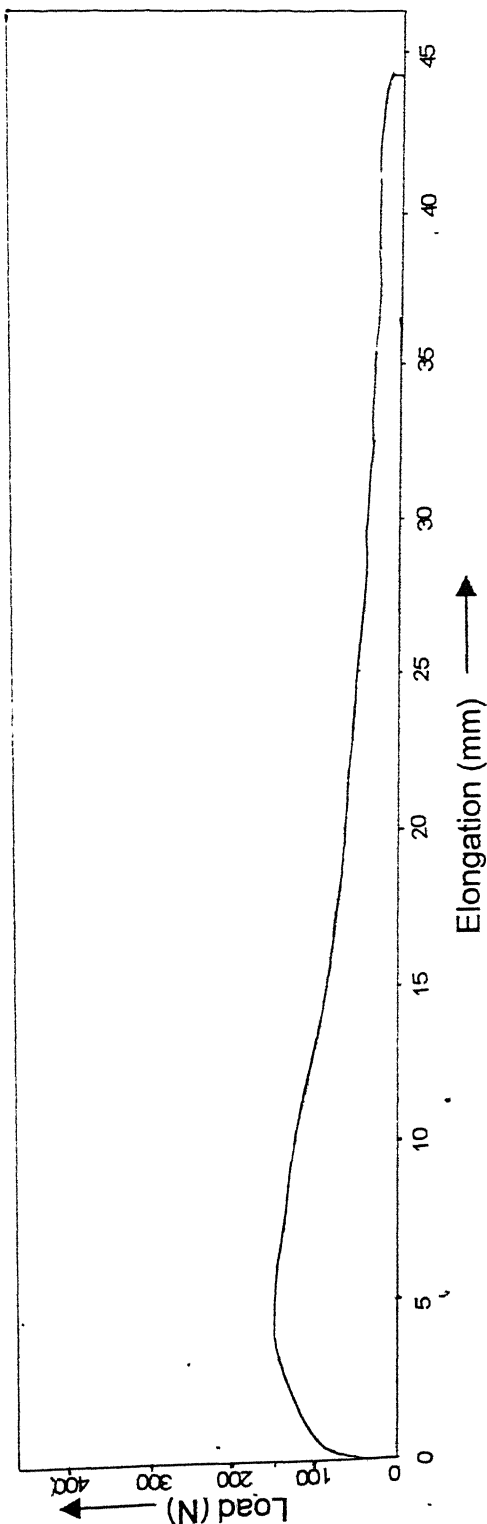


Figure 4.32(c) Load – Elongation Curve upto Failure for Route III  
Tested at 850°C at  $\varepsilon = 7.4 \times 10^{-4}$

Figure 4.32(c)



**Figure 4.32(d) Load – Elongation Curve upto Failure for Route IV  
Tested at 850°C at  $\varepsilon=1.4 \times 10^{-3}$**

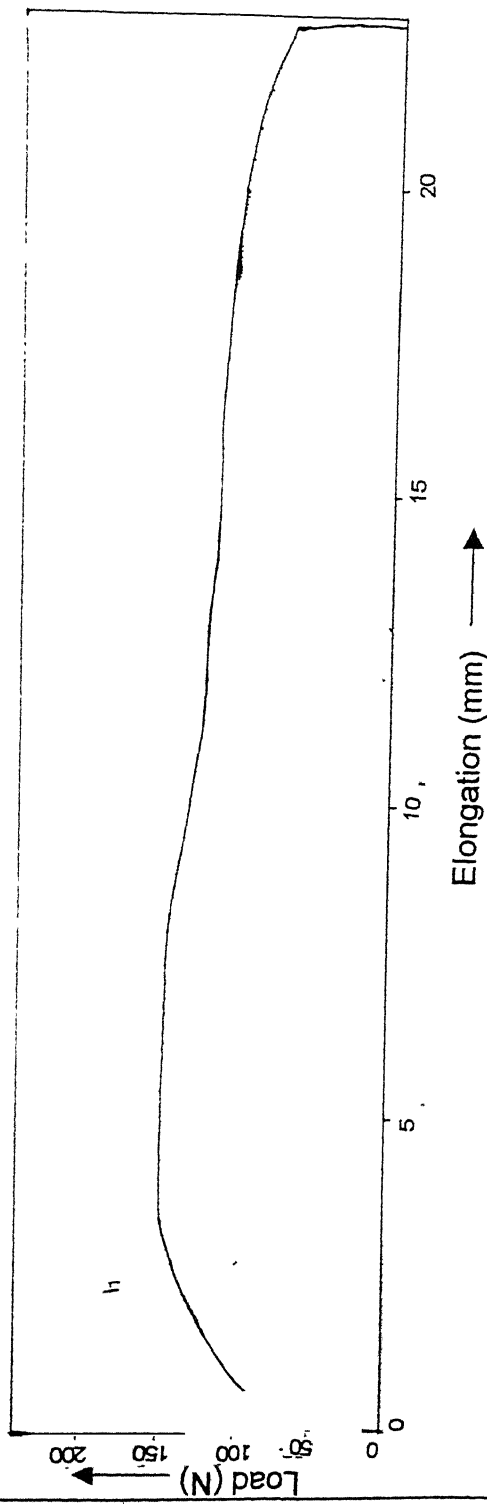
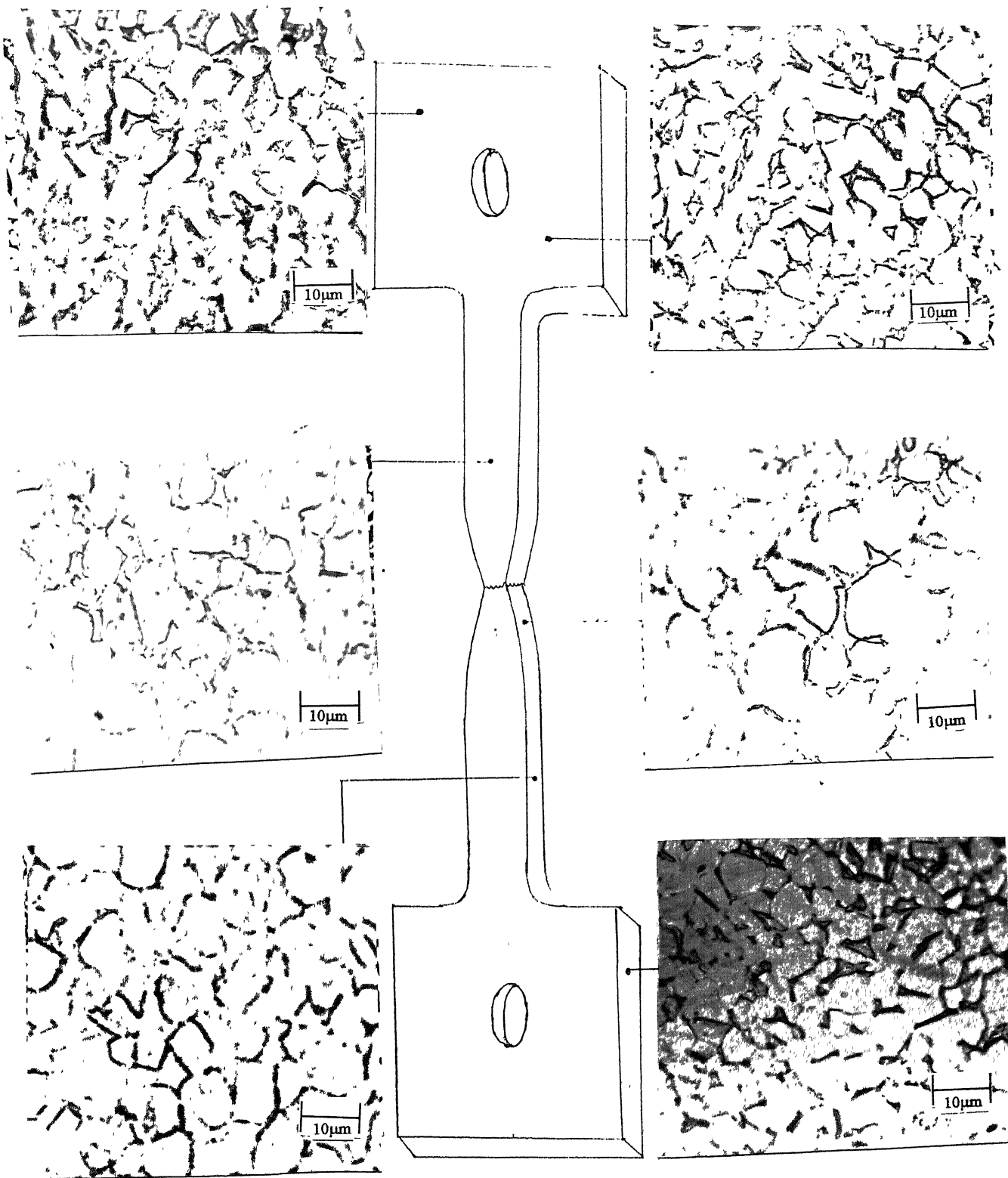


Figure 4.32(e)

Load - Elongation Curve upto Failure for Route V  
Tested at 850°C at  $\epsilon = 1.68 \times 10^{-4}$



**Figure 4.33 Microstructures of the Elongated Sample Treated Through Route IV at Various Locations** (tested at 850°C)

Processing Routes	Grain Size After Recrystallization	Grain Size After Superplastic Testing
I	3.28	10.29
II	3.19	8.38
II	3.00	8.99
IV	3.29	7.81
V	3.53	11.19

**Table 4.1    Equivalent Grain Size Value After Recrystallization Annealing and after Superplastic Testing at 850°C**

the conventional thermo-mechanical processing route. The variables studied in these works are (i) the grain size distribution and the mean size of  $\alpha$  grains [77,108,109], (ii) aspect ratio and the aspect ratio distribution of non-equiaxed  $\alpha$  grains, when present, [102] (iii) the concurrent grain growth occurring in the alloy during superplastic deformation [75,110], (iv) minor alloying elements when present in the alloy[80] and (v) the texture present in the material[111]. On the other hand, the present work was undertaken to study the superplastic behaviour of Ti-6-4 alloy microstructurally refined by adopting new unconventional thermo-mechanical processing routes incorporating processing variables to modify the morphology of prior  $\beta$  grains.

- (2) While earlier reported works are confined to the normal grades of Ti-6-4 alloy containing about 1100 to 1500 ppm of oxygen deliberately added to the alloy, the present work was undertaken to study the superplastic behaviour of the extra-low interstitial (ELI) grade of Ti-6-4 alloy. Thus, while the  $\beta$ -transus of the material used in earlier studies is reported to be lying between 980°C and 990°C, that of the material used in the present investigation was lower and was found to be  $950 \pm 5^\circ\text{C}$ .
- (3) Many of the earlier reported studies have used round bars or thicker plates for preparing tensile samples. However, sheets of thickness ranging from 1.8 mm to 2.0 mm, produced by different thermo-mechanical processing routes were used in the present investigation. Also, due to (i) the maximum length limitation of the superplastic testing set-up and (ii) the limited availability of the thermo-mechanically processed alloy for all the five processing routes, non-standard samples of the gauge length of 6.00

mm were tested in the present study. Further, the high-temperature tensile tests were conducted under atmospheric conditions.

The volume fractions of  $\alpha$  and  $\beta$  phases is known to have an effect on the strain rate sensitivity,  $m$ , and the % total elongation displayed by the material. Figures 4.34 and 4.35 show the effect of volume % of the  $\beta$  phase for various two-phase titanium alloys on their strain rate sensitivity and % total elongation. The volume fraction of  $\alpha$  phase, as a function of soaking temperature below the  $\beta$ -transus temperature, for the present alloy has been shown in Figure 4.36. Thus, it may be inferred that various thermo-mechanically processed samples used in the present study and tested at 850°C contained about 55% of the  $\beta$  phase at the testing temperature. For similar volume fractions of  $\alpha$  and  $\beta$  phases the reported values of the strain rate sensitivity and % total elongation are about 0.8 and 580-590% respectively. Highest values of the strain rate sensitivity,  $m$ , and % total elongation for the alloy processed through each processing route are shown in Table 4.2. It must be noted that the alloy processed through routes II and IV

Table 4.2 Superplastic Properties in Different Processing Routes

Processing Route	Max. $m$ Value	%Total Elongation
I	0.57	335
II	0.55	625
III	0.70	330
IV	0.68	730
V	0.87	450

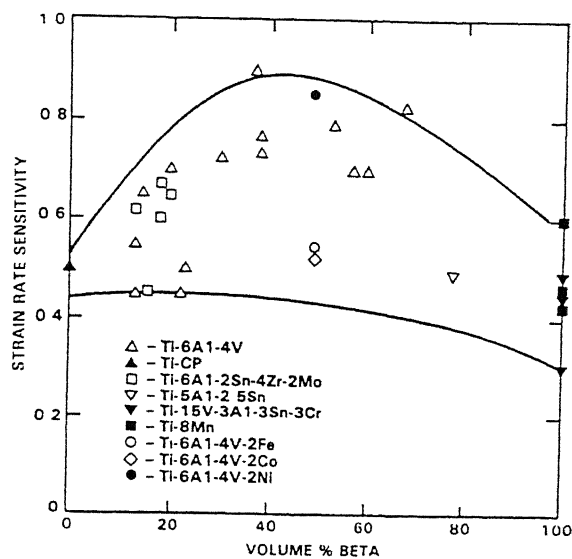


Figure 4.34  $m$  as a Function of  $\beta$  Phase Content for Different Ti Alloys

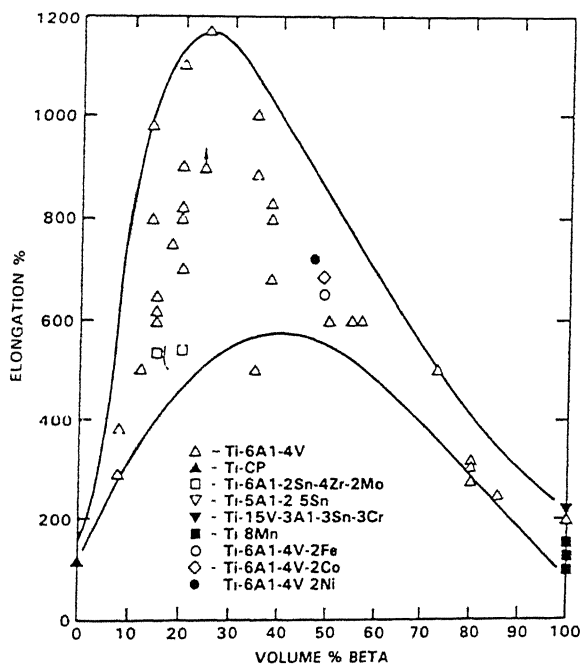
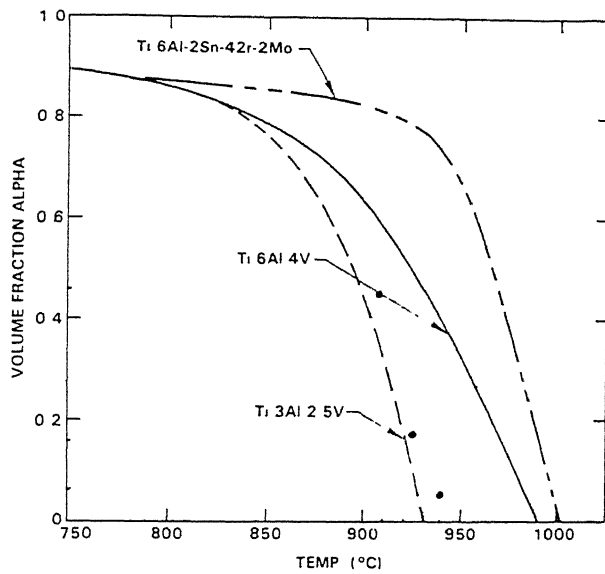


Figure 4.35 Total Elongation as a Function of  $\beta$  Phase Content for Different Ti Alloys



**Figure 4.36 Variation of  $\alpha$  Volume Fraction with Temperature for Different Ti Alloys** (circles represent points corresponding to present investigation)

#### Chapter 4: Results and Discussion

provide higher % total elongation. The very fact that the tensile tests in the present investigation were conducted on thinner and shorter samples without the presence of the protective atmosphere and yet superior % total elongation values are obtained, shows that the alloy processed through the newly conceived thermo-mechanically processing routes must be having even superior superplastic behaviour when studied under comparable testing conditions.

## CHAPTER 5

### CONCLUSIONS

Extra-Low Interstitial (ELI) grade of Ti-6Al-4V alloy was processed through unconventional thermo-mechanical processing routes involving (a) conditioning of prior  $\beta$  grains and (b) altering the morphology of  $\alpha$  lamellae prior to working of the alloy in the  $(\alpha+\beta)$  phase field. Microstructural features of the alloy processed through five different processing routes were analysed. The alloy processed through different routes and subsequently subjected to the  $(\alpha+\beta)$  recrystallization annealing treatment was subjected to analyse its superplastic behaviour by the step strain rate as well as the elongation-to-failure tests. Microstructural features of failed samples were also examined. The following conclusions can be drawn from the results of the present study.

- (1) The alloy Ti-6-4, during its processing in the  $\beta$  phase field up to the rolling temperature of  $980^{\circ}\text{C}$ , i.e. about  $30^{\circ}\text{C}$  above the  $\beta$ -transus temperature does not undergo dynamic recrystallization even at a deformation as high as 60%. However, the alloy undergoes rapid recrystallization and grain growth during subsequent annealing in the  $\beta$  phase field.
- (2) The condition of  $\beta$  grains prior to their water-quenching has considerable effect on (a) the morphology of the martensitic needles and (b) acicular  $\alpha$  plates/lamellae formed prior to hot rolling of the alloy in the  $(\alpha+\beta)$  phase field.
- (3) Results from the X-ray diffraction clearly indicate that both orthorhombic as well as hexagonal martensites,  $\alpha''$  and  $\alpha'$ , form when the alloy is quenched from the  $\beta$  phase field. However, the quenched structure of the alloy comprises primarily of the orthorhombic

## Chapter 5: Conclusions

martensite,  $\alpha''$ . In contrast, when the alloy is quenched from the two-phase ( $\alpha+\beta$ ) phase field the  $\beta$  phase present in the alloy transforms only to the hexagonal martensite,  $\alpha'$ . Thus the alloy quenched after  $\beta$  processing and further heated to the ( $\alpha+\beta$ ) phase field for its preheating before rolling in the two-phase field is found to contain orthorhombic martensite,  $\alpha''$ , indicating that the orthorhombic martensite is stable even at the heating temperature of 850°C.

- (4) The  $\beta$  processed alloy undergoes a considerable microstructural refinement during rolling in the ( $\alpha+\beta$ ) phase field at 860°C by the thickness reduction of 70%
- (5) Recrystallization annealing in the ( $\alpha+\beta$ ) phase field helps in transforming the structure from mixed morphology consisting of acicular and equiaxed primary  $\alpha$  to a nearly equiaxed one. However, it is observed that those recrystallized microstructural states which contain higher volume fraction of equiaxed  $\alpha$  grains undergo faster grain growth during superplastic testing than those which contain a wider distribution of the aspect ratio of  $\alpha$  grains.
- (6) Unrecrystallized alloy treated through Route IV gives 375% total elongation when tested at the temperature of 800°C at the strain rate of  $1.7 \times 10^{-4} \text{ sec}^{-1}$ .
- (7) Among the five different thermo-mechanical processing routes studied in the present investigation, the maximum total elongation was obtained for the recrystallized samples prepared by Route IV when tested at 850°C at the strain rate of  $1.4 \times 10^{-3} \text{ sec}^{-1}$ . The % total elongation displayed by the alloy under these conditions was found to be 730%. The next highest % total elongation (630%) was obtained in the recrystallized alloy processed through Route II when tested at the temperature of 850°C at the strain rate of  $7.2 \times 10^{-4} \text{ sec}^{-1}$ .

## Chapter 5: Conclusions

- 
- (8) Microstructural examination of failed samples indicate that alloy samples processed through routes IV and II, which also displayed maximum % total elongation, underwent the least grain growth.
  - (9) The results of the present work thus indicate that the  $\beta$  processing variables studied in the present investigation serve as a useful method for the microstructural refinement and enhanced superplastic characteristics of extra-low interstitial (ELI) grade of Ti-6Al-4V alloy.

## REFERENCES

1. H.T.Clerk ; "Trans. Amer. Inst. Min (Metall.) Engrs.", v. 185, 1949, pp.588.
2. W.Burgers, F.Z.Jacobs ; "Kristallogr.", v. 94, 1936, pp.299.
3. A.D.McQuillon, M.K.McQuillon ; "Titanium", Butterworths Scientific Publications, 1956, London.
4. E.W.Collings ; "The Physical Metallurgy of Titanium Alloys", American Society for Metals, 1984, USA.
5. K.B.Mallikarjun; M.Tech. Thesis, I.I.T., Kanpur, 1998.
6. J.L.Everhart ; "Titanium and Titanium Alloys", Rein hold Publishing Corporation, 1954, New York
7. G.Shujun, Q.Rongshi, Z.Suisheng, W.Xiaojng ; Fatigue crack growth for Ti-6Al-4V Alloy In Water, "Proc. of 1<sup>st</sup> Int. Conf. on Metallurgy and Material Science of W, Ti, RE, Sb", Ed. by F. Chongyue, v. II, pp.987.
8. European Productivity Agency of the organization for European Economic Co-operation ; "Titanium, Zirconium and Some Other Elements of Growing Industrial Importance", Project No 247, Sept. 1956, Paris.
9. C.Sugui, M.Suland, L.Shizhuo ; Cavitation Damage of Ti-6Al-4V Alloy, "Proc. of 1<sup>st</sup> Int. Conf. on Metallurgy and Material Science of W, Ti, RE, Sb", Ed. by F. Chongyue, v.II, pp.906
10. S.Ashley ; Boeing 777 Gets a Boost From Titanium, "Mechanical Engg.", v. 115, no. 7, July, 1993, pp.60
11. "Titanium for Energy and Industrial applications", Ed. by D.Eylon, The Metallurgical Society of AIME, pp.19,71,84.
12. H.E.Friedrich, R.Furlon, M. Kullick ; SPF/DB on the way to the production stage for Ti and Al applications within military and civil projects, "Superplasticity and superplastic forming, Int. Conf. proc., Ed. by C.H.Hamilton,N.E.Patron; TMS, August,1988, Washington, pp.649.

## References

13. R.Furlon, P.J.Winkler, D.Hagg, L.Reisinger ; Production of Ti-6Al-4V componenets for a new turbo-fan engine, ibid, pp.665.
14. A.S.Ramamoorthy ; Titanium for underwater applicatrions, "National seminar on titanium and superalloys", Conf. Proc., Hyderabad, 28-29 July, 1996.
15. J.R.Myers, H.B.Bomberger, F.H.Froes ; Corrosion behaviour and use of titanium and its alloys, "Jornal of Metals", October, 1984, pp.50.
16. L.S.Richardson, N.J.Grant ; "Trans. Amer. Inst. Min. (Metall.) Engrs.", Vol. 200, 1954, pp.69.
17. E.S.Bumps, H.D.Kessler, M.Hansen ; "Trans. Amer. Soc. Metals", Vol.45, 1953, pp.1008.
18. L.Qingyun, L. Weihong ; Status for China's titanium processed materials, "Proc. 1<sup>st</sup> Int Conf. on metallurgy and material science of W,Ti, RE, Sb", Ed. by F. Chongyue, Vol.1, pp.23-33.
19. E K.Molchanova , "Phase diagrams of titanium alloys", Israel programme for scientific translations, Jerusalem, 1965.
20. U.Zwicker : "Titan and titanlegierungen" , Springer-Verlag, 1974(as sited in ref.4).
21. B.W.Levinger ; "Trans. Amer. Inst. Min. (Metall.) Engrs.", Vol.197, 1953, pp.195.
22. H.W.Rosenborg ; Titanium alloying in theory and practice, "Sci. Tech. and Appl. Of titanium", Proc. 1<sup>st</sup> Int. Conf. on titanium, Ed. by R.I.Jaffee and N.E.Promisel, Pergamon press, London, 1970, pp.851-859.
23. "Facts about metallography of titanium", RMI Company, Niles, Ohio.
24. R A.Wood ; "Titanium alloys handbook", Metals and Ceramic information centre, Battelle, December, 1972.
25. D.R.Salmon ; "Low temperature data handbook, Titanium and titanium alloys", National Physical Laboratory, May, 1979.
26. I.V.Gorynin, B.B.Chechulin, S.S.Ushkov, A.I.Baluyev ; A study of the nature of the ductile-brittle transition in β-Titanium alloys, "Titanium Science and Tech.", Proc. 2<sup>nd</sup> Int. Conf. on Titanium, Ed. by R.I.Jaffee and H.M.Brute, Plenum press, 1973, pp.1109-18.

## References

27. K.H.Mishra ; "Materials Engineering", Reinhold Publishing Company Inc., 1974, pp.61-80.
28. S M.L Shastri, P S.Rao, K.K.Shankaran ; High Temperature Deformation of Ti-6Al-4V, "Titanium'80 Science and Technology", Conf. Proc., Ed. by Kimura and Izumi, Japan, May 1980, pp.873-86.
29. S.Abkowitz, J.J.Burke, R.H.Hiltz ; "Titanium in Industry", D.Van Norstand Company Inc., USA, January 1955.
30. "Emerging Materials for Automotive Applications", An ISTE Course package developed by S.Bhargava, Dept. of MME, IIT Kanpur, pp.24.
31. H.D.Kessler, R.P.Sullivan ; Seamless Ti-15V-3Cr-3Sn-3Al Alloy Tubing for Aerospace and Other Applications, "Titanium 1986, Int. Conf. Proc. on Titanium Products and Applications", Titanium Development Association, Dayton, Vol-1, 1987, pp.72-83.
32. J.Charles, A.Suiger, J.P.Doucet ; Corrosion Behaviour And Use in Offshore Applications of Ti-6Al-4V Titanium Alloy, ibid, pp.256-81.
33. M.Sen ; Development of a Titanium Base Alloy for Medical Implants, ibid, Vol. 2, pp. 712-20.
34. T.Shepard, J. Norley ; Deformation Characteristics of Ti-6Al-4V, " Mat. Sc. And Tech.", Vol. 4, No. 10, Oct 1988, pp. 903-8.
35. F.D.Rosi, C.A.Dube, B.H.Alexandar ; "Trans. Amer. Inst. Min.(Metall.) Engrs.", Vol.197, 1953, pp.257.
36. A.T.Churchman ; "Nature", London, Vol.171, 1953, pp.706.
37. F.D.Rosi, F.C.Perkins ; "Journal of Metals", Vol.5, 1953, pp.1083.
38. C.J.Mcttargue, J.P.Hamond ; "Acta Met.", Vol.1, 1953, pp.700.
39. Metals Handbook, 8<sup>th</sup> Edition, Vol. 4, ASM, pp. 437-46.
40. S.L.Semiatin, D.Lahoti ; The Occurance of Shear-Bands in Non-isothermal Hot Forging of Ti-6Al-2Sn-4Zr-2Mo-0.1Si, "Met. Trans. A", Vol.14A, January1983, pp.105-15.
41. Metals Handbook, 9<sup>th</sup> Edition, Vol.3, ASM Committee on Ti and Ti alloys, 1980, pp.361-71.
42. Microstructural Standards for  $\alpha+\beta$  Titanium Alloy Bars, Prepared by The Technical Committee of European Titanium Producers,1979.

## References

43. W.A.Reinsch , Terminology for Titanium Microstructures, "Metal Progress", Vol.121, No.2, February1982, pp.51-56.
44. G.Welsch, R.Boyer ; Technical Note 1: Metallography and Microstructure, pp.1051-60.
45. D.R.Thornburg, H.R.Piehler ; Cold Rolling Texture Development in Ti and Ti-Al Alloys, "Titanium Sc. And Tech.", Int. Conf. Proc. on Titanium, Ed. by R.I Jaffee, H.M.Burte, Boston, 1973, pp.1187-97.
46. H.Inagaki ; Development of Cold Rolling Textures in Pure Ti, "Z. Metalkd.", October 1991, pp.79-89.
47. H.Inagaki ; Hot rolling Textures in Ti, "Z. Metalkd.", April1990, pp.282-92
48. H.Inagaki ; Hot rolling Textures in High strength Ti alloys, "Z. Metalkd.", August1990, pp.540-55.
49. H.Inagaki ; Evolution of Textures and Microstructures in TMP of Ti-6Al-4V, "Z. Metalkd ", June1990, pp.433-45.
50. S.F.Frederick, G.A.Lenning ; Producing Basal Textured Ti-6Al-4V Sheet, "Met. Trans.", Vol.6B, December1975, pp.601-5.
51. A.A.Babreko, I.V.Egiz, O.S.Belova, M.M.Dobrodeyeva ; The Formation of a Basal Texture of Sheets of a Psedo  $\alpha$  Alloy of the Ti-Al-V System in Different Conditions of Rolling, " Phys. Met. Metallo.", Vol.65, No. 5, 1988, pp.100-7
52. R.A.Adanesku, G.I.Denisenko, A.S.Kudryavtsev, G.V.Turchaninova, Ye.V.Chudakov ; Influence of Annealing on The Texture of a Titanium  $\alpha+\beta$  Alloy, "Phys. Met. Metallo.", Vol.63, No.5, 1987, pp.139-43.
53. M.F.Amateau, D.L.Dull, L.Reymond ; The Effect of Processing on Plastic Anisotropy of Ti-6Al-4V, "Met. Trans. A", Vol.5A, March1974, pp.561-64.
54. G.V.Shakhanova, O.G.Ukolova ; Features of The Texture of Hot Upsetting and Its Influence on The Structure of Titanium Alloy VTZ-1, "Phys. Met. Metallo.", Vol.71, No.4, 1991, pp.143-48.

## References

---

55. H.Liping ; The Study of Reducing Superplastic Temperature in Titanium Alloys, "Superplasticity and Superplastic Forming", Int. Conf. Proc., Ed. by C.H.Hamilton, N.E.Paton, TMS, 1988, pp.435-39.
56. A.K.Singh, C.Ramachandra, M.Tavafoghi, V.Singh ; Structure of Martensite in Titanium Alloy Ti-6Al-1.6Zr-3.3Mo-0.3Si, "J. of Mat. Sc. Letters", 12, 1993, pp.697-99.
57. JCPDS Files – International Centre for Diffraction Data.
58. G.Sridhar, D.S.Sarma ; On The Influence of Microstructure on The Room-temperature Deformation Behaviour of a Near  $\alpha$  Ti Alloy, " Met. Trans. A", Vol.22A, No.5, May1991, pp.1122-25
59. K.A.Padmanabhan, G.J.Davies ; "Superplasticity – Mechanical and Structural Aspects, Environmental Effects, Fundamentals and Applications", Springer-Verlag, Berlin, Heidelberg, 1980.
60. M.M.I.Ahmed, T.G.Langdon ; Exceptional Ductility in The Superplastic Pb-62%Sn Eutectic, " Met. Trans.A", Vol.8A, No.11, November1977, pp.1832-33.
61. K.Higashi, T.Ohnishi, Y.Nakatami ; Superplastic Behaviour of Commercial Aluminium Bronze , "Scr. Met.", Vol.19, no.7, July1985, pp.821-24.
62. C.H.Hamilton ; Superplasticity in Titanium Alloys, "Superplastic Forming", Proc. of Symposium by ASM, Ed. by. S.P.Agrawal, ASM, 1984, pp.13-22.
63. G.J.Davies, J.W.Edington, C.P.Cutler, K.A.Padmanabhan ; "J. of Mater. Sc.", Vol.5, 1970, pp.1091-
64. J.Pilling, N.Ridley ; "Superplasticity in Crystalline Solids", The Institute of Metals, London, 1989.
65. W.A.Backfen, I.R.Turner, D.H.Avery ; "Trans. ASM Quart.", Vol.57, 1964, pp.980-
66. C.Liu ; Dependance of Total Elongations Of Superplastic Materials on m, "Met. Trans.A", Vol.17A, No.4, April1986, pp.685-90.
67. C.Liu ; The C.L. m- $\delta$  Equation of Superplasticity, "Met. Trans.A", Vol.17A, No.4, April1986, pp.679-84.

## References

68. Y.Ito, A.Hasegawa ; Deformation Behaviour of Ti-6Al-4V Alloy Under Superplastic Condition, "Titanium'80 Science and Technology", Proc. Of 4<sup>th</sup> Int. Conf. on Titanium, Ed. by H.Kimura, O.Izumi, 1980, pp.983-92.
69. J.Cui, Q.Wu, L.Ma ; Effect of Grainsize on Region Transition Behaviour in Superplastic Deformation, " Superplasticity and Superplastic Forming", Int. Conf. Proc., Ed. by C.H.Hamilton, N.E.Paton, TMS, 1988, pp.245-49.
70. B.P.Kashyap, A.Arieli, A.K.Mukherjee ; On Structure Property Correlation During Superplastic Deformation, "Trans. Of IIM", Vol.39, No.4, August1986, pp.341-56.
71. A.K.Ghosh, C.H.Hamilton ; Influences of Material Parameters and Microstructure on Superplastic Forming, "Met. Trans.A", Vol.13A, No 5, May1982, pp.733-43.
72. B P.Kashyap, G.S Murty ; "Met. Trans.A", Vol 13A, No.1, January1982, pp.53-
73. R.G.Gifkins ; "Met. Trans.A", Vol.8A, 1977, pp.1507-
74. C.H.Caceres, D.S Wilkinson ; Large Strain Behaviour of a Superplastic Cu Alloy, "Acta. Met.", Vol 32, 1984, pp.415-422.
75. A.K.Ghosh, C.H.Hamilton ; "Met. Trans.A", Vol.10A, 1979, p.699.
76. N.Furushiro, H.Ishibashi, S.Shimoyama, S.Hori ; Factors Influencing The Ductility of Superplastic Ti-6Al-4V Alloy, "Titanium'80 Science and Technlogy", Proc. of 4<sup>th</sup> Int. Conf. on Titanium, Ed. by H. Kimura, O.Izumi, 1980, pp.993-1000.
77. C.H.Hamilton, A.k.Ghosh ; Characterization of Superplastic Deformation Properties of Ti-6Al-4V, ibid, pp.1001-14.
78. E.Sato, K.Kuribayashi, R.Horiuchi ; Superplastic Deformation Induced Graingrowth in Microduplex and Second-phase Induced Alloys, "Superplasticity and Superplastic Forming", Int. Conf. Proc., Ed. by C.H.Hamilton, N.E.Paton, TMS, 1988, pp.115-19.
79. O.A.Kaibyshue, I.V.Kazachkov, R.M.Galeev ; "J. of Mat. Sci.", Vol.16, 1981, pp.2501

## References

80. C.H.Hamilton, A.K.Ghosh, M.M.Mahoney ; Microstructure and Phase Ratio Effects on The Superplasticity of Ti-6Al-4V, "Advanced Processing Methods for Titanium", Conf. Proc., Ed. By D.F.Hasson, C.H.Hamilton, TMS – AIME, pp.129-144.
81. J.S.Kim, Y.W.Chang, C.S.Lee ; The Effects of  $\alpha/\beta$  Volume Fraction on The Superplastic Deformation Behaviour of Ti-6Al-4V alloy, "Light Weight Alloys for Aerospace Applications IV", Ed. by E.W.Lee, W.E.Fraizer, N.J.Kim, K.Jata, TMS, 1997,pp.141-49.
82. L.R.Zhao, S.Q.Zhang, M.G.Yan, Improvement in The Superplasticity of Ti-6Al-4V Alloy by Hydrogenation, "Superplasticity and Superplastic Forming", Int. Conf. Proc., Ed. by C.H.Hamilton, N.E.Paton, TMS, 1988, pp.459-64.
83. H.Liping, The Study of Reducing Superplastic Temperature in Ti Alloys, ibid, pp.435-39.
84. W.B.Morison ; The Elongation of Superplastic Alloys, "Trans Met Soc Of AIME", Vol. 242, 1968, pp.2221-27.
85. A.Arieli, A.K.Mukherjee, Factors Affecting The Ductility of Superplastic Ti-6Al-4V Alloy, "Proc. of 5<sup>th</sup> Int. Conf. on The Strength of Metals And Alloys", Ed. by P.Hassen et. al., Aachen, August 1979, Vol.1,pp.375-80.
86. H.Inagaki, Enhanced Superplasticity in High Strength Ti Alloys, " Z. Metallkd", Vol.86, No.9, 1995, pp.643-50.
87. H.Inagaki, Mechanism of Enhanced Superplasticity in Thermomechanically Processed Ti-6Al-4V, " Z. Metallkd", Vol.87, No.3, 1996, pp.179-86.
88. M.E.Rosenblum, P.R.Smith, F.H.Froes ; Microstructural Aspects of Superplastic Forming of Titanium Alloys, " Titanium'80 Sc. And Tech.", -Int. Conf. Proc., Ed. by H. Kimura, O.Izumi, 1980, pp.1015-24.
89. A.K.Ghosh, C.H.Hamilton ; Influences of Material Parameters and Microstructure on Superplastic Forming, "Met. Trans.A", Vol.13A, May1982, pp.733-43.
90. A.Arieli, A.Rosen, Superplastic Deformation of Ti-6Al-4V Alloy, "Met. Trans.A", Vol.8A, Oct.1977, pp.1591-96.

## References

91. M.T.Cope, N.Ridley ; Superplastic Deformation Characteristics of Microduplex Ti-6Al-4V Alloy, "Mat. Sc. And Tech.", Vol.2, Feb.1986, pp.140-45.
92. M.T.Cope, D.R.Evetts, N.Ridley ; Superplastic Deformation Characteristics of Two Microduplex Titanium Alloys, "J.of Mat. Sc.", Vol.21, 1986, pp.4003-08.
93. E.Girault, J.J.Blandin, A.Verlooteanx, M.Surey, Y.Combres ; Low Temperature Superplasticity of A Metastable  $\beta$ -Ti Alloy, "Scr. Met.", Vol.29, No.4, 1993,pp. 503-08.
94. S.Yamazaki, T.Oka, Y.Mae, Superplastic Properties of The Cold Formable Ti Alloy SP35, "Superplasticity And Superplastic Forming", Int. Conf. Proc., Ed. by C.H.Hamilton, N.E.Paton, TMS, 1988, pp.407-11.
95. M.j.Donachie ; " Titanium And Titanium Alloys: A Source Book", ASM, 1982.
96. M.Peters, G.Lutjering, G.Ziegler ; Control of Microstructures of  $\alpha+\beta$  Titanium Alloys, "Mat. Sc. And Tech.", Vol.4, No.903, Oct.1988, pp.274-82.
97. D.Bourell, H.J.McQueen ; "J. of Applied Metal Work", Vol.5, 1987, pp.53-73.
98. J.C.Chesnutt, C.G.Rhodes, J.C.Williams ; Relationship Between Mechanical Properties, Microstructure And Fracture Topography in  $\alpha+\beta$  Titanium Alloys, "Fractography – Microscopic Cracking Processes", ASTM, 1976, pp.99-138.
99. M.A.Greenfield, C.M.Pierce, J.A.Hall ; The Effect of Microstructure on The Control of Mechanical Properties in  $\alpha+\beta$  Titanium Alloys, "Titanium Science And Technology", Proc. of 2<sup>nd</sup> Int. Conf., Ed. by R.I.Jaffee, H.M.Burte, Vol.3, 1973, pp.1731-43.
100. V.Shukla, S.Bhargava ; Effect of Thermomechanical Treatment on Microstructural Refinement in Ti-6.8Al-3.2Mo-1.8Zr-0.3Si Alloy, "National Seminar on Titanium And Superalloys", Hyderabad, July1996.

## References

101. G.Wirth, K.J.Grundhoff, A TMT For The Improvement of Microstructure of PM And IM Ti-6Al-4V Possessing A Combination of High RT Fatigue Strength And Good Creep Rupture Strength, "6<sup>th</sup> World Conference on Titanium", France, 1988, pp.1307-18.
102. I.Weiss, F.H.Froes, D.Eylon, G.E.Welsch ; Modification of  $\alpha$  Morphology in Ti-6Al-4V by Thermomechanical Processing, " Met. Trans.A", Vol.17A, Nov.1986, pp.1935-46.
103. O.A.Kaibyshev, R.A.Lutfullin, G.A.Salishchev ; "Phys. Metal and Metallo.", Vol.66, No.6, 1988, pp.1163-71.
104. D.L.Bourell, H.J.McQueen ; Thermomechanical Processing of Iron, Titanium and Zirconium Alloys in the BCC structure , "J. Mater. Shaping Tech.", Vol.5,No.1, 1987,pp.53-73.
105. H.Oikawa, K.Nishimura, M.X.Cui ; "Scr. Met.", Vol.19, 1985, pp.825-828.
106. B.D.Cullity ; "Elements of X-Ray Diffraction", Addison-Wesley Publishing Co., 1978.
107. R.M.German ; "An Introduction to Powder Metallurgy"
108. D.Lee,W.A.Backofen ; " Trans. TMS-AIME", Vol. 239,1967, p.1034.
109. N.E.Paton,C.H.Hamilton ; "Met. Trans. ", Vol.10A, 1979, p.241.
110. A.Arieli, B.J.Maclean, A.K.Mukherjee ; An Evaluation of the Concurrent Grain Growth during Supreplastic Flow of the Ti-6Al-4v Alloy, "Titanium'80 Sc. & Tech.", Ed. by H.Kimura, O.Izumi, 1980, pp.-1047-1056.
111. O.A.Kaibyshev, I.V.Kazachkov, R.M.Galeev ; "J. Mat. Sci.", Vol.16, 1981, p. 2501.

A 130842

130842

## Date Slip

This book is to be returned on the  
date last stamped.



A130842